

REPUBLIC OF IRAQ

MINISTRY OF HIGHER EDUCATION

AND SCIENTIFIC RESEARCH

AL-FURAT AL-AWSAT TECHNICAL  
UNIVERSITY

ENGINEERING TECHNICAL  
COLLEGE- NAJAF



# DESIGN AND PERFORMANCE EVALUATION OF HORN NANOANTENNAS FOR MODERN APPLICATIONS

A THESIS

SUBMITTED TO THE COMMUNICATION TECHNIQUES  
ENGINEERING DEPARTMENT

IN PARTIAL FULFILLMENT OF THE REQUIREMENTS FOR  
THE MASTER OF TECHNIQUES DEGREE IN

COMMUNICATION TECHNIQUES ENGINEERING

BY

**Doaa Maryam Abbas Mohammed**

Supervised by

**Asst. Prof. Faris Mohammed Ali, Ph.D.**

**Salim Muhsin Wadi, Ph.D.**

October 2019

# بِسْمِ اللَّهِ الرَّحْمَنِ الرَّحِيمِ

﴿اللَّهُ نُورُ السَّمَوَاتِ وَالْأَرْضِ مِثْلُ نُورِهِ كَمِثْقَاةٍ فِيهَا مِصْبَاحٌ الْمِصْبَاحُ فِي زُجْجَةٍ

الزُّجْجَةُ كَأَنَّهَا كَوْكَبٌ دُرِّيٌّ يُوقَدُ مِنْ شَجَرَةٍ مُبَارَكَةٍ زَيْتُونَةٍ لَّا شَرْقِيَّةٍ وَلَا غَرْبِيَّةٍ يَكَادُ

زَيْتُهَا يُضِيءُ وَلَوْ لَمْ تَمْسَسْهُ نَارٌ نُورِ عَلِيِّ نُورٌ يَهْدِي اللَّهُ النُّورَ مِنْ بَيْتَاءَ وَيَضْرِبُ اللَّهُ

الْأَمْثَالَ لِلنَّاسِ وَاللَّهُ بِكُلِّ شَيْءٍ عَلِيمٌ ﴿﴾

صَدَقَ اللَّهُ الْعَلِيُّ الْعَظِيمُ

## DEDICATION

*To the greatest person in this world*

*AL-IMAM AL-MAHDI AL-MUNTATHAR*

*To the one I am so proud to carry his name, to the one who  
taught me giving, to the spirit of my father.*

*To my love, devoted, tender, affectionate, merciful, to life's  
smile, to the essence of existence, who gave me the ability to  
achieve my dreams, to my beloved mother.*

*To loyalty and sincerity, to that which encouraged me, in  
my life, to my family.*

*DOAA MARYAM*

*2019*

## Acknowledgement

In the beginning, I would like to thank *Allah* Almighty, the most gracious, the most merciful, for giving me the determination and the strength to complete this research work in the field of communications technology engineering.

I appreciate the guidance and advice that I have received from the supervisors **Assistant Prof. Dr. Faris Mohammed Ali** and **Dr. Salim M. Wadi** for their continues support and encouragement .

I would also like to express my thanks to **Assistant Professor Dr. Ali Jabbar Salim**, **Assistant Professor Dr. Musa H. Wali** and **student PhD. Gufran Mahdi** for providing advice throughout the research period.

I am very grateful to my **family** for their help, understanding, patience, and encouragement. Finally, I say to thank my **mother** for her patience, long suffering and great encouragement; to her I owe everything in my life from birth to death.

## Supervisors Certifications

We certify that this thesis titled “**Design and Performance Evaluation of Horn Nanoantennas for Modern Applications**” which is being submitted by **Doaa Maryam Abbas Mohammed** was prepared under my/our supervision at the Communication Techniques Engineering Department, Engineering Technical College-Najaf, AL-Furat Al-Awsat Technical University, as a partial fulfillment of the requirements for the degree of Master of Technical in Communication Techniques Engineering.

Signature:

Name: **Asst. Prof. Dr. Faris  
Mohammed Ali**  
(Supervisor)

Date:     /     / 2019

Signature:

Name: **Lecture, Dr. Salim M.  
Wadi**  
(Supervisor)

Date:     /     / 2019

In view of the available recommendation, we forward this thesis for debate by the examining committee.

Signature:

Name: **Dr. Salim M. Wadi**  
(Head of Comm. Tech. Eng. Dept.)

Date:     /     / 2019

## Committees Reports

We certify that we have read this thesis titled "**Design and Performance Evaluation of Horn Nanoantennas for Modern Applications**" which is being submitted by **Doaa Maryam Abbas Mohammed** and as Examining Committee, examined the student in its contents. In our opinion, the thesis is adequate for award of degree of Master of Technical in Communication Engineering.

Signature:

Name: **Asst. Prof. Dr. Faris Mohammed Ali**

(Supervisor)

Date:     /     / 2019

Signature:

Name: **Lecture, Dr. Salim M. Wadi**

(Supervisor)

Date:     /     / 2019

Signature:

Name: **Asst. Prof. Dr.**

(Member)

Date:     /     / 2019

Signature:

Name: **Asst. Prof. Dr.**

(Member)

Date:     /     / 2019

Signature:

Name: **Asst. Prof. Dr.**

(Chairman)

Date:     /     / 2019

### Approval of the Engineering Technical College- Najaf

Signature:

Name: **Asst. Prof. Dr. Ali Albakry**

Dean of Engineering Technical College- Najaf

Date:     /     / 2019

## Abstract

The main objective of this thesis is to design and simulate a new horn nanoantenna that operates in THz region. It includes several applications of infrared and optics wireless communication, such as smart lighting, sensing, imaging, energy harvesting and other applications required wideband.

The horn antenna is used in engineering because of the attractive properties, such as directivity, gain and broadband. Many researchers have studied this type of antennas, including the conical and the pyramidal. The proposed designs have the same general shape, but it is different in the sidewall and studies the effect of the shape on characteristic of an antenna. We use the cylindrical and square vias and different in material used to reduce the leakage of signal through waveguide.

In this thesis, we have designed and simulated four Horn Nanoantenna designs, where the proposed designs operate in terahertz range and have multiband or broadband of frequencies. All the proposed four-horn antennas are composed of two layers of gold metal because it represents a perfect electric conductor which does not change the characteristics at nan scale, the thickness of gold layer is 50nm. The waveguide port is used to excite this type of horn nanoantenna through the transmission line. The dimension of the two layers of gold used for the four proposed antenna designs are in the same range: the length of waveguide ( $\ell_{wg}$ ) is 4000nm; the length horn ( $\ell_{horn}$ ) is 2000nm; width of waveguide ( $w_{wg}$ ) is 2500nm; and the thickness is 50 nm. In order to implement the performance of each proposed Horn Nanoantenna, a

commercial available software simulator called CST STUDIO SUITE 2018 is used to reach the desired goal.

The first Horn Nanoantenna design consists of only two layers of transmission line called Simple Horn Nanoantenna (SHNA). This antenna gives multiband with three resonant frequencies, where the range bandwidth are (29.3-36) THz, (49.3-57.3) THz and (67.6-75.7) THz.

The second design consists of two layers of gold by inserting square and silicon vias inside the transmission line. This design is called Gold-Silicon Horn Nanoantenna (G-SHNA). This Nanoantenna gives a broadband. The range of bandwidth is from (200 - 300) THz.

The antenna designs of the third and fourth horn nanoantenna are made of two layers of gold with an addition of cylindrical vias inside the transmission line, but the latter design is different. The material uses a dielectric between the two layers of gold. Drill holes into the insulating material are made and then filled with the same conductive material so to get the best match. Therefore, it is called a Cylindrical-Gold Horn Nanoantenna (C-GHN) and Substrate Integrate Waveguide Horn Nanoantenna (SIW-HNA). These two types give the same bandwidth range of (200-300) terahertz.

## Contents

Title	Page No.
Acknowledgement	I
Supervisors Certifications	II
Committees Reports	III
Abstract	V
Contents	VII
Nomenclatures (Symbols)	X
Abbreviations	XII
List of Figures	XIII
List of Tables	XV
List of Publications	XVI
<b>Chapter One: Introduction</b>	
1.1 Introduction	1
1.2 Horn antenna	3
1.3 Applications for the Nanoantenna	4
1.4 Motivation	7
1.5 Aim of the work	7
1.6 Thesis Contributions	8
1.7 Thesis layout	8
<b>Chapter Two: Literatures Review</b>	
2.1 Introduction	9
2.2 Literature review	10
<b>Chapter Three: Theory and Design Configuration</b>	
3.1 Introduction	22
3.2 Analysis of nanoantenna structures	23
3.3 Basic definitions of antenna parameters	26
3.3.1 Reflection Coefficient	26
3.3.2 VSWR	27
3.3.3 Current distribution	28
3.3.4 Radiation pattern	28
3.3.5 Gain	29

3.3.6 Directivity	30
3.3.7 Efficiency	31
3.3.8 Bandwidth	32
3.4 The proposed first model; Simple Horn Nanoantenna (SHNA)	33
3.4.1 Parametric study of SHNA design	35
3.4.1.1 The effect of different thickness of air	35
3.4.1.2 The effect of various radius of flare or curvatures	37
3.5 The proposed second model; Gold –Silicon Horn Nanoantenna (G-SHNA).	39
3.5.1 Parametric study of the proposed antenna design	41
3.5.1.1 The effect various of the length of square gold side(a)	41
3.6 The proposed third model, Cylindrical-Gold Horn Nanoantenna (C-GHNA)	43
3.6.1 Parametric study of C-GHNA design	47
3.6.1.1 The effect various of radius of via	47
3.7 The proposed fourth model; Substrate Integrate Waveguide Horn Nanoantenna (SIW-HNA)	49
3.7.1 Parametric study of the proposed antenna design	51
3.7.1.1 The effect various of dielectric thickness ( $ts$ )	52
<b>Chapter Four: Result, Discussion and Performance Evaluation</b>	
4.1 Introduction	53
4.2 Characteristic of Simple Horn Nanoantenna (SHNA)	53
4.2.1 Reflection coefficient ( $S_{11}$ ) for SHNA	53
4.2.2 VSWR for SHNA	54
4.2.3 Current distribution for SHNA	55
4.2.4 Radiation pattern for SHNA	56
4.2.5 3D Gain for SHNA	60
4.2.6 3D Directivity for SHNA	61
4.2.7 Efficiency and bandwidth for SHNA	62
4.3 Characteristic of Gold – Silicon Horn Nanoantenna(G-SHNA)	63
4.3.1 Reflection coefficient ( $S_{11}$ ) for G-SHNA	63
4.3.2 VSWR for G-SHNA	64
4.3.3 Current distribution for G-SHNA	65

4.3.4 Radiation pattern for G-SHNA	66
4.3.5 3D Gain for G-SHNA	71
4.3.6 3D Directivity for G-SHNA	72
4.3.7 Efficiency and bandwidth for G-SHNA	73
4.3.8 Compression between the first (SHNA) and second (G-SHNA) proposed antenna.	74
4.3.9 The proposed designs validation	75
4.4 Characteristic Cylindrical-Gold Horn Nanoantenna(C-GHNA)	76
4.3.1 Reflection coefficient ( $S_{11}$ ) of C-GHNA	76
4.3.2 VSWR of C-GHNA	77
4.3.3 Current distribution of C-GHNA	77
4.3.4 Radiation pattern of C-GHNA	79
4.3.5 3D Gain of C-GHNA	83
4.3.6 3D Directivity of C-GHNA	84
4.3.7 Efficiency and bandwidth of C-GHNA	85
4.5 Characteristic of Substrate Integrated Waveguide Cylindrical-Gold Horn Nanoantenna (SIW-HNA).	86
4.3.1 Reflection coefficient ( $S_{11}$ ) of SIW-HNA	86
4.3.2 VSWR of SIW-HNA	87
4.3.3 Current distribution of SIW-HNA	88
4.3.4 Radiation pattern of SIW-HNA	89
4.3.5 3D Gain of SIW-HNA	96
4.3.6 3D Directivity of SIW-HNA	98
4.3.7 Efficiency and bandwidth of SIW-HNA	100
4.5.8 Compression between the third (C-GHNA) and fourth (SIW-HNA) proposed antenna	100
4.5.9 Validation the two design with other reference	101
4.6 Comparison of four proposed antennas	102
<b>Chapter Five: Conclusions and Suggestions</b>	
5.1 Introduction	103
5.2 Conclusion	103
5.3 Suggestions	105
References	

## Nomenclatures (Symbols)

Symbol	Meaning
E-	Amplitude of wave reflection
E+	Amplitude of wave incident.
$\Phi$	Azimuth angle
$P(\theta, \phi)$	Angular radiation in one direction
$P_{rad}$	Angular radiation in all direction
$\alpha$	Angle of flare
$Z_0$	Characteristic impedance
$f_c$	Center frequency
$D(\theta, \phi)$	Directivity
$d$	Diameter of cylindrical via
$\theta$	Elevation angle
$w_{eff}$	Effective widths of waveguide
$\eta_{rad}$	Efficiency
$B$	Flux density
$G$	Gain
Au	Gold material
$f_h$	High frequency
$h$	High
$E_{inc}$	Incident field
$V_i$	Incident voltage
$P_{in}$	Input power (accepted power)
$Z_L$	Load impedance
$P_{LA}$	Losses antenna
$f_l$	Low frequency
$\ell_{wg}$	Length of waveguide
$\ell_{horn}$	Length of horn
$a$	Length of the square side
$\delta$	Loss tangent
$V_{max}$	Maximum voltage
$V_{min}$	Minimum voltage

$f_{max}$	Maximum frequency
$f_{min}$	Minimum frequency
$n$	Number of layers
$P_{acc}$	Net power accepted.
$\lambda$	Operating waveguide
$\epsilon_0$	Permittivity
$\mu$	Permeability
$U$	Power intensity
$p$	Pitch (distance between center two vias)
$\epsilon_r$	Relative electrical permittivity of the nanoantenna
$\Gamma$ or $S_{11}$	Reflection coefficient
$V_r$	Reflection voltage
$rf$	Radius of curvature
$r$	Radius of via
$\epsilon_r$	Relative permittivity of the antenna
Ag	Silver material
A	The magnetic vector potential
$\varphi$	The electric scalar potential
$E$	The total electric field
$J_{eff}$	The volume current
$k_n$	The wavenumber
$G_A^{mn}$	The Green's function of A
$G_q^{mn}$	The Green's function of $\varphi$
$\rho$	The charge density
$d_{Au}$	Thickness of gold
$d_{air}$	Thickness of air
$t_s$	Thickness of dielectric material
$w_{wg}$	Width of waveguide
$w$	Width of waveguide

## Abbreviations

Abbreviation	Meaning
BW	Bandwidth
CST	Computer Simulation Technology
C-GHNA	Cylindrical –Gold horn nanoantenna
dB	Decibel
DMLS	Direct Metal Laser Sintering
FBW	Fraction bandwidth
GHz	Gigahertz
G-SHNA	Gold-Silicon horn nanoantenna
GPR	Ground penetrating radar
IEEE	Institute of Electrical and Electronics Engineers
MPIE	mixed potential integral equation
NDT	Non-destructive technical
nm	Nanometer
NIR	Near infrared
PV	Photovoltaic
Cu–15Sn	polished material
RF	Radio frequency
RT5880	Roger dielectric material
SiO <sub>2</sub>	Silicon Dioxide
THz	Terahertz
SIW	Substrate integrate waveguide
SHNA	Simple horn nanoantenna
SIW-HNA	Substrate integrate waveguide-horn nanoantenna
3D	Three dimension
2D	Two dimension
TWTL	Two wire transmission line
TE <sub>10</sub>	Transvers Electric mode
VSWR	Voltage Standing Wave Ratio

## List of Figures

<b>Figure No.</b>	<b>Figure Title</b>	<b>Page No.</b>
Fig. 3.1	Power Pattern (radiation pattern)	29
Fig. 3.2	Transverse section of transmission line	33
Fig. 3.3	Horn Nanoantenna Geometry	34
Fig. 3.4	The different thickness of air for proposed antenna	37
Fig. 3.5	Simulate reflection coefficient for various radius of flare for proposed design	38
Fig. 3.6	Overview G-SHNA design	40
Fig. 3.7	Gold-silicon via have shaped in this geometrical lattice	41
Fig. 3.8	Comparison of reflection coefficient for different values of the length square side.	42
Fig. 3.9	C-GHNA only two layers of Gold	43
Fig. 3.10	C-GHNA design (a) cylindrical gold vias have shaped in this geometrical lattice. (b) C-GHNA design over view	44
Fig. 3.11	Geometric of SIW	47
Fig. 3.12	Simulate reflection coefficient at different radius of via (r)	48
Fig. 3.13	SIW-NHA two gold and Rogers RT5880	49
Fig. 3.14	Geometric lattice of via through dielectric material (a) Dielectric material is worked holes (b) The holes are filled conductive	51
Fig. 3.15	Simulated reflection coefficient for various thickness of dielectric	52
Fig. 4.1	Simulated reflection coefficient of the SHNA	54
Fig. 4.2	Simulated VSWR of SHNA	54
Fig. 4.3	Simulated current distributions of proposed horn antenna	55
Fig. 4.4	Far-field radiation patterns for the total electric field of simple horn nanoantenna	59

Fig. 4.5	Simulated 3D far-field gain patterns for SHNA	61
Fig. 4.6	Simulated 3D far-field directivity pattern of SHNA	62
Fig. 4.7	The simulated reflection coefficient $S_{11}$ of G-SHNA	64
Fig. 4.8	The simulated results of VSWR for G-SHNA	64
Fig. 4.9	The simulated results of current distribution for different resonant frequency of G-SHNA	66
Fig. 4.10	The simulated far field radiation pattern of G-SHNA at three resonant frequencies 276.47THz, 298.21THz and 320.98THz	70
Fig. 4.11	The simulated gain for different frequencies	72
Fig. 4.12	The simulated directivity of G-SHNA.	73
Fig. 4.13	The simulation of reflection coefficient of C-GHNA	76
Fig. 4.14	VSWR of the proposed model C-GHNA	77
Fig. 4.15	The simulated results current distribution for different resonant frequency of C-GHNA	78
Fig. 4.16	The simulated radiation pattern for proposed antenna	82
Fig. 4.17	3D far-field gain of different resonant frequencies	84
Fig. 4.18	3D far-field directivity of three resonant frequencies of C-GHNA	85
Fig. 4.19	The simulated reflection coefficient $S_{11}$ of SIW-HNA	87
Fig. 4.20	Simulated VSWR of the proposed model	87
Fig. 4.21	Simulated current distribution of proposed model	89
Fig. 4.22	The simulated result of 2D radiation pattern	95
Fig. 4.23	Simulation Gain at three various frequencies	97
Fig. 4.24	The directivity for different frequencies	99

## List of Tables

<b>Table No.</b>	<b>Table Title</b>	<b>Page No.</b>
Table 2.1	The horn Nanoantenna designs references at Gigahertz band frequencies	17
Table 2.2	The horn Nanoantenna designs references at Terahertz band frequencies	19
Table 3.1	The dimensions of SHNA	35
Table 3.2	Comparison of proposed antenna design based thickness of air	36
Table 3.3	Compression results for different radius of flare of SHNA antenna	38
Table 3.4	The dimensions of G-SHNA design	40
Table 3.5	Comparison between different values of the length square side	42
Table 3.6	The dimensions of C-GHNA	45
Table 3.7	Comparison proposed module for different the radius of via	48
Table 3.8	The dimension of SIW-HNA	50
Table 4.1	The characteristic of far-filed radiation pattern of SHNA	56
Table 4.2	The efficiency and bandwidth for SHNA	63
Table 4.3	The simulated radiation pattern characteristic for three resonant frequencies of G-SHNA.	67
Table 4.4	The results of efficiency and bandwidth for G-SHNA	74
Table 4.5	The compression between two proposed antennas	74
Table 4.6	The compression the proposed designs and other reference	75
Table 4.7	The characteristic of far field power radiation of C-GHNA	79
Table 4.8	Efficiency and bandwidth	86

Table 4.9	The characteristic of radiation pattern of SIW-HNA	90
Table 4.10	The simulated results of efficiency and bandwidth for various frequencies.	100
Table 4.11	The comparison between the last two proposed designs	101
Table 4.12	Comparison between the last two proposed designs	101
Table 4.13	The simulation results for four proposed horn antenna design	102

### **List of Publications**

<b>Paper No.</b>	<b>Paper Title</b>	<b>Paper Status</b>
Paper 1	“A new design and simulation of cylindrical-gold horn Nano-antenna at terahertz region for energy harvesting application” International Journal of Engineering & Technology, 2018	published

# CHAPTER ONE

## INTRODUCTION

### 1.1 Introduction

In the last few decades, there has been a rapid development involving satellite and wireless communications because the world communication depends on it. Therefore, the current trend in the evolution of the communications system commercial and government entities focuses on small size and low cost. [1].

Antenna is defined in different ways. The Institute of Electrical and Electronics Engineers (IEEE) defines it as "a means of transmitting and sending radio waves". The other definition of antenna is "a device that converts electrical energy into electromagnetic energy to be transported through free space" [2].

Communications in both fields (wire and wireless) have been enabled among devices with polymorphous in the abilities and the dimensions, beginning from the center computer devices and laptop computers to the electronic devices used in buildings, sensing elements and mobile phones. Alongside diminish in the device's measurements. In this time, nanotechnology provides new collections for designing and fabricating small components, such as physical, chemical fields and nano sensors relating to biology. Most of the modern devices need to exchange information, among themselves, to wireless communications.

The world trend to reduce the size of devices leads to minimize the size of antenna. So, we have to reduce the size of antennas to some of the micrometers within a wide range of high frequencies that start from infrared bands to optical frequencies [3].

Nano science was far from being a reality. In 1959, Richard Feynman delivered his speech at the yearly meeting of the American Physical Society, under the title “There's a lot of room at the base”. In his speech, Feynman foresaw the greater part of the exploratory fields and issues of concern. Over twenty years, they have ended up as key issues in the comprehension of phenomena at the nanometer scale. Discussing the likelihood of building nanoscale electric circuits, the question was whether it was possible to emit light from the full set of antennas. For example, an organized group of antennas emits radio waves to carry radio programs to Europe [4].

Which is similar to emit light out in a definite direction with very high intensity. Today it can be said that Feynman's proposal has become a reality and the research on nanoantennas working in optical frequencies has been developed particularly in nano-optics. The aim of based on this research is to explain the current understanding of optical antennas from the background of evolution in antenna engineering [5].

The most important topic in this field is the subject of feeding or the extraction from the electromagnetic energy sent by the transmitter or receiver of nanoantenna. Many applications are related to this subject (like energy harvesting and wireless communication) as mentioned above [6] [7].

Optical energy also can be focused around the antenna because of its resonant behavior in the receiving state where the energy extraction from the antenna itself is not a simple task at all [8].

The purpose of this thesis is to design new horn nanoantennas. These intended to achieve high frequencies operating in the field of infrared and optical frequencies, taking into account the gain and directivity.

## 1.2 Horn antenna

The horn antenna is one of the simplest antennas or perhaps the most widely used in optical and infrared frequency range. It was found in the late 19<sup>th</sup> century. Although neglected at the beginning of 1900s, it was almost restored in the late 1930's because of the interest in microwave and transmission lines waveguide during World War II. Since 1939, many papers have been written describing optimal design methods, radiation mechanism and applications. Papers deal to the principle of work and the basic theory as well as century horn designs [9].

The horn antenna is a hollow tube of different cross sections. It has eventually, be taper or flared into a larger opening. The overall performance of the element as radiator affect with respect to direction, types and amount of curvature of opening end of antenna. [10].

The horn antenna is used as a feeder called (horn feed) for larger antennas as the parabolic antennas. It is used as standard for measuring the gain of other antennas, and directive antennas for devices such as radar guns, automatic door opening. The horn antenna provide wide bandwidth, high gain and low voltage standing wave ratio (VSWR), it is used in space applications in the Megahertz, Gigahertz to currently in Terahertz [11].

The horn nanoantenna is composed of the same structure as the standard structure of horn but with a compact size up to several nanometers. The Horn Nanoantenna has many uses especially in near infrared and visible region, for example harvesting energy and radar.

### 1.3 Applications of the Nanoantenna

The nanoantenna at present has entered into many fields. Several applications will be briefly listed as follows:

- **In microscopy:** Many researchers have been able to develop near-field optical microscopy because of nanostructures. This technique of optical imaging can be used to break the diffraction limit around. It is also used in near-field microscopic optical mapping distribution of nanoscale antenna that can be attained by detecting the scattering response from a sharp probing end [12].
- **In communication:** Because of the increasing demand for high-speed communications and data high rate speed, there has a need to use the

higher operating frequency of the electromagnetic spectrum. High operating frequencies are set for communication link in the Terahertz (THz) area. The nanoantenna plays a large and important role in wireless communication, which is extended in THz frequencies zone. To improve communication link, the gain of antenna is an important factor [13]. The techniques of THz antennas with the special attention to the planar techniques, which leads to the compact, inexpensive, and low - profile future THz wireless communication system design [14].

- **In sensing:** The nanostructure makes antenna more sensitive to environmental changes, and therefore any change in the refractive index of the surrounding medium leads to a change in the position of the signal of the far field region [15].
  
- **In energy harvesting:** The nanoantenna array includes many applications [16]:
  - 1- Through the body radiation generating electricity.
  - 2- Heating and cooling processes within clothing.
  - 3- Cooling systems through the conversion of infrared thermal radiation IR to another type of radiation.
  - 4- Energy collectors and cooling electronic devices such as that is used to reduce the heat of personal computers (Laptops) instead of traditional fans.

- **In solar plane:** The nanoantenna have many advantages:

1- Photovoltaic cells must be thick for better absorption of the solar spectrum. However, a large part of the solar spectrum, especially between wavelengths between 600-1100nm, the absorption is weak. The use of dense photovoltaic cells reduces efficiency, so the use of solar cells nanoantenna can be reduced while maintaining the optical thickness constant [17].

2- Solar photovoltaic cells rely on a fundamental principle in their operation. The process relies on the generation of hole - electron pairs which are limited to certain band. Solar radiation that reaches the earth contains photons that have higher energy than the hole in silicon. Therefore, the solar cells will absorb the higher energy photons. Waste of energy can cause as heat because of the difference between the hole and the electron in the silicon. However, the solar nanoantenna cells can absorb our entire energy without any problem. It is with noting, that the reception of the nanoantenna characteristics are almost constant during all operating frequencies [18].

The proposed designs can be applied in wireless communications, power harvesting, smart lighting and other applications according to the resonant frequencies obtained.

## 1.4 Motivation of work

Antennas consist of different shapes and types. All types of antenna operate according to the same electromagnetic principle. However, horn antenna is distinguished from another type with some characteristics, such as wide bandwidth and high directivity. In recent years, the horn nanoantenna has been used in many applications of wireless communications including radar and energy harvesting.. Many researchers have implemented different types of nanoantennas to solve the problem between the minimize size of the antenna and the high gain because the gain is reduced with respect the effective area. So, in this thesis decided to design four horn nanoantenna to operate in THz range to cover the visible region and infrared.

## 1.5 Aims of the work

The present work aims to:

1. Design four new horn nanoantennas with extreme frequency in Terahertz and wide band to include a range of applications.
2. Evaluate a comprehensive study of the results in terms of gain, bandwidth, reflection coefficient and efficiency.
3. Comparing between the types of proposed aperture horn nanoantennas, by using the commercially available EM simulator the Microwave Studio (CST-2018).

## 1.4 Thesis Contributions

The main contributions in this work are:

- Design and Simulate different shapes of horn nanoantennas so as to obtain high directivity as well as wideband and multiband for different resonant frequencies which can be applied in many applications.
- Comparing the obtained results of the different proposed designs in term of gain, bandwidth and efficiency. In order to choose the highest bandwidth to include a range of applications in terms of easy of manufacturing in the future.

## 1.5 Thesis Layout

This thesis consists of five chapters each chapter is arranged as follow:

**Chapter One:** It is a general introduction about antenna and nanoantenna, horn antenna, application of nanoantenna, motivation of work, aim of the work, thesis contribution, and summary about the thesis content.

**Chapter Two:** It includes an introduction to the horn antenna and literature review.

**Chapter Three:** It covers theory of the horn antenna and deals with the proposed design of horn nanoantennas.

**Chapter Four:** It includes the simulation process, results and discussion of the proposed horn nanoantennas.

**Chapter Five:** It obtains the conclusion of the results in this work as well as future recommendations.

# CHAPTER TWO

## LITERATURE REVIEW

### 2.1 Introduction

This chapter deals with an introduction to nanoantenna and review of literatures. Modern wireless communications need a wide range of bandwidth and high data rate because of its congestion in conventional spectrum levels. In recent times, researchers face task to design a miniature size antenna with excellent characteristics for energy consumption taking into consideration the cost [19] [20].

Antenna illustrates a key-component in the scheme of wireless systems and the most part its physical measurements are corresponding for using wavelength. Little scales, equivalent to the wavelength of visible beam, describe optical antennas. In these days, we can come with the utilization of novel best down nanofabrication devices (e.g. centered particle pillar processing and electron-shaft lithography) and base up self-get together plans [21].

Nanoantenna is also known as optical antenna. The only difference is that it works at the optical frequencies of the electromagnetic spectrum, this depends on the wavelength measurements of the antenna. This is achieved by making antenna measurements in nano scale in order to obtain resonance in optical frequencies [22] [23].

Currently, most of the efforts have been made in the field of nanoantenna propose innovative designs that have the ability to give better matching impedance with free space, efficiency, higher gain, directivity and wide bandwidth of operation.

In this work, it is intended to design more than one new optical horn nanoantennas and compare them depending on the results from the first design and other designs. The proposed design are applied to achieve effective results such as gain and bandwidth as well as directivity and suitability for modern wireless communications applications.

## 2.2 Literature review

It is divided into two sections, the first section deals Gigahertz range frequencies and the other section deals Terahertz range.

### A. Literatures review for Gigahertz range frequency

- **In 2009, Majid Abbas-Azimi *et al*, [24]** suggested a new conical corrugated-horn antennas. The design proposed constant beamwidth and wideband taking into consideration design and construction with less complexity. For a corrugated-horn antenna, the frequencies are of 8 to 18 GHz operating. Electromagnetic performance was measured where the results obtained for the design of the antenna confirmed that they achieved the required antenna in terms of verifying the validity of the design procedure required.

- **In 2010, Hao Wang *et al*, [25]** proposed sectorial horn antenna, (SIW) substrate integrated waveguide. Loaded dielectric and the horn antenna is integrated by utilizing the same substrate, a substrate with dielectric constant  $\epsilon_r$  of 4.8, thickness of 2.5 mm, the length of 22mm, the width of waveguide 5.5mm and a working frequency of 27 GHz. Two antennas are designed with elliptical and rectangular shapes and fabricated by loaded dielectric. These antennas have two shapes E-plane and H-plane, the same qualities in terms of high gain and narrow beam width.
- **In 2014, Mahdi Oliaei and Mohammad Sadegh Abrishamian, [26].** proposed design substrate integrate waveguide (SIW) coaxial feeding technique used. The corrugated SIW H-plane sectorial horn antenna is used Substrate of Rogers RT/5880 with relative permittivity  $\epsilon_r=2.2$  and loss tangent  $\delta=0.0009$  has been used for this antenna. The design have good and suitable gain 10 dB and overall bandwidth 2GHz from (23.8 - 25.7 GHz) and radiation efficiency about 95%.
- **In 2016, J.-P. Adam and M. Romier, [27]** proposed corrugate horn antenna cover quad band (18GHz, 28GHz, 38GHz and 48GHz). This design split into two parts, the first which design consist of proper mode converter capable of produce low cross polarization and hybrid modes in the bands (28GHz, 38GHz and 48GHz), so corrugated design used to the pure polarization at high frequencies. The second part at low frequency (18GHz) band the design operated as smooth wall to achieve high efficiency for aperture antenna.

- **In 2016, Bing Zhang *et al*, [28]** studied the use of the metallic three dimension (3D) technology of printing for the operating antennas up to 325GHz. The use of two techniques and materials printing different. The develop series of conical horn antenna by choosing a polished material Cu–15Sn, the horn antenna work at multi bands E (60-90GHz) ,D (110-170GHz ) and H band (220-325GHz). Three-dimension (3D) metallic printed horn antenna have some features low cost, short turnaround time and environmental friendliness compared with conventional metallic horn antenna, it used injection molding and micromachining for implementation. Another compared with nonmetallic three-dimension (3D) printed antenna technique, where the (3D) metallic printed antenna technology characterized by simply and mechanical.
- **In 2017, Muhannad A. Al-Tarifi and Dejan S. Filipovic<sup>1</sup>, [29]** suggested a square horn antenna with radiation pattern is stable and the frequencies are almost alternating within the entire W-band from (75-110 GHz) is demonstrated. The flaring of horn antenna designed to support two perpendicular polarization, the radiation patterns very similar in both polarization. The horn antenna fabricated in two techniques: by using 3D metallic printed (DMLS) Direct Metal Laser.
- **In 2017, Ariffuddin Joret *et al*, [30]** studies the use of the Ground Penetrating Radar GPR system to detect underground objects, as this system is known as a non-destructive technical (NDT) system where it does not need to dig the surface of the earth. GPR technology depends on the reflection of the electromagnetic wave signal produced and detected by the transmitter and receiving antenna. Use a horn antenna as

transceiver antenna to study the GPR technique. The current signal of an antenna with a Gaussian signal with a frequency band of 8-12GHz produces electromagnetic signal.

## B. Literatures review for Terahertz range frequency

- **In 2011, D. Ramaccia *et al*, [31]** proposed a horn nanoantenna composed of two layers of metal thickness of 50nm Ag-air-Ag nanoscale of transmission line in tapered horn and used silver pillars cylindrical organized in triangular lattice to get a lateral confinement of the field inside the transmission line. The length of waveguide and opening horn 6000nm and 2000nm respectively, the width of waveguide was 3250nm and the height was 2000nm. This design operated at near infrared (NIR) frequencies. The results obtained from the proposed design include broadband frequencies and the gain of antenna was greater than 10 dB. These results can be applied in many technical and scientific fields such as optical wireless communications and smart lighting.
- **In 2011, Davide Ramaccia *et al*, [32]** studies characteristics of radiation and electrical of horn nanoantenna. The proposed design composed of Ag-Sio<sub>2</sub>-Ag nano scale of transmission line in tapered horn, the lengths of the waveguide and the horn respectively, are 1000 nm and 500 nm, respectively. The vertical aperture h is set to 300 nm. It working at near infrared (NIR) frequencies. The results of design in

terms of gain and bandwidth are involved in some applications as energy harvesting and telecommunications.

- **In 2012, Davide Ramaccia *et al*, [33]** suggested pyramidal horn nanoantenna to achieve broadband nano optical concentration. The pyramidal horn nanoantenna is assumed to be excited by a plane wave normally impinging on the aperture. The plane wave is progressively transformed by the horn into a guided mode that impinges on the PV converter placed at its end. This design operated through bands are 150THz and 320 THz. Although this approach leads to reasonable gain levels (around 11 dB).
- **In 2013, T.V. Bondarenko *et al*, [34]** studied the development radiating antennas for THz source's radiation. They suggested circular antenna is the most conventional type of antenna. The opening angle was varied while the horn length was kept  $L=1$  mm and taken another case change the length  $L=2$  mm to study effective with electrodynamic characteristics. The second type of considered horns are variable cross-section (transfer from circular to rectangular). The horn is attached directly to the coated capillary. The transition from circular to rectangular cross-section is done directly inside the opening. the maximum case study when set 15 degrees opening angles in both planes. The results of design directivity equal 22.5 dB with the horn length 2 mm, band of 0.7-1.1 THz and the reflection coefficient -20 dB.

- **In 2014, Yuanqing Yang *et al*, [35]** suggested plasmonic sectorial nano horn antenna working in near infrared frequencies wavelength about 1550nm. The plasmonic antenna still has some attractive features, for example, the simplicity of manufacturing, high directivity that are compressible and easy to couple with waveguide. As a specific application is to exploit these results of the proposed plasmonic horn nanoantenna to develop optical nano link wireless are used, the received power increased about 60 % compared with dipole antennas.
- **In 2014, Sumukha Prasad.U *et al*, [36]** Presented design of a horn Nanoantenna for operating at near infrared NIR range, with a good directivity and return loss, as well as the range of bandwidth 200 to 300 THz. In this paper, the researchers sought to address the problem of Plasmonic a combination the Silver (Ag) and Silicon Dioxide (SiO<sub>2</sub>) was considered for the antenna, the flaring angle and the radius of aperture of antenna were changed for the considered range of bandwidth. The best results were obtained after several antenna iterations are: Directivity is 14.22dBi, Radiation efficiency is 66.93%, S<sub>11</sub> is below -15 dB, and Side lobe level is -10 dB.
- **In 2016, Zhongyu Li *et al*, [37]** presented novel design and good performed of Terahertz horn antenna with microstrip feed. The overall proposed shape is divided into two parts, the horn antenna and microstrip feed. Where the horn antenna can radiated well during open space with new microstrip feed of graded shape stimulating it. The results obtained of design high frequency. This design presented small

scale, so the characteristic of reflection coefficient less than (-10 dB ) and the gain more than (5 dB ), as well as, the design work at wide band from (0.7-0.765) THz.

- **In 2016, Adeel Afridi and Sukru Ekin Kocabas, [38]** suggested a plasmonic horn nanoantenna consist of two wire transmission line (TWTL) are formed and flare in the end of horn. They analyze the effect of the thickness of the substrate on the antenna radiation pattern and show the beam steering in a wide range of elevation angle. In addition, they analyze the impact of ground plane on impedance matching between TWTL and the antenna. the directivity pattern of the antenna which has a maximum value of 14.5 dB at wavelength 1550nm and the total radiation efficiency is around 0.61.

All the previous studies of the above-mentioned references have been cleared for some basic factors such as Fraction Bandwidth (FBW), resonant frequency, type of design and design shape. They have been classified by frequency band, Gigahertz band frequency as shown in Table 2.1 and Terahertz band frequency as shown in Table 2.2.

Table 2.1: The horn Antenna designs references at Gigahertz band frequencies

No.	Ref. No.	Year	FBW	Freq. band	Type of horn	Illustration
1	[24]	2009	---	8-18 GHz	Conical (corrugate)	
2	[25]	2010	---	26-27 GHz	H-plane E-plane	
3	[26]	2014	8%	23.8-25.7 GHz	H-plane	

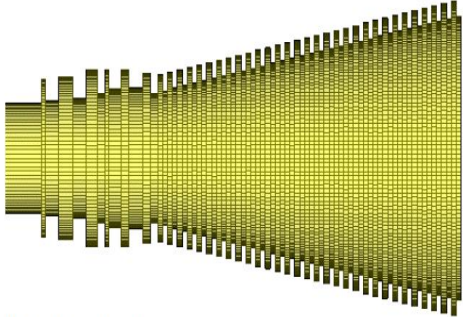
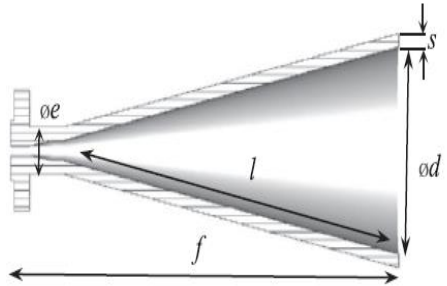
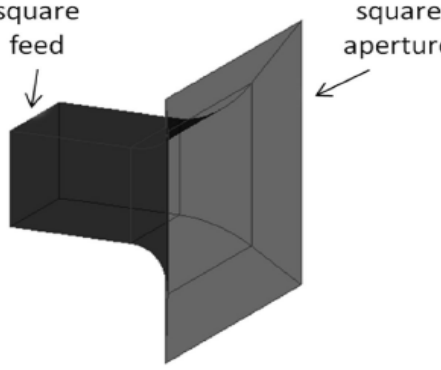
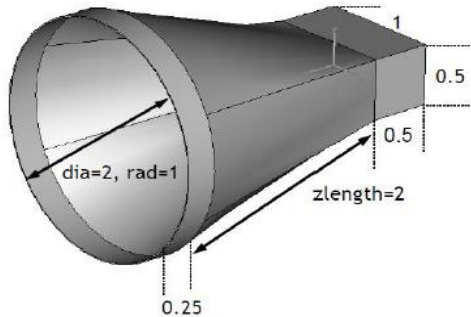
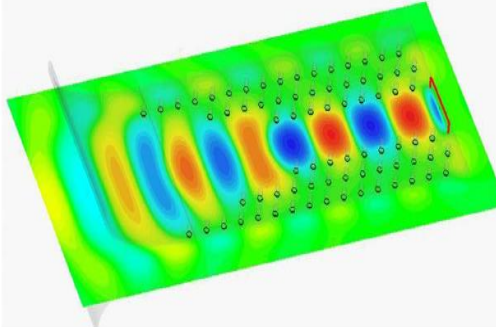
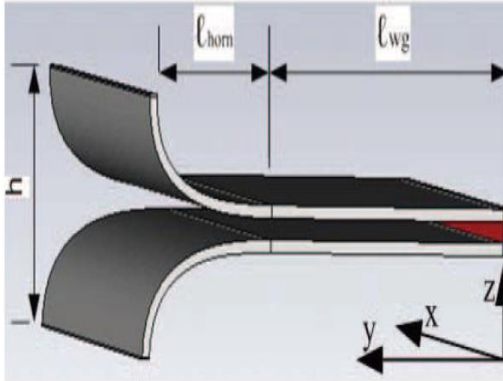
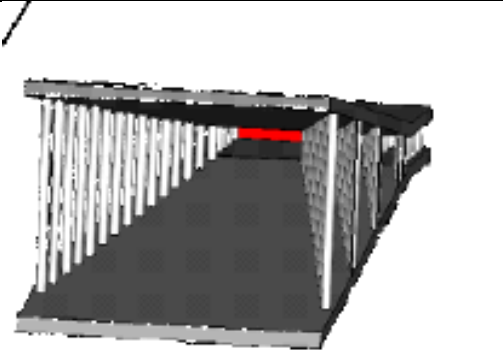
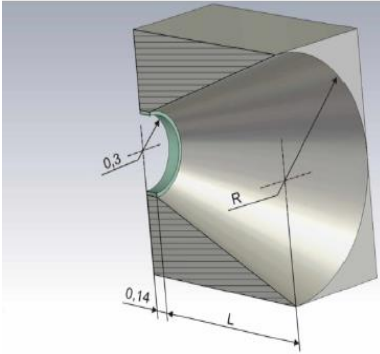
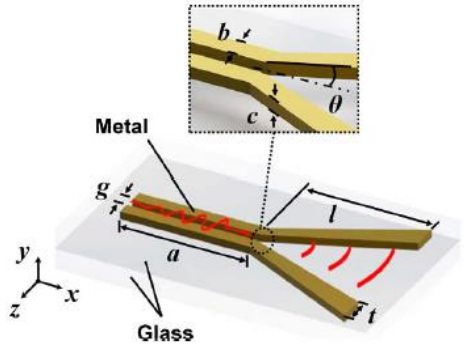
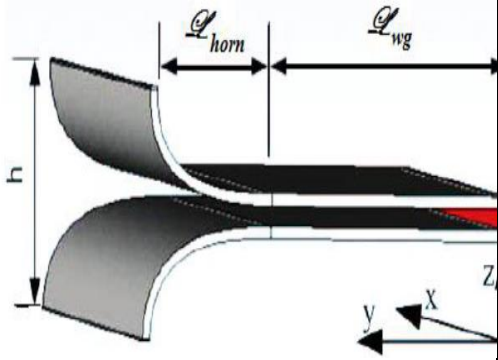
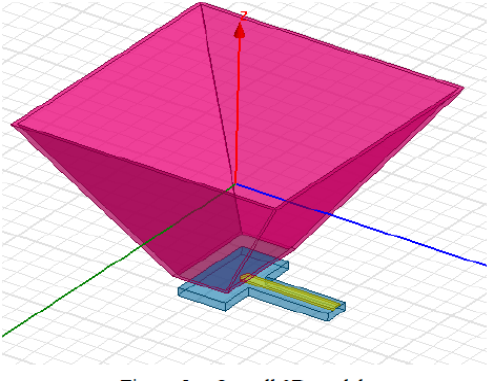
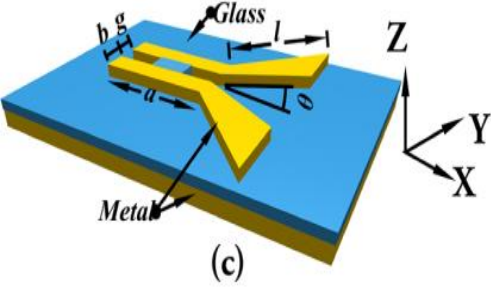
4	[27]	2016	8,1, 2, 6 %	18,28,3 8,48 GHz	conical	
5	[28]	2016	40, 37, 38 %	(60-90) (110- 160) (220- 325) GHz	Conical	
6	[29]	2017	37%	75-110 GHz	Pyramidal	
7	[30]	2017	40%	8-12 GHz	Conical	

Table 2.2: The horn Antenna designs references at Terahertz band frequencies

No.	Ref. No.	Year	FBW	Freq. band	Type of horn	Illustration
1	[31]	2011	---	160-240 THz	H-plane	
2	[32]	2011	37%	185-270 THz	E-plane	
3	[33]	2012	70%	150-320 THz	Pyramidal	

4	[34]	2013	44%	0.7-1.1 THz	conical	
5	[35]	2014	----	193 THz	E-plane	
6	[36]	2014	40%	200-300 THz	E-plane	

7	[37]	2016	8%	0.7-0.765 THz	Pyramidal	
8	[38]	2016	---	193 THz	H-plane	

# **CHAPTER THREE**

## **THEORY AND DESIGN CONFIGURATION**

### **3.1 Introduction**

This chapter, an introduction to define nanoantenna as well as analysis nanoantenna structure and definition of the basic parameters of antenna,. Then discuss the design of four shapes horn nanoantennas by using waveguide port to excite the transmission line. The effect different shapes of horn nanoantenna are discussed and analyzed to choose the best one. The performance of the proposed nanoantennas is evaluated all of the presented nanoantennas by CST STUDIO SUITE software version 2018.

The first and second designs have two layers of transmission line flared at end opening. The first design consists of only two layers, but the second proposed design has square gold and silicon vias arranged alternately in geometric shape. The third and fourth proposed designs have the same two layers of transmission line; they have cylindrical gold vias arranged in geometry lattice. However, the difference between them is stuffed the material inside transmission line. The third design consists of Au-Air-Au, but the last design consists of Au-Roger RT5880-Au.

## 3.2 Analysis of nanoantenna structures

Nanoantennas are optical wave radiating structures working based on the same physical principles equivalent to fundamental of their radio frequency. However, in the optical range of frequency the physical properties of materials are caused different response to the incident electromagnetic field appearing a new application in this field [39].

The conventional methods for the design and analysis of antennas requirement to be modified for nanoantenna structures. In this section, using the complex shape Green's function technique is used to model the optical wave interactions with nanoantennas in multi-layer media [40].

Using the optical properties of metals, metallic nanostructures are able of connecting with the free space propagating optical waves with plasmonic resonances to concentrate the incident waves by several orders of magnitude in the areas the wavelength much larger. These structures can applied many applications especially in bio sensing, nanolithography and also be used to the nonlinear effects and radiation efficiency [41].

To design complicated structures, the method is needed accurate and fast. Different schemes have been proposed to design and optimize nanoantennas. Considering some the concept of antenna impedance, optical Nano circuit elements are used steering to optimize their performance [42] [43].

In this thesis is presented a fast and accurate analysis method for a general configuration of nanoantennas. The method as described below is based on dyadic Green's functions with complex images, which will be used in the method of moments [44].

The total electric field can be described by the magnetic vector potential ( $A$ ) and the electric scalar potential ( $\varphi$ ) and flux density as shown in 3.1 and 3.2 equations following:

$$B = \nabla \times A - \frac{\nabla \times E_{inc}}{j\omega} \quad \dots (3.1)$$

$$E = -j\omega A - \nabla\varphi + E_{inc} \quad \dots (3.2)$$

Where  $E_{inc}$  is define the incident field which placed the Maxwell's equations in the layered media in the absence of nanoantennas. Replacement the nanoantennas by the volume current  $J_{eff}$ , the Green's functions for a two layers media. The modify equations of the magnetic vector potential and the electric scalar potential in the two layers are written as

$$\nabla^2 A + k_n^2 A = -\mu J_{eff}^n \quad \dots (3.3)$$

$$k_n^2 = \omega^2 \mu \epsilon_0 \epsilon_{rn} \quad (n = 1,2) \quad \dots (3.4)$$

$$J_{eff}^n = j\omega \epsilon_0 (\epsilon_r - \epsilon_{rn}) E \quad \dots (3.5)$$

Where:

$k_n$ : is the wavenumber

$n$ : is number of layers

$\epsilon_r$ : relative electrical permittivity of the nanoantenna

The Lorentz gauge condition is represented by equation 3.6:

$$\nabla \cdot A = -j\omega\mu\epsilon_0\epsilon_r\varphi \quad \dots (3.6)$$

The total electric field in each region can be achieved through the mixed potential integral equation (MPIE) as (3.7):

$$E = -j\omega \int_v G_A^{mn}(r, r') \cdot \mu J_{eff}^n(r') dv' - \nabla \int_v G_q^{mn}(r, r') \rho_v^n(r') dv' + E_{inc} \dots (3.7)$$

Where: The antenna regions  $G_A^{mn}$  and  $G_q^{mn}$  are denoted the dyadic Green's function of (A) and the Green's function of ( $\varphi$ ), respectively. The  $m$ th layer due to an electric dipole placed in the  $n$ th layer of the two layers and  $v$ -directed electric dipole source placed in the  $n$ th layer.

The charge density is defined in equation (3.8)

$$\rho = -\nabla \cdot J / j\omega \quad \dots (3.8)$$

Where the numerical evaluation for all possible source and field points is a very time consuming process. This is one of the major challenges in solving the (MPIE) for the unknown current distribution  $J_{eff}$ .

### 3.3 Basic definitions of antenna parameters

Some parameters of antenna will be explained in this section.

#### 3.4.1 Reflection coefficient

Reflection coefficient (or known amplitude reflection coefficient) is defined as the ratio between power reflections to power incident. It shows characteristic of antennas' operation by using figure of merit. This parameter calculates amount of electromagnetic wave (voltage) or power reflected from interface between two mediums different impedance [45]. The amplitude reflection coefficient is represented by:

$$|\Gamma| = |E^-/E^+| \quad \dots (3.9)$$

Where:

$E^-$  Represents amplitude of power reflection.

$E^+$  Represents amplitude of power incident.

Another equation is used to calculate reflection coefficient shown in equation (3.10) [46].

$$\Gamma = \frac{Z_L - Z_0}{Z_L + Z_0} \quad \dots (3.10)$$

Where:

$Z_L$  =load impedance

$Z_0$  =characteristic impedance

### 3.4.2 VSWR

Standing Wave Ratio is the ratio of the maximum voltage ( $V_{max}$ ) to the minimum voltage ( $V_{min}$ ). The transmission line is terminated by impedance. When this impedance is not matched with the characteristic impedance, the new signal incident to transmission line collides with the part reflected back to it from the previous signal. This is caused by the so-called standing wave ratio as shown in the following equations [47], where  $V_i$  is incident voltage and  $V_r$  is reflected voltage.

$$V_{max} = V_i + V_r \quad \dots (3.11)$$

$$V_{min} = V_i - V_r \quad \dots (3.12)$$

$$VSWR = \frac{V_{max}}{V_{min}} \quad \dots (3.13)$$

There is also another relationship between the standing wave ratio and reflection coefficient.

$$VSWR = \frac{1+\Gamma}{1-\Gamma} \quad \dots (3.14)$$

### 3.4.3 Current distribution

When the source of microwave is connected with Microstrip antenna, the charge will establish distribution in the lower and the upper planes of the antenna.

There are two mechanisms: that are used to control the charge distribution: attractive and repulsive. The attractive force is between the opposite charges on the ground plane and patch; it creates a current density at the bottom of the patch inside the dielectric. The repulsive force is between the same charges; it pushes the charges from the bottom of patch around the edge of the patch to the top of the patch. So as to that is create another current density [46].

### 3.4.4 Radiation pattern

The antenna radiation pattern can be defined as a geographical or mathematical representation of the radiation characteristics of the antennas determined in the far field as function special coordinates usually spherical.

The radiation properties include: power pattern, directivity, polarization or filed pattern. The power pattern of antenna shown in Fig 3.1 is a function of spherical coordinate system, where:  $r$  is considered magnitude,  $\Phi$  is considered azimuth angle,  $\theta$  is considered elevation

angle. The radiation pattern has two parts; major lobes and minor lobes [2].

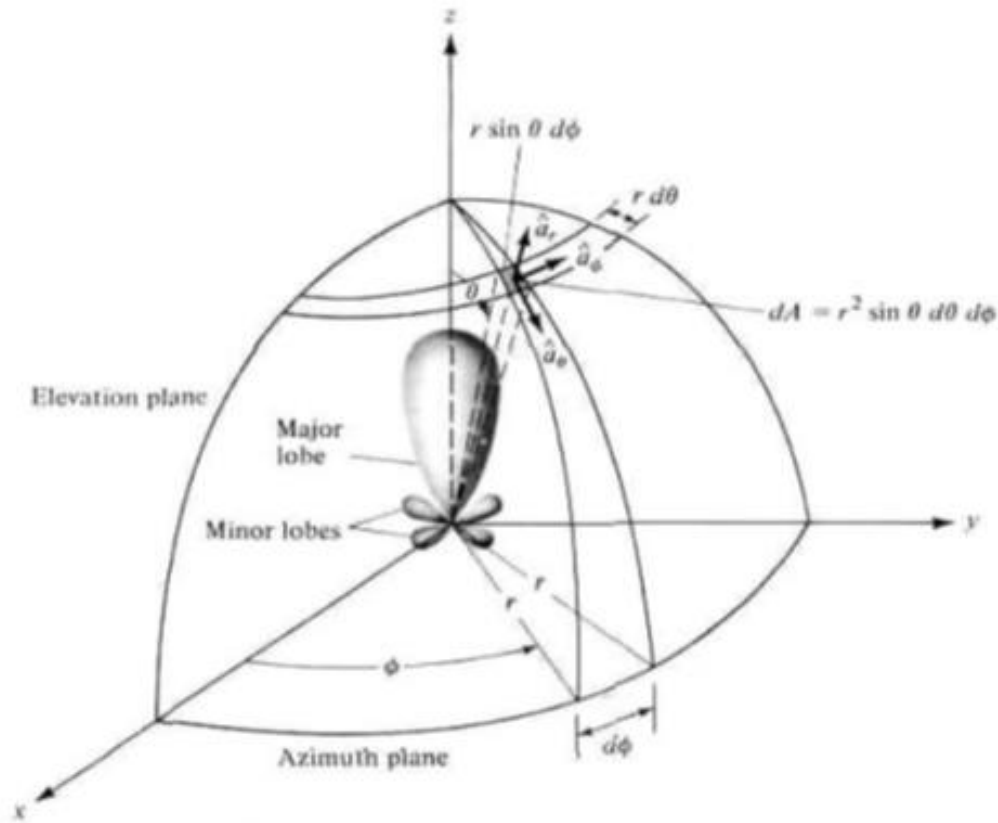


Fig 3.1: Power Pattern (radiation pattern)

### 3.4.5 Gain

Antenna gain can describe by the ratio of the power intensity transmitted in the direction of peak radiation to the power intensity of an isotropic antenna, as shown in equation 3.15. Gain is more common than the directivity of antenna characteristics in papers

because it takes into account the actual losses that occur. The power intensity radiation of an isotropically antenna can be calculated from the power accepted (input) divided by  $4\pi$  [10].

$$G = \frac{4\pi U}{P_{in}} \quad \dots (3.15)$$

Where:

$U$  : Power intensity

$P_{in}$  :input power (accepted power)

### 3.4.6 Directivity

Directivity is one of the most important parameters affecting the design and analysis of the antenna, through which the antenna operations are recognized [2].

Directivity can be defined as the ratio between the angular radiation intensity in special direction to the angular radiation intensity in general direction as shown in the following equation:

$$D(\theta, \phi) = 4\pi (P(\theta, \phi))/Prad \quad \dots (3.16)$$

Where:

$P(\theta, \phi)$  : represents the angular radiation in one (special) direction.

$Prad$  : represents the angular radiation in all (general) direction.

$\theta, \phi$  : represents elevation angle and azimuth angle alternately.

### 3.4.7 Efficiency

Antenna efficiency can be calculated from the ratio of the total power radiated by the antenna to the net acceptable power by the antenna as shown in equation 3.17. The losses at the input terminals; the losses within the structure of the antenna; the loss caused by the mismatched between the transmission line and the antenna as well as the loss of the dielectric and conductor material are taken into account when calculating the efficiency of the antenna [48].

$$\eta_{rad} = \frac{P_{rad}}{P_{acc}} = \frac{P_{rad}}{P_{rad} + P_{LA}} \quad \dots (3.17)$$

Where:

$P_{acc}$ : Net power accepted.

$P_{LA}$ : Losses antenna.

In addition, there are other ways to calculate efficiency, It can be calculated from the gain and directivity.

Efficiency can calculate the radiation efficiency from another relationship, the relative between gain to directivity as shown below [49]:

$$\text{Radiation efficiency} = \frac{\text{gain}}{\text{directivity}} \times 100\% \quad \dots (3.18)$$

### 3.4.8 Bandwidth

The antenna bandwidth can be defined as a range of frequencies or difference between maximum frequency and minimum frequency including antenna performance and certain characteristics which correspond to a specific standard. Bandwidth can be considered on both sides of the central frequency where antenna characteristics (such as pattern, directivity, beam width, side lobe level, gain, beam direction, radiation efficiency...etc.) are acceptable values within central frequency [2].

The Fraction Bandwidth (FBW) can be calculated in the percentage of ratio between the upper frequencies minus the minimum to the central frequency as shown in the equation below [50]:

$$FBW = \frac{f_{max} - f_{min}}{f_c} \quad \dots (3.19)$$

Where:

$f_{max}$ : the maximum frequency

$f_{min}$ : the minimum frequency

$f_c$ : the center frequency

Bandwidth can be calculated, which is defined by [22]

$$BW = 2 \frac{f_h - f_l}{f_h + f_l} \quad \dots (3.20)$$

Where  $f_h$  and  $f_l$  represent the higher and the lower frequency operational of antenna frequencies respectively.

### 3.4 The proposed first model: Simple Horn Nanoantenna

The first design of Simple Horn Nanoantenna (SHNA) consists of two metallic layers representing waveguide shape and increasing the physical aperture at the end of transmission line. Waveguide port is used to excite transmission line and the expected forward propagation of the fundamental mode has been correctly obtained at the design frequency.

In proposed antenna, the Au-Air-Au symmetric transmission line represents, Fig 3.2 show the diagram of transmission line.

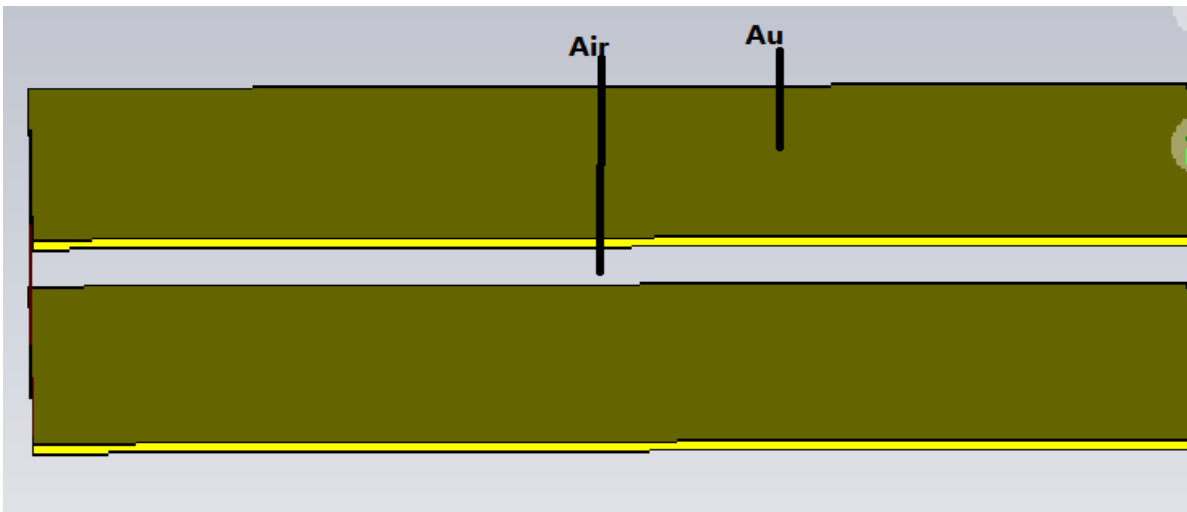


Fig 3.2: Transverse section of transmission line

The plasmonic antenna behavior of gold at Terahertz frequencies let to obtain the required series inductance behavior along the transmission line, while the dielectric (air) returns the shunt capacitance. Therefore, such a configuration supports a fundamental forward mode restricted between

the two metal layers. Gold is represented by the complex permittivity model that is presented in a Drude model with damping and plasma frequencies set to 4.35 THz and 2175THz, while the dielectric (air) is considered permittivity function model. According to these models, both dispersion and material losses are taken into account. [25] [26].

To have propagation in the terahertz frequencies, the thicknesses of gold and air layers have been set to 50 nm and 500nm, respectively.

The length of waveguide  $\ell_{wg}$  and length horn  $\ell_{horn}$  are set to 4000nm and 2000nm respectively and the height  $h$  is set 1500nm, Fig 3.3 shows the dimension in the table 3.1.

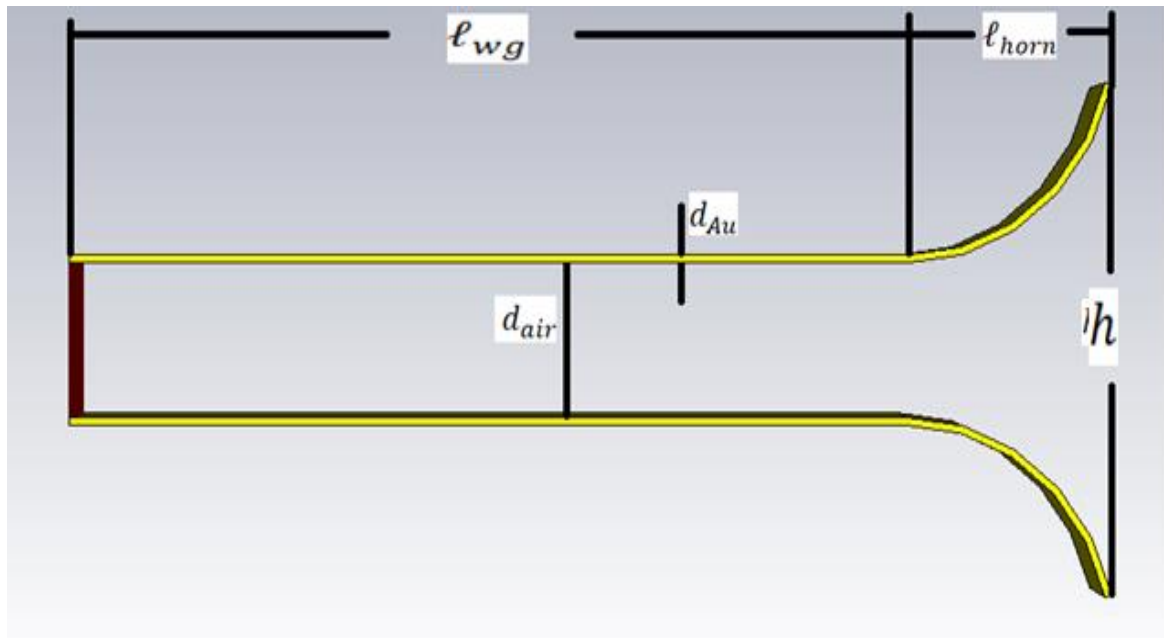


Fig 3.3: Horn Nanoantenna Geometry

Table 3.1: The dimensions of SHNA.

No.	parameters	symbols	amounts
1	Length waveguide	$l_{wg}$	4000 nm
2	Length horn	$l_{horn}$	2000 nm
3	Width of waveguide	$w_{wg}$	2500 nm
4	Height	$h$	1500 nm
5	Thickness of gold	$d_{Au}$	50 nm
6	Thickness of air	$d_{air}$	500 nm
7	The radius of curvature	$rf$	1500 nm
8	Angle of flare	$\alpha$	45°

### 3.4.1 Parametric study of SHNA design

The study parameter of the proposed design will changing dimension of parameter. There are several results selected the best them with respect gain and efficiency, are explaining:

#### 3.4.1.1 The effect of different thickness of air

One parameter of the proposed antenna is changed to a different thickness of air layer as shown in table 3.2. It is clear that when increasing thickness of air layer ( $d_{air} = 500nm$ ) the smoothness harmonic signal will be obtained. In addition, efficiency of

radiate and gain are enhanced from other thickness suggested and amount of reflection coefficient increased where -22.28 dB, -41.09dB and -24.27dB at frequencies 32.9, 53.49 and 71.35 THz respectively. So it is significant to show that the antenna parameters (reflection coefficient, efficiency of radiation and gain) can be enhanced by increasing the thickness of air layer. The reflection coefficient  $S_{11}$  calculated at different frequencies for different thickness of air layer are shown in Fig 3.4.

Table 3.2: Comparison of proposed antenna design based on thickness of air

Thickness of air $d_{air}$	$S_{11}$ (dB)	Frequency resonant (THz)	Efficiency (%)	Gain (dB)
$d_{air}=300\text{nm}$	-24.29	30.32	35	0.233
	-13.4	49.62	91	5.32
	-14.82	70.43	94	9.65
$d_{air}=400\text{nm}$	-36.73	32.106	71	1.02
	-19.84	52.74	92	5.82
	-22.39	71.29	95	9.8
$d_{air}=500\text{nm}$ (proposed)	-22.28	32.9	72	1.05
	-41.09	53.49	93	5.99
	-24.27	71.35	96	9.82

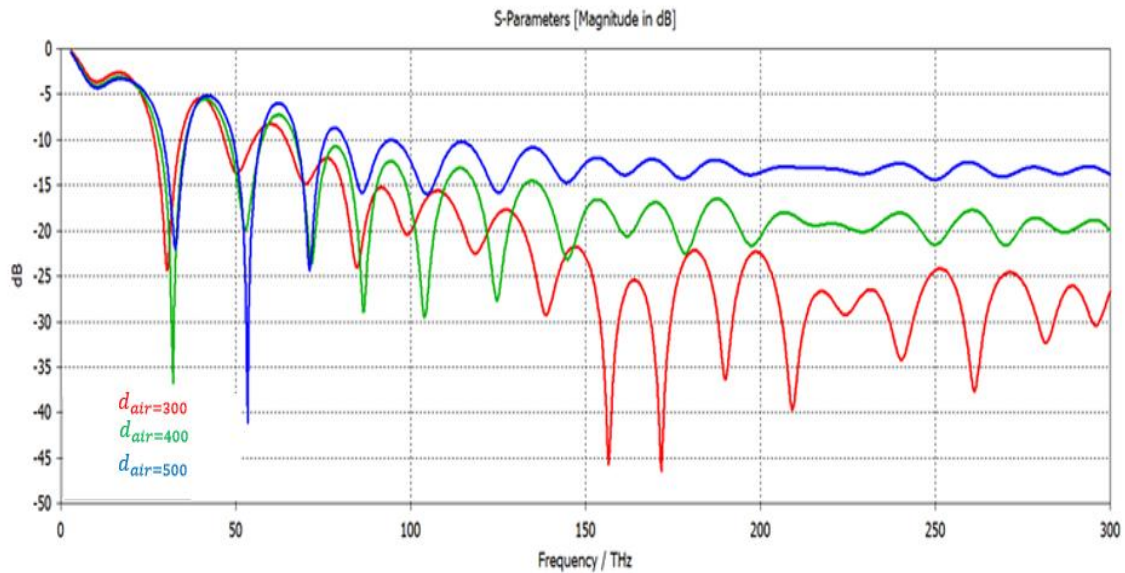


Fig 3.4: The different thickness of air for the proposed antenna

### 3.4.1.2 The effect of various radius of flare or curvatures

The radius of curvatures  $rf$  is optimized to achieve the best reflection coefficient and we can note the effect of  $rf$  alteration on the proposed design performance as summarized in Table 3.3. Initially, the  $rf$  value is taken 1500nm and increased by 100nm until reaching 1700nm. It is noted that when  $rf$  is equal to 1500nm, the best reflection coefficient  $S_{11}$  values can be achieved. Also, a comparison of reflection coefficient  $S_{11}$  at various frequencies for different values of  $rf$  is shown in Fig 3.5.

Table 3.3: Compression results for different radius of flare of SHNA antenna

Radius of curvatures	$S_{11}$ (dB)	Frequency resonant (THz)	Efficiency (%)	Gain (dB)
$rf = 1500\text{nm}$ (proposed)	-22.28	32.9	72	1.05
	-41.09	53.49	93	5.99
	-24.27	71.35	96	9.82
$rf = 1600\text{nm}$	-19.56	32.75	71	0.962
	-31.46	53.204	92	5.85
	-24.2	71.607	94	9.47
$rf = 1700\text{nm}$	-18.68	32.766	70	0.962
	-28.31	52.839	92	5.77
	-21.92	71.307	94	9.41

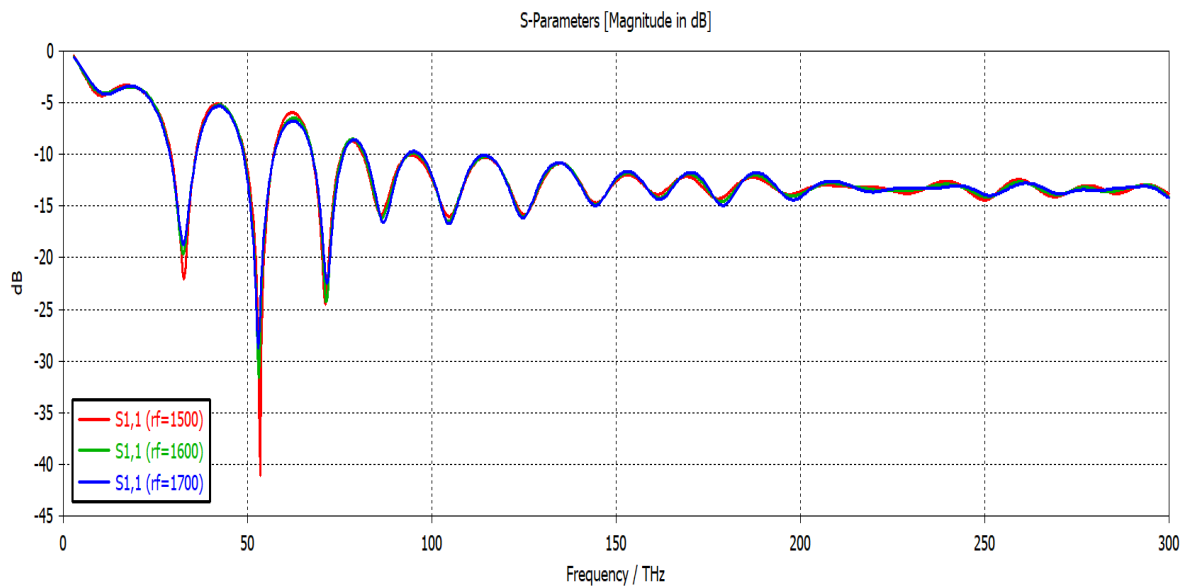


Fig 3.5: Simulate reflection coefficient for various radius of flare for proposed design

Although the proposed antenna obtains the result of the Terahertz, but there are some disadvantages: for example, the signal has harmonic, and the bandwidth is very narrow and low directivity. Accordingly, we conclude that there is signal leakage so, we will do some new techniques to get a better result and we will elaborate in detail the second proposed design.

### **3.5 The second proposed model: Gold –Silicon Horn Nanoantenna (G-SHNA).**

The first goal to be considered in the new design of Gold-Silicon Horn Nanoantenna (G-SHNA) is calculated parameters of the transmission line because the feeding of the horn depends on it. It is obtain propagation in the high frequencies (near infrared and optical frequencies). Waveguide port is used to excite transmission line. The proposed design, consisting of two layers of gold, intersects the air and inserting set of square vias as shown in Fig 3.6. The thicknesses of gold layers have been set to 50 nm and the air layer to 400nm, the lengths of the horn ( $\ell_{horn}$ ) is 2000 nm and the lengths of waveguide ( $\ell_{wg}$ ) is 4000 nm, as shown in Table 3.4.

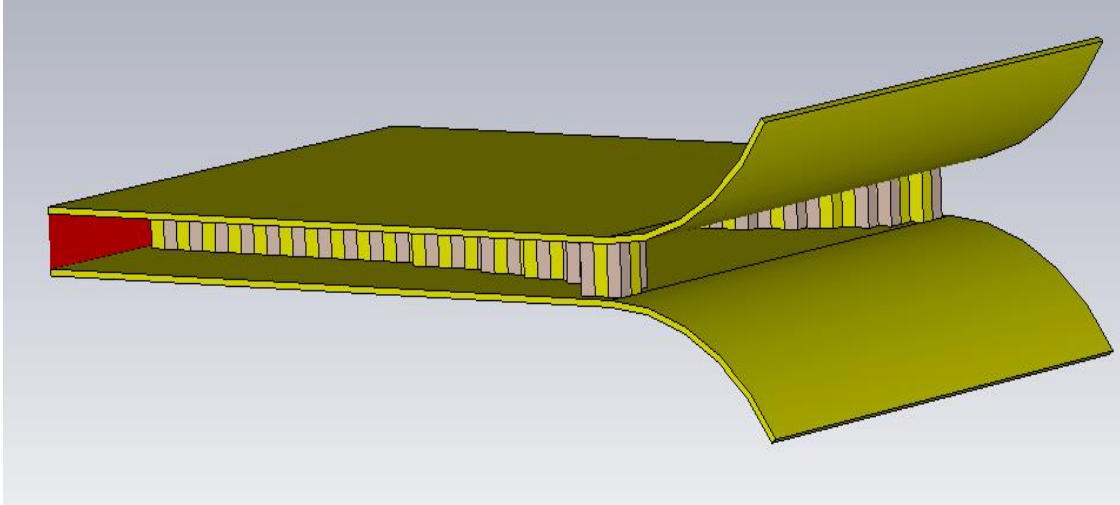


Fig 3.6: Overview G-SHNA design

Table 3.4: The dimensions of G-SHNA design

No.	parameters	symbols	amounts
1	Length waveguide	$\ell_{wg}$	4000 nm
2	Length horn	$\ell_{horn}$	2000 nm
3	Width of waveguide	$w_{wg}$	2500 nm
4	High	$h$	1500 nm
5	Thickness of gold	$d_{Au}$	50 nm
6	Thickness of air	$d_{air}$	400 nm
7	The radius of curvature	$r_f$	1500 nm
8	Angle of flare	$\alpha$	45°
9	Length of the square side	$a$	140 nm

The arranged of set of square via conductive material and dielectric material alternately are arranged in a geometrical shape, as shown in Fig 3.7. The internal confinement of field through the boundary of the sides during the waveguide is shown in Table 3.4.

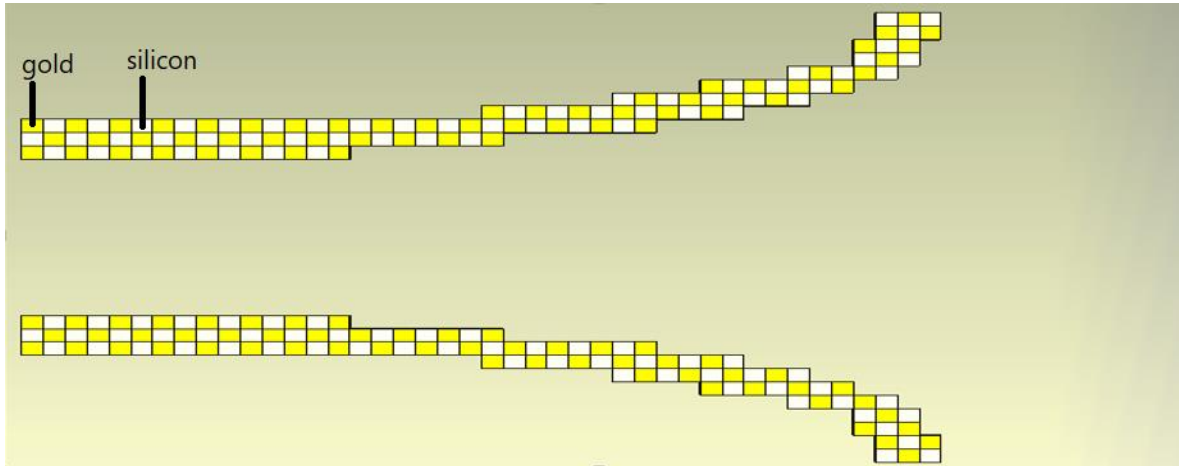


Fig 3.7: Gold-silicon square vias have shaped in the proposed geometrical lattice

### 3.5.1 Parametric study of the proposed antenna design

The study effect changing the dimension of length of square gold with respect some characteristics.

#### 3.5.1.1 The effect various of the length of square gold side ( $a$ )

A comparison between different values of square gold side ( $a$ ) is shown in Table 3.5. It is obvious that when  $a$  is 140nm, we can realize the best reflection coefficient value from other values. Therefore, this value of ( $a$ ) is utilized in the implementation of antenna as a length of square side. Also, a comparison of reflection coefficient for different values of ( $a$ ) is illustrated in Fig 3.8.

Table 3.5: Comparison between different values of the length square side

The length of square side	$S_{11}$ (dB)	Frequency resonant (THz)	Efficiency (%)	Gain (dB)
$a=120\text{nm}$	-16.74	270.5	85	10.8
	-18.29	293.7	83	10.8
	-23.01	321.16	83	10.8
$a =130\text{nm}$	-19.95	272.57	85	10.9
	-23.89	296.53	83	10.7
	-26.74	320.3	83	10.9
$a =140\text{nm}$ (proposed)	-25.97	276.42	85	10.9
	-33.42	298.17	82	10.6
	-26.43	321	86	10.9

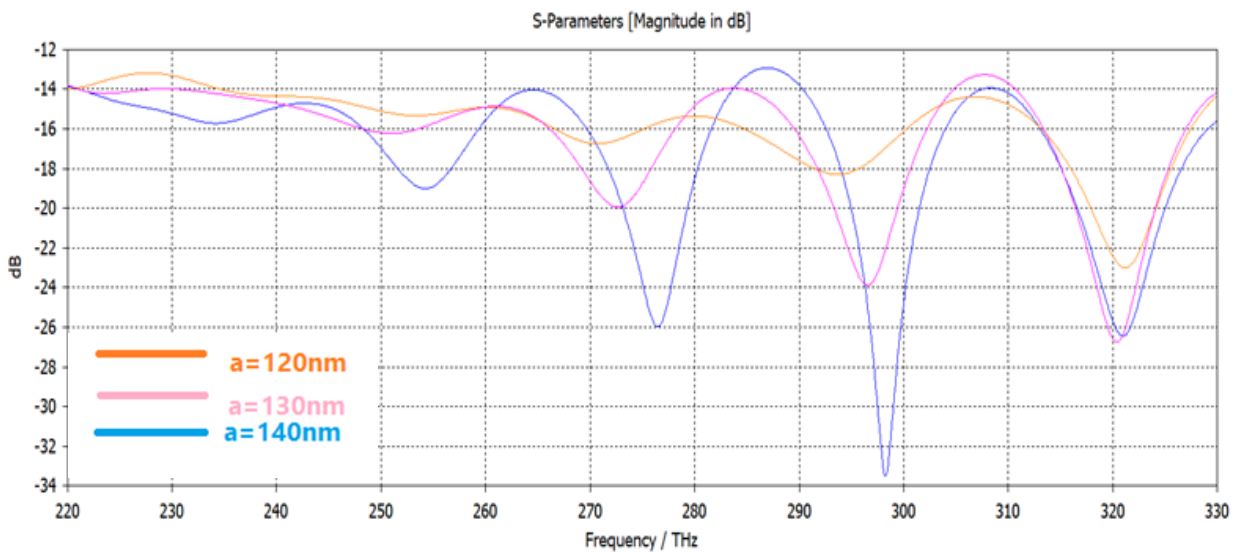


Fig 3.8: Comparison of reflection coefficient for different values of the length square side.

It is obvious that the resonant frequencies are affected when changing amount of (a). It is noted that reflection coefficient tends to decrease as value of (a) parameter increase.

### 3.6 The third proposed model: Cylindrical-Gold Horn Nanoantenna (C-GHNA)

The proposed horn nanoantenna (C-GHNA) consists of two gold layers at one-end of the waveguide representing transmission line and flared at the end opening. The dimension of the proposed design represents the thicknesses of the gold and the air layers have been set to 50 nm and 400nm respectively, as shown in Fig 3.9.

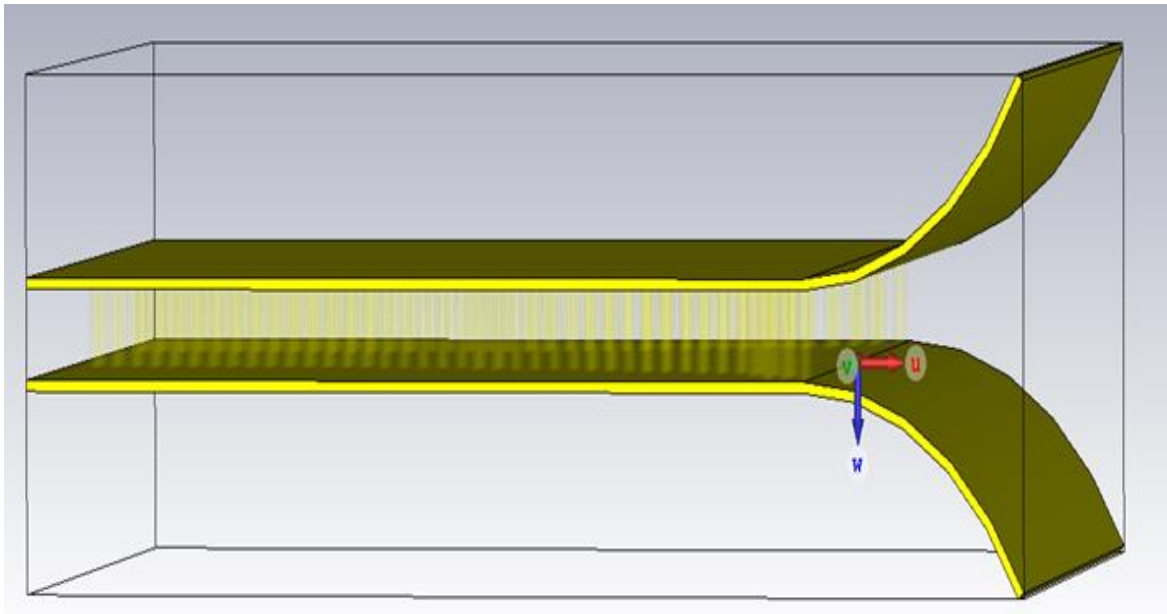
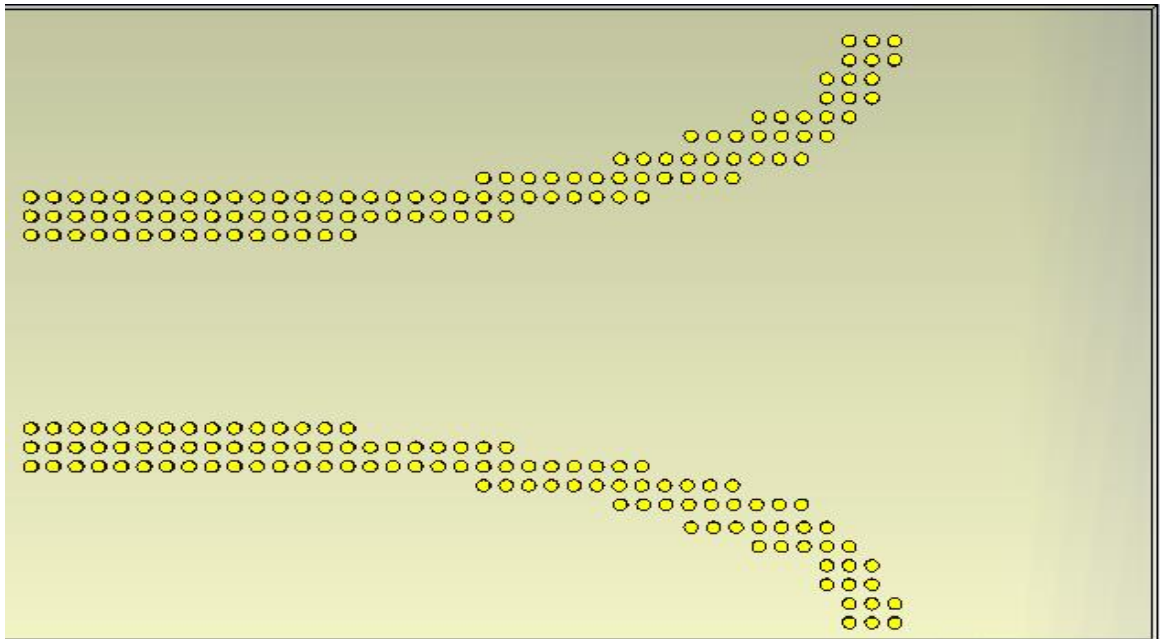
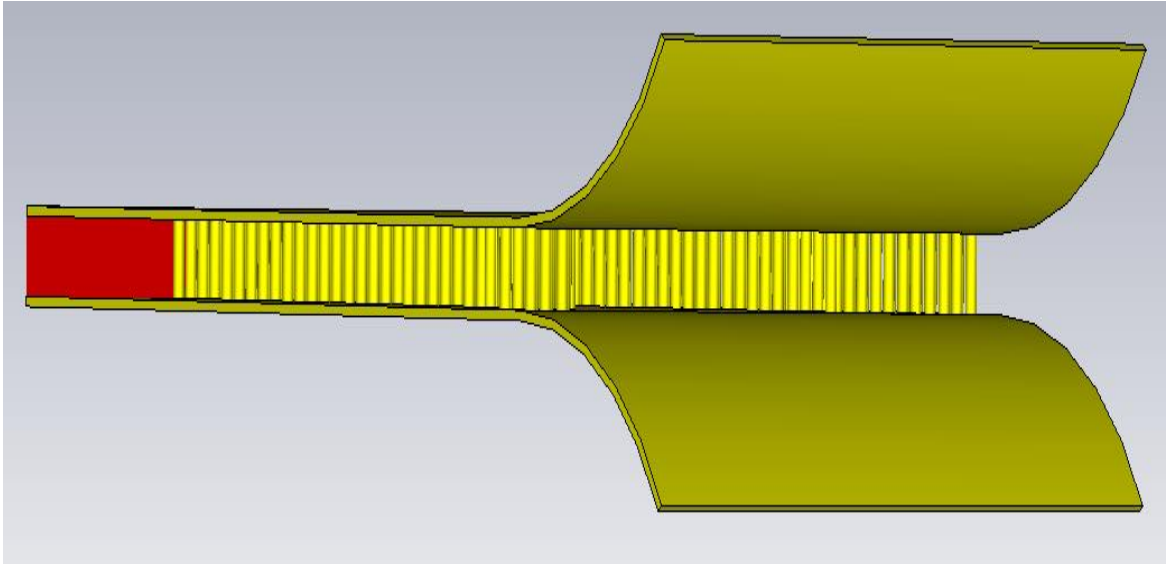


Fig 3.9: C-GHNA only two layers of Gold

The shape of horn antenna consists of metallic waveguide in such a way to increase the physical aperture thus, the antenna gain and progressively the impedance matching of the waveguide to free-space. The length of the horn ( $\ell_{horn}$ ) is 2000 nm and the length of waveguide ( $\ell_{wg}$ ) is 4000 nm. The height vertical aperture ( $h$ ) is set to 1500 nm, the radius of curvature and angle of flare is very important parameters which effect on the directivity and the gain of antenna results. Which are set 1500nm and  $45^\circ$  respectively. Cylindrical gold vias are arranged in the geometrical lattice as shown in Fig 3.10 a, b to reduce leakage of the electromagnetic signal during the waveguide. The dimension of the proposed design is shown in Table 3.6.



(a)



(b)

Fig 3.10: C-GHNA design (a) cylindrical gold vias have shaped in this geometrical lattice. (b) C-GHNA design over view

Table 3.6: The dimensions of C-GHNA

No.	Parameters	symbols	amounts
1	Length waveguide	$\ell_{wg}$	4000 nm
2	Length horn	$\ell_{horn}$	2000 nm
3	Width of waveguide	$w_{wg}$	2500 nm
4	Height	$h$	1500 nm
5	Thickness of gold	$d_{Au}$	50 nm
6	Thickness of air	$d_{air}$	500 nm
7	The radius of curvature	$r_f$	1500 nm
8	Angle flare	$\alpha$	45°
9	Diameter of cylindrical via	$d$	45 nm
10	Pitch	$p$	60 nm

In order to ensure radiation free from leakage loss or less leakage loss through waveguide section, the effect of  $p$  and  $d$  parameter is studied. These parameters can be determined according to equations (3.20 and 3.21) [51], [52]. To make it more comprehensible the analysis, conductor and dielectric losses are neglected, only the loss comes from radiation. In order to minimize the leakage losses or signal return can be used metal vias, the diameter of via should be within the permissible limits of geometric according to the following equations [53].

$$d < \frac{\lambda}{5} \quad \dots (3.20)$$

$$p \leq 2d \quad \dots (3.21)$$

Where:

$d$ : diameter of hole or via

$p$ : pitch or distance between two holes

$\lambda$ : operating wavelength.

The similarity between rectangular waveguide and Substrate Integrate Waveguide SIW can produce empirical relations; these relations have been obtained due to the effective widths of rectangular waveguide  $w_{eff}$  and geometrical dimensions of the SIW with safety of the same propagation characteristics [54].

$$w_{eff} = w - \frac{d^2}{0.95p} \quad \dots (3.22)$$

Where  $d$  is the diameter of the metal vias,  $p$  is longitudinal spacing and  $w$  represents transverse spacing as shown in Fig.3.11 [55].

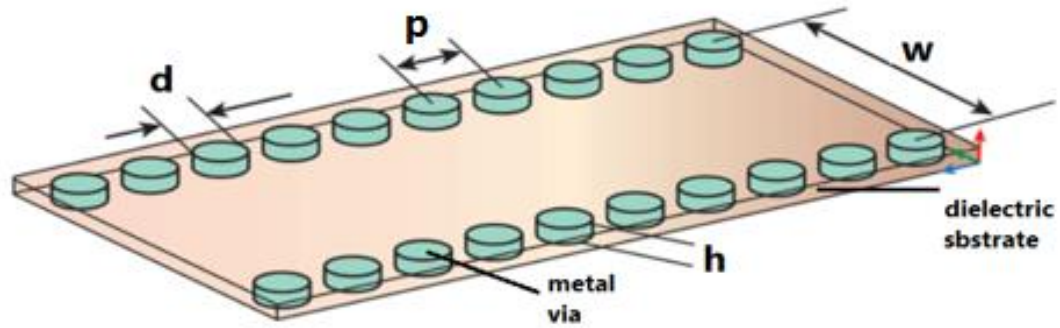


Fig 3.11: Geometric of SIW

This relation can be defined in another form [56] in the following equation:

$$w_{eff} = w - 1.08 \frac{d^2}{p} + 0.1 \frac{d^2}{w} \quad \dots (3.23)$$

### 3.6.1 Parametric study of C-GHNA design

In this section study effect characteristics of proposed design when selected different values of radius of via.

#### 3.6.1.1 The effect various of radius of via (r)

The radius of via or hole (r) value is selected. Three readings are taken to explain results of the proposed antenna, as shown in Table 3.7. The radius of via is taken three different values 25nm, 35nm and 45nm. It is the good impedance matching at 45 nm. Comparison of reflection coefficient at different frequencies as shown in Fig 3.12.

Table 3.7: Comparison proposed module for different the radius of via

Radius of via	$S_{11}$ (dB)	Frequency resonant (THz)	Efficiency (%)	Gain (dB)
r=25nm	-18.11	215.92	87	9.93
	-18.25	249.35	86	9.83
	-17.99	287.54	86.7	11.1
r=35nm	-19.4	218.29	87	9.93
	-20.17	248.2	85.7	9.95
	-20.73	272.53	85.8	10.3
r=45nm (proposed)	-23.58	239.45	86.8	10.6
	-23.89	263.65	85	9.29
	-23.96	289.22	87	11.2

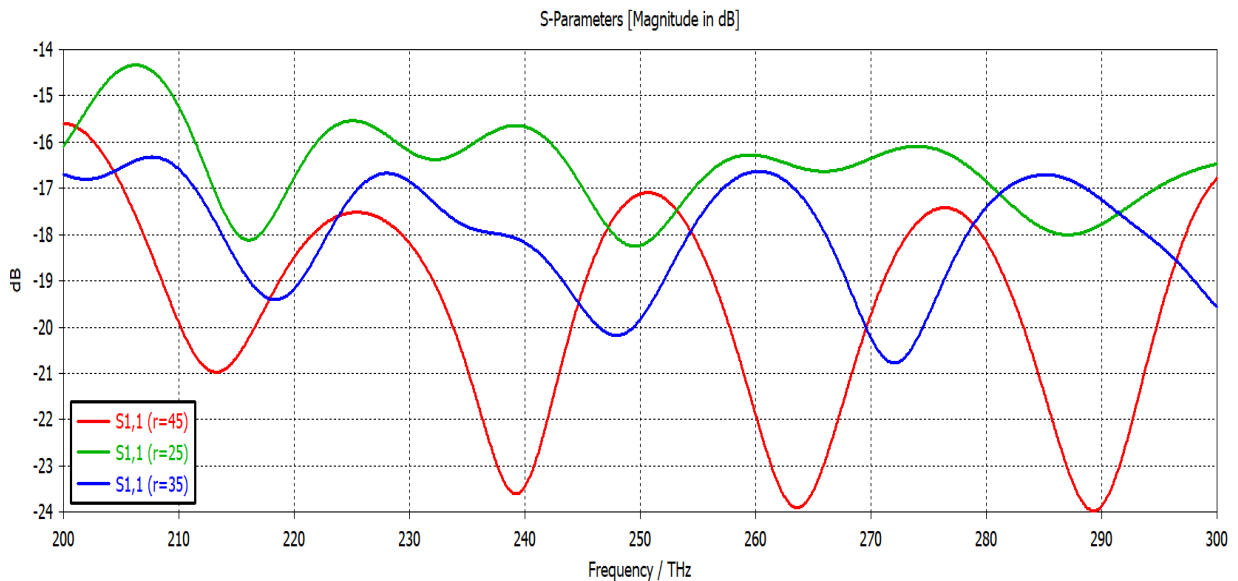


Fig 3.12: Simulate reflection coefficient at different radius of via (r)

### 3.7 The fourth proposed model: Substrate Integrate Waveguide Horn Nanoantenna (SIW-HNA)

A new technique which is called substrate integrate waveguide (SIW) is used in fourth design of horn nanoantenna in this thesis. This technique represents the performance of fundamental metallic waveguide, and is fabricated by using two layers of metal; one at the top and the other is below. Two rows of vias are located at the sidewalls to achieve compact size and low weight waveguide antenna as an alternative to conventional metallic waveguide. The proposed design SIW-HNA consists of two metallic layer representing transmission line excited by waveguide ports and progressively the impedance matching of the waveguide to one free-space. The thickness of gold 50nm inserting between the two gold layers dielectric layer of Rogers RT5880 thickness of it is 800nm, permittivity  $\epsilon_r = 2.2$  and loss tangent  $\delta = 0.0009$  as shown in Fig 3.13.

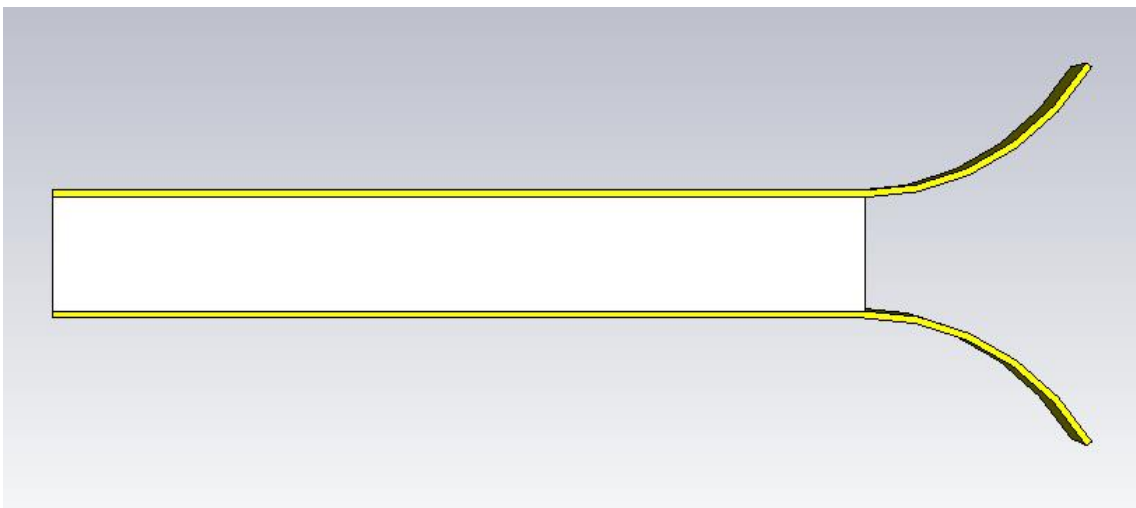
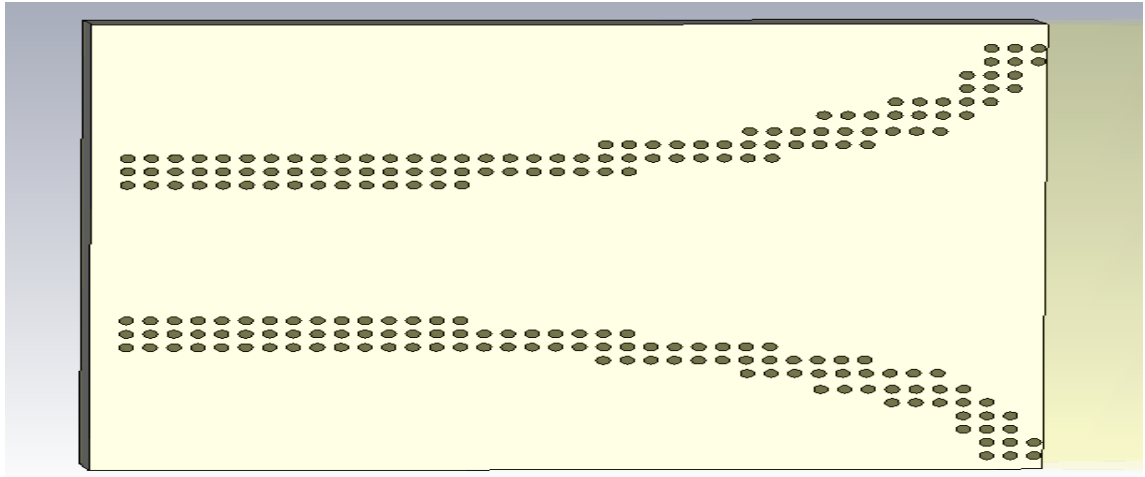


Fig: 3.13: SIW-NHA two gold and Rogers RT5880

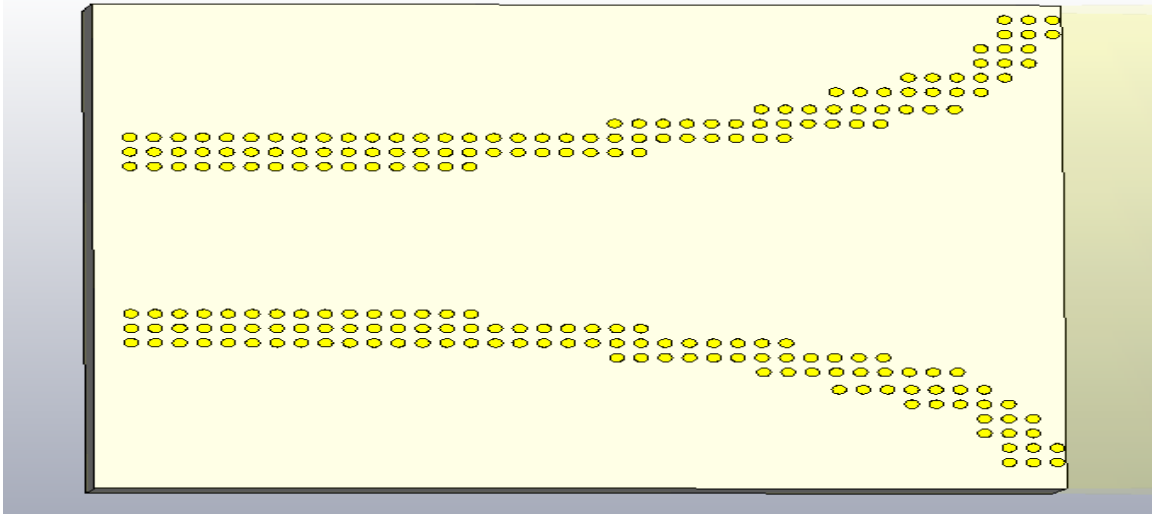
Table 3.8 illustrates the dimension of the proposed antenna. In the substrate layer is done holes in the form of specific geometrical shape. These holes are filled with a conductive material called vias, preferably from the same type of layers to obtain a more matching as shown in Fig 3.14 a, b.

Table 3.8: The dimension of SIW-HNA

No.	parameters	symbols	amounts
1	Length waveguide	$\ell_{wg}$	4000 nm
2	Length horn	$\ell_{horn}$	2000 nm
3	Width of waveguide	$w_{wg}$	2500 nm
4	Height	$h$	1500 nm
5	Thickness of gold	$d_{Au}$	50 nm
6	Thickness of substrate	$ts$	800 nm
7	The radius of curvature	$r_f$	1500 nm
8	Angle of flare	$\alpha$	45°
9	Diameter of cylindrical via	d	45 nm
10	Pitch	p	60 nm



(a)



(b)

Fig 3.14: Geometric lattice of via through dielectric material

(a) The holes are worked dielectric material

(b) The vias are used to fill holes

### 3.7.1 Parametric study of the proposed antenna design

The study parameter for different thickness of dielectric to note affect with respect reflection coefficient.

### 3.7.1.1 The effect various of dielectric thickness ( $ts$ )

Thickness of dielectric material is investigated by selecting three values. It is obvious that at the thickness 800nm the reflection coefficient  $S_{11}$  has the best value equal to -44.37dB, -42.4dB, -29.63dB, -27.09dB at the resonant frequency of (203.61, 234.7, 250 and 282.68) THz and bandwidth equal 100 THz. In addition, a comparison of various thickness of dielectric is shown in Fig 3.15 to identify the reflection coefficient characteristic.

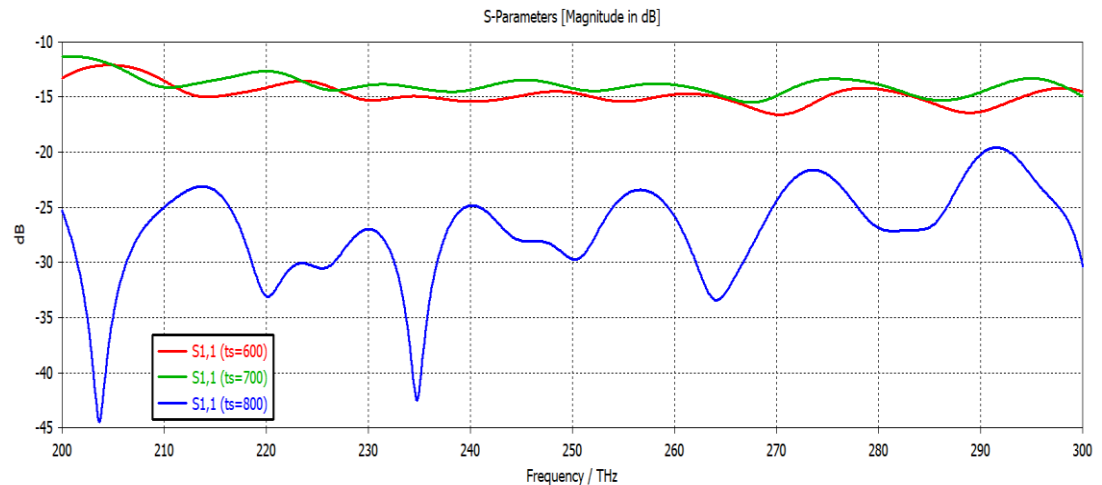


Fig: 3.15: Simulated reflection coefficient for various thickness of dielectric

We conclude from the study parameter for various thickness of dielectric, when the thickness of the material changes 600 and 700 there isn't resonant frequency but when changed the thickness 800 note to give wide band of frequencies.

# **CHAPTER FOUR**

## **RESULT AND DICCUSSION**

### **4.1 Introduction**

This chapter presents the calculated characteristics of the four proposed horn nanoantennas, which include reflection coefficient  $S_{11}$ , VSWR, 2D radiation pattern, 3D directivity, 3D gain, radiation efficiency, bandwidth and current distribution. A comparison of all proposed horn nanoantennas in terms of reflection coefficient  $S_{11}$ , resonant frequencies, impedance bandwidth, radiation efficiency, gain, directivity and their applications are presented.

### **4.2 Characteristic of Simple Horn Nanoantenna (SHNA)**

The simulation results of the first proposed antenna for various parameters are dealt with presented in the following sub sections:

#### **4.2.1 Reflection coefficient ( $S_{11}$ )**

The relationship between the reflection coefficient wave  $S_{11}$  to frequency in Terahertz of the first proposed antenna SHNA is shown in Fig 4.1. Simple horn nanoantenna resonates at 32.9THz, 53.49THz and 71.32THz with reflection coefficient values of  $-22.28$  dB,  $-41.09$  dB and  $-24.27$ dB respectively.

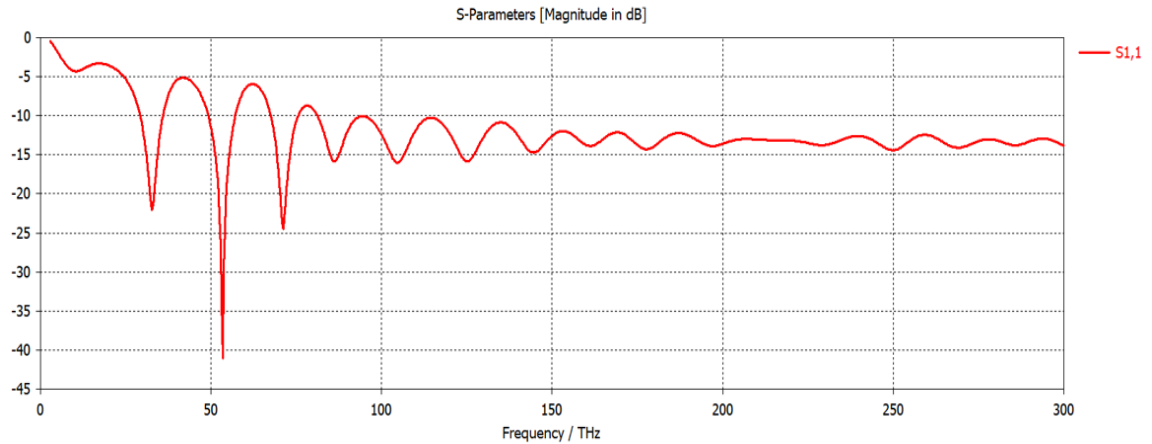


Fig 4.1: Simulated reflection coefficient of the SHNA

### 4.2.2 VSWR

The VSWR wave of the proposed antenna with respect to frequency (THz) is shown in Fig 4.2. It has an acceptable value according to standard value less than 2 at resonant frequencies 32.9 THz, 53.49 THz and 71.32 THz according to the value of reflection as shown in the previous chapter.

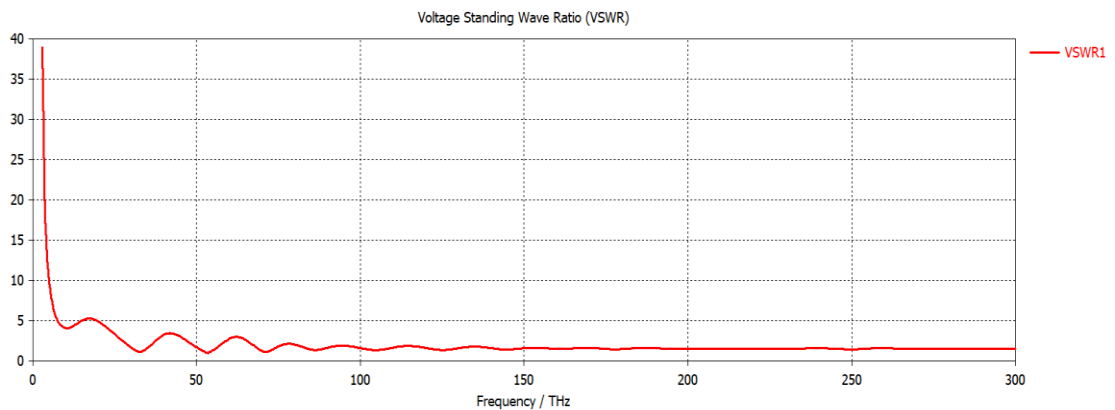
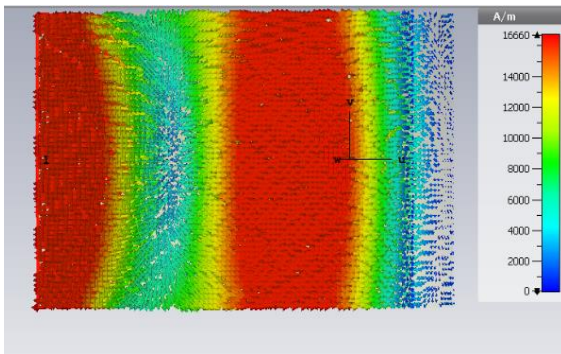


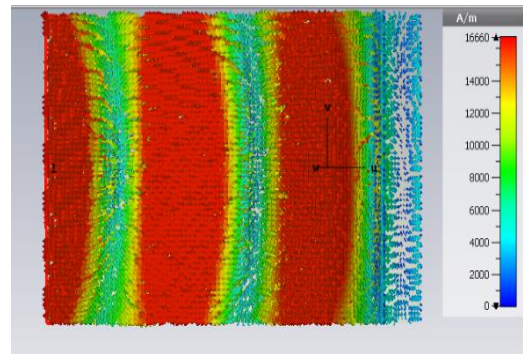
Fig 4.2: Simulated VSWR of SHNA

### 4.2.3 Current distribution

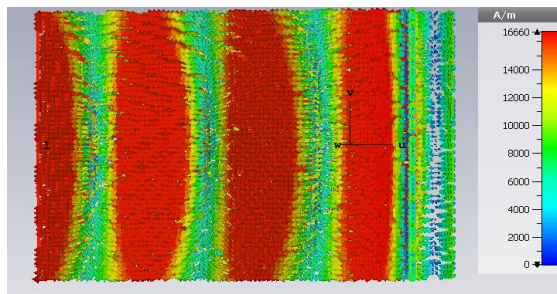
The simulated current density generation for the first proposed design at different resonant frequencies is shown in the Fig 4.3, where Fig 4.3 (a) illustrates the current distribution at first resonant frequency 32.9 THz. It is obvious that most of the current concentration are in two regions only of the waveguide of horn antenna. Figure 4.3(b) shows the current distribution at the second resonant frequency 53.49 THz. The current distribution increases in the largest region; it operates about three zones. However, the third resonant frequency 71.32 THz shows the current density distributed along path of waveguide of horn antenna.



(a)



(b)



(c)

Fig 4.3: Simulated current distributions of proposed horn antenna (a) the current distribution at 32.9THz (b) the current distribution at 53.49THz (c) the current distribution at 71.32THz.

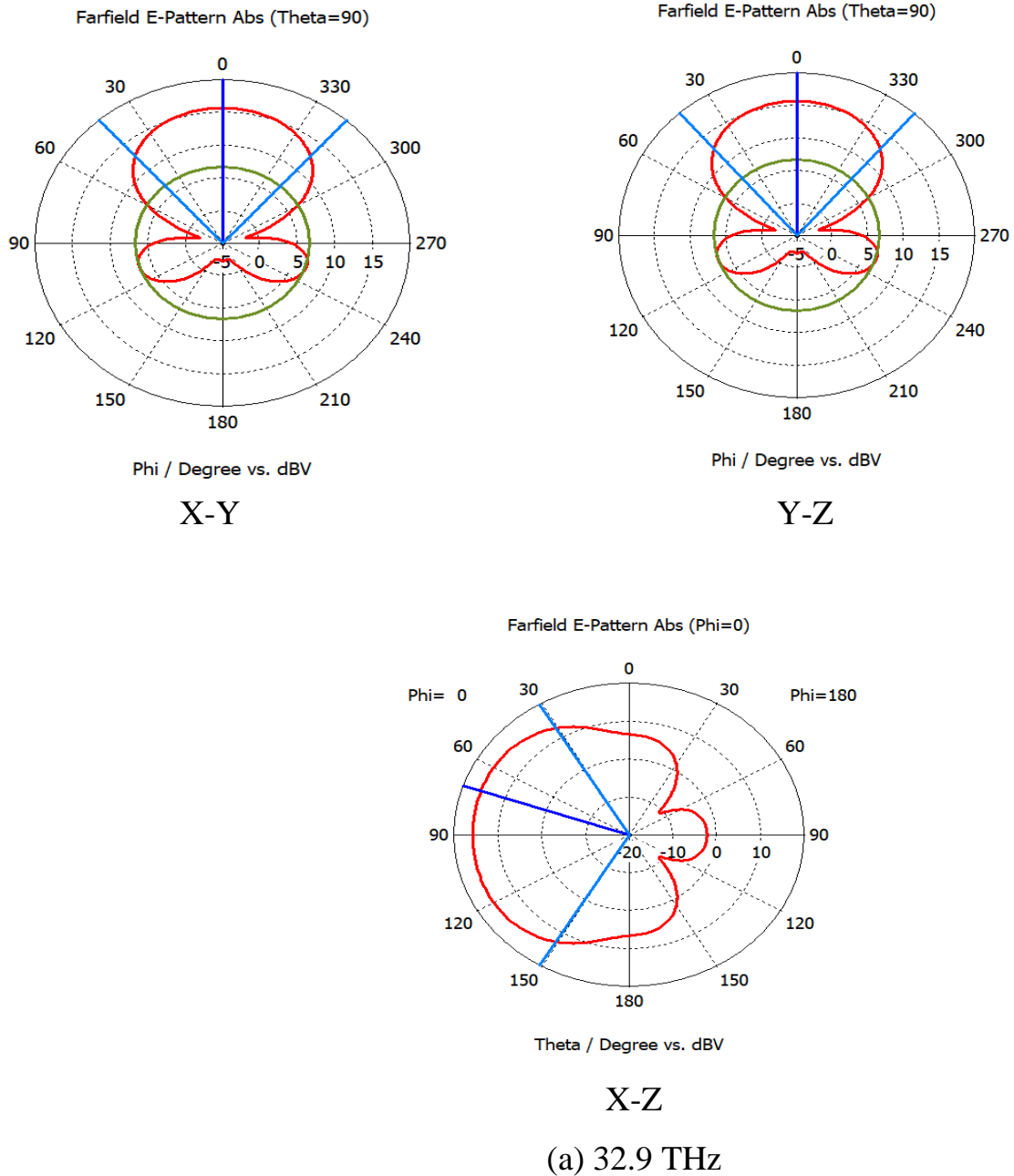
#### 4.2.4 Radiation Pattern

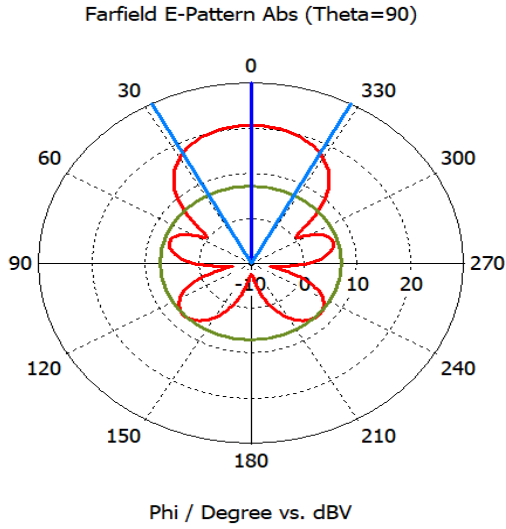
The characteristic of far-field radiation pattern of the proposed horn nanoantenna is shown in Table 4.1.

Table 4.1: The characteristic of far-field radiation pattern of SHNA

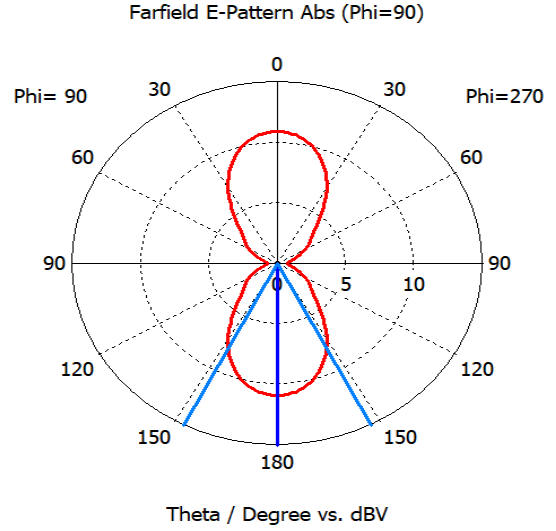
Frequency (THz)	Parameter	x-y plane $\theta=90$	y- z plane $\Phi=90$	x-z plane $\Phi=0$
32.9	Main lobe magnitude(dB)	15.7dB	6.51dB	15.7dB
	Main lobe direction	0°	0°	71°
	Angular width (3dB)	82.4°	72.7°	118.2°
	Side lobe level (dB)	-9dB	-2.3dB	-
53.49	Main lobe magnitude(dB)	20.6dB	10.9	20.6dB
	Main lobe direction	0°	180°	99°
	Angular width (3dB)	55.8°	54.1°	98.9°
	Side lobe level (dB)	-13.8dB	-	-
71.32	Main lobe magnitude(dB)	24.5dB	11.5dB	24.5dB
	Main lobe direction	0°	180°	90°
	Angular width (3dB)	40.7°	41.8°	75.4°
	Side lobe level (dB)	-18dB	-25.6dB	-12.5dB

The simulated far- field radiation patterns for the total electric field in the x-y plane ( $\theta=90$ ), the x-z plane ( $\Phi=0$ ), and the y-z plane ( $\Phi=90$ ) at frequencies of the three resonant bands of proposed nanoantenna are shown in Fig 4.4.

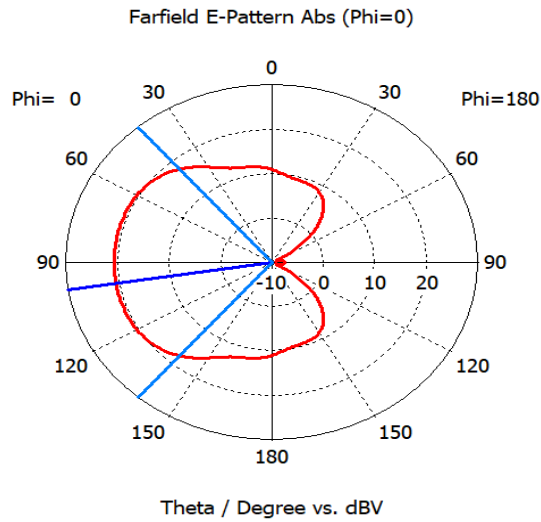




**X-Y**

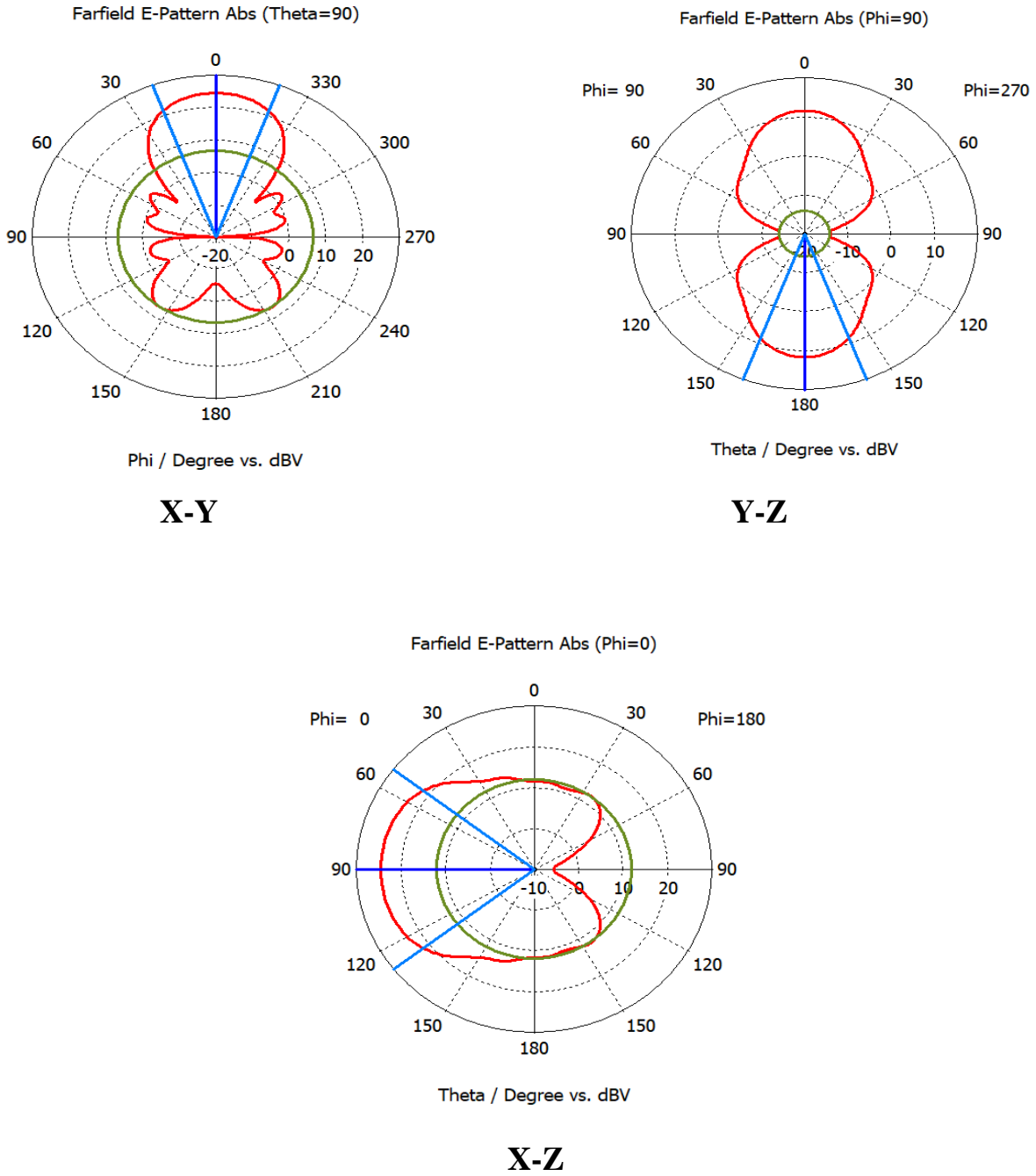


**Y-Z**



**X-Z**

(b) 53.49 THz

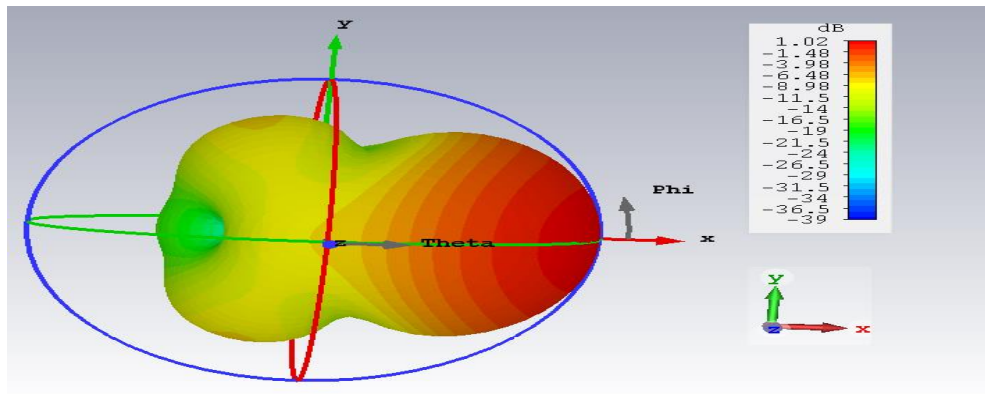


(c) 71.32 THz

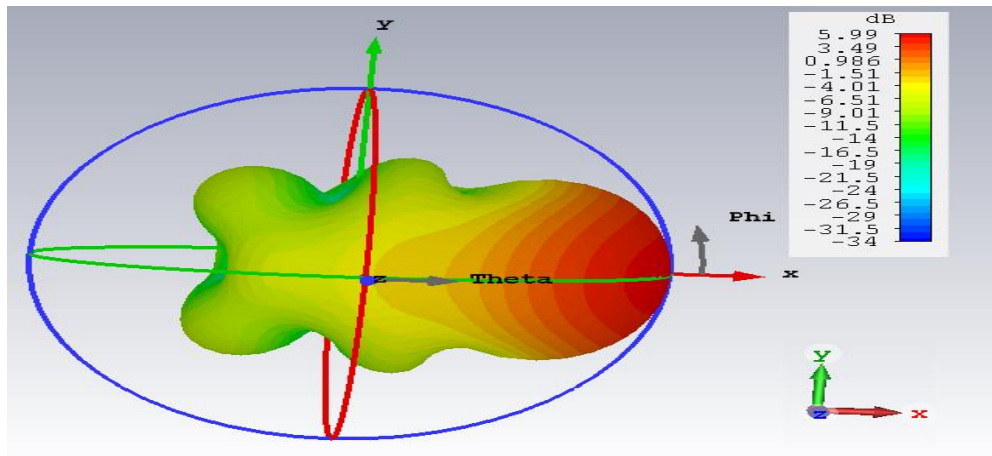
Fig 4.4: Far-field radiation patterns for the total electric field of simple horn nanoantenna

### 4.2.5 3D Gain

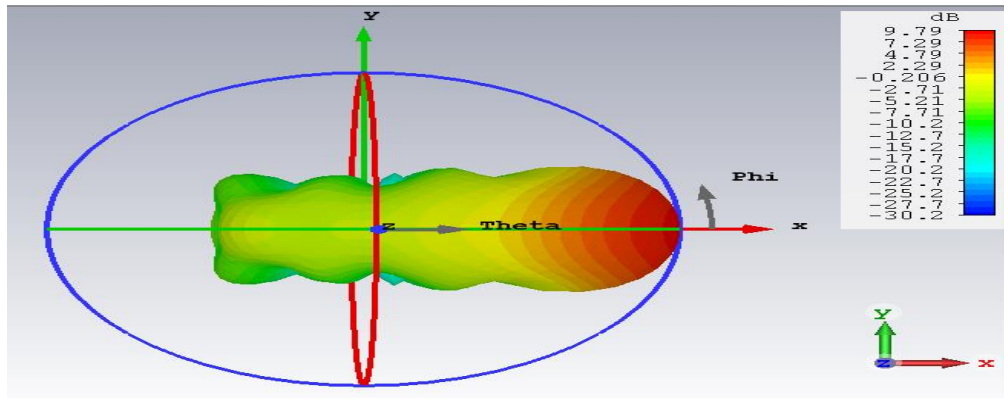
The simulated 3D far-field gain of simple horn nanoantenna for three resonant frequencies are as follow: the gain at the first frequency 32.9THz is 1.02dB the second frequency 53.49 THz has gain 5.99dB and the last frequency 71.32 THz has gain 9.79dB. Note that gain increases with the increasing frequency value as shown in Fig 4.5.



(a) Gain at 32.9THz



(b) Gain at 53.49THz

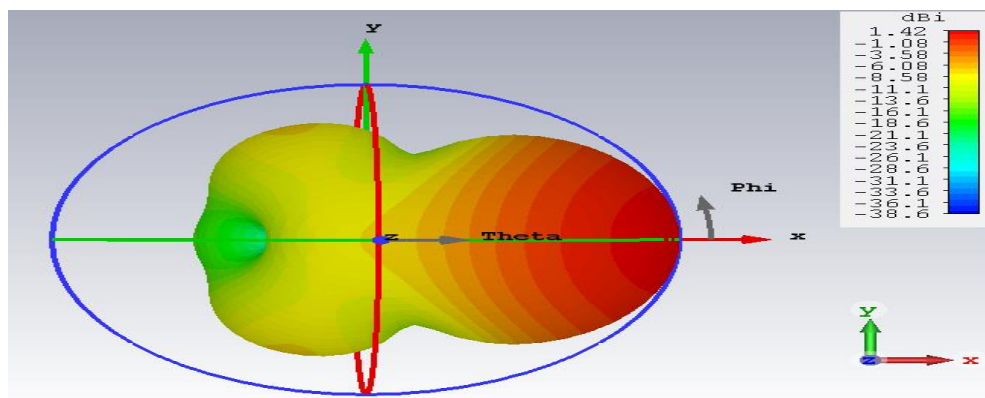


(c) Gain at 71.32THz

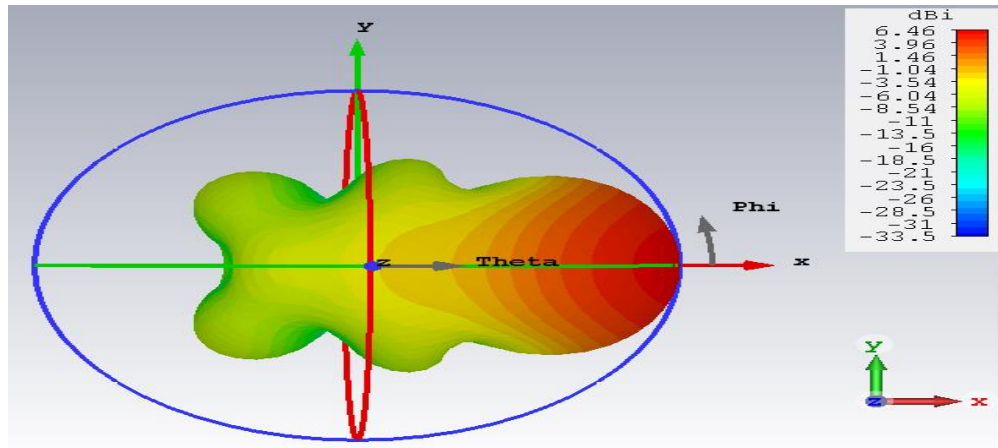
Fig 4.5: Simulated 3D far-field gain patterns for SHNA

#### 4.2.6 3D Directivity

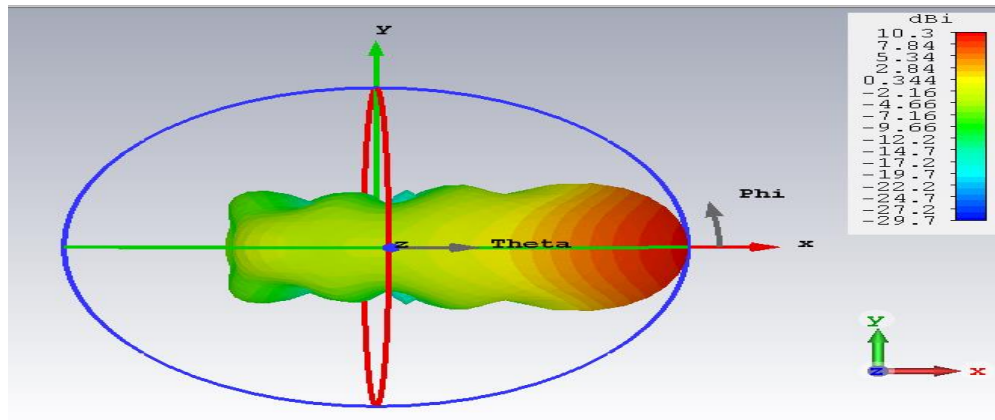
The simulated 3D far filed radiation pattern directivity of simple horn nanoantenna design at three resonant frequencies 32.9THz has directivity 1.42dB, increases at second frequency 53.49THz is 6.46dB and directivity 10.3 at the last resonant frequency 71.32THz, as shown in Fig 4.6. It is clear that the directivity is increased with the increase of the value of frequency.



(a) Directivity at 32.9THz



(b) Directivity at 5.49THz



(c) Directivity at 71.32THz

Fig 4.6: Simulated 3D far-field directivity pattern of SHNA

#### 4.2.7 Efficiency and bandwidth

From the directivity and gain values, we can calculate the radiation efficiency and bandwidth of SHNA according to equation (3.18, 3. 20)

In the Table4.2 below is demonstrated the efficiency at three resonant frequencies as well as the bandwidth of the proposed design.

Table 4.2: The efficiency and bandwidth for SHNA

Frequency THz	32.9	53.49	71.32
Efficiency %	72	93	95
Bandwidth THz	6.78	7.77	8.38

### 4.3 Characteristic of Gold – Silicon Horn Nanoantenna(G-SHNA)

The simulation results for important parameters of the second proposed antennas, which have gold-silicon vias horn nanoantenna, are presented and discussed in the following sections.

#### 4.3.1 Reflection coefficient ( $S_{11}$ )

The reflection coefficient wave of the second proposed antenna (G-SHNA) is illustrated in Fig 4.7. Simulation results reveal that the antenna demon started a wideband behavior with resonant frequency at about 276.47 THz, 298.21THz and 230.98THz with reflection coefficient -25.48 dB, -32.29 dB and -26.09 dB respectively.

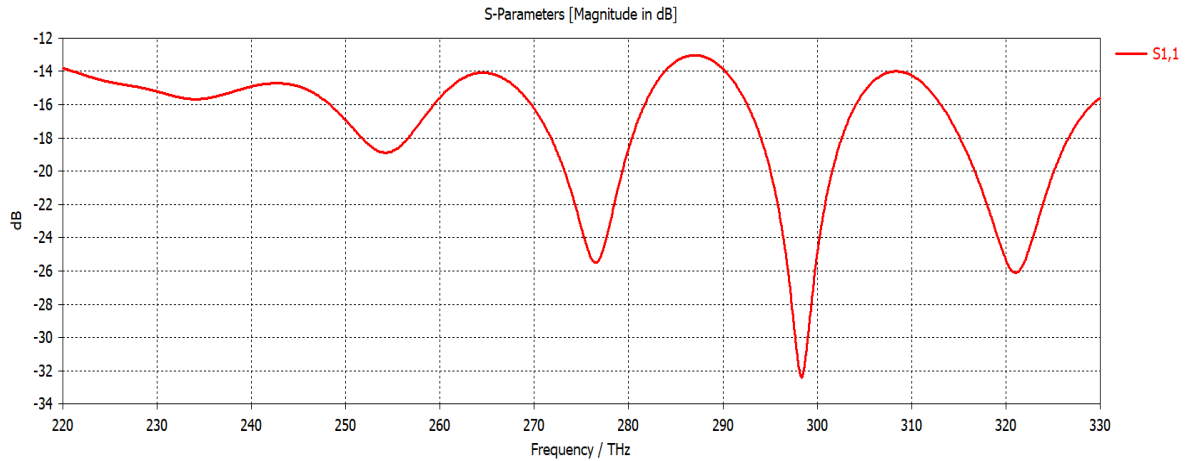


Fig 4.7: The simulated reflection coefficient  $S_{11}$  of G-SHNA

### 4.3.2 VSWR

The VSWR of the proposed model G-SHNA is shown in Fig 4.8. It has value at three resonant frequencies 276.47 THz, 298.21 THz and 320.98 THz located below standard value of VSWR 2 ( $VSWR < 2$ ).

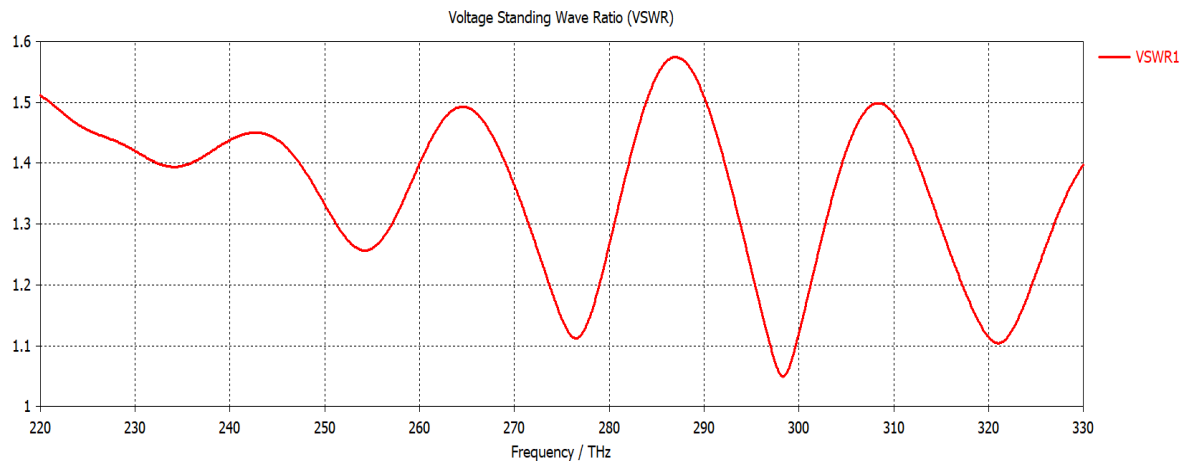
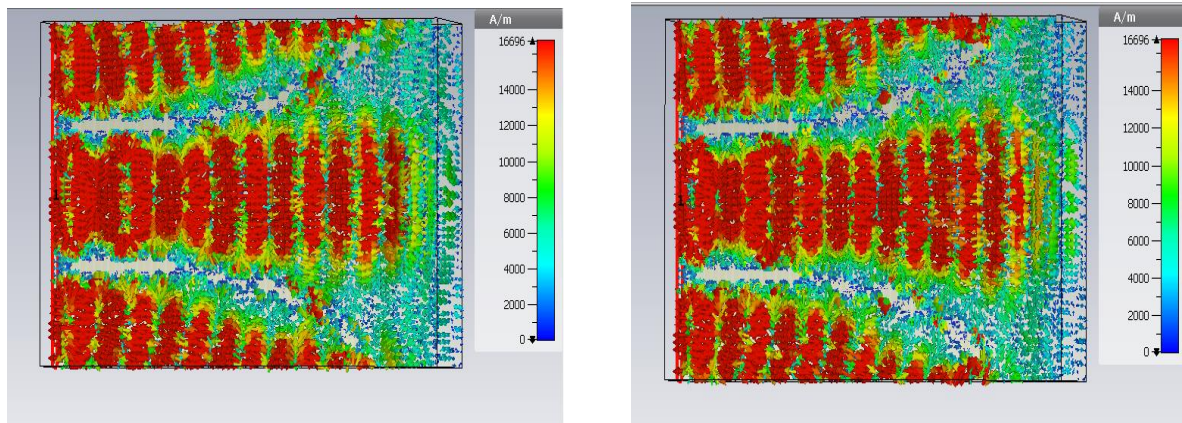


Fig 4.8: The simulated results of VSWR for G-SHNA

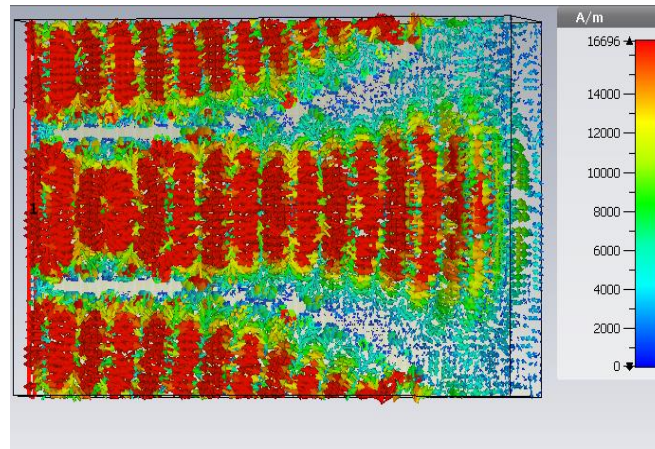
### 4.3.3 Current distribution

The current distribution simulation of the nanoantenna for different resonant frequencies is shown in Fig 4.9. Where Fig 4.9 (a) illustrates the current distribution at 276.47THz, which indicates the current concentration, is along the transmission line and arrived to the end of nanoantenna. Also, Fig 4.9 (b) illustrates the current distribution at 298.21THz which indicates the concentration of the current from the starting transmission line and extended to the flare end. Finally, Fig 4.9 (c) illustrates the current distribution at the last frequency 320.98 which is concentration the starting waveguide and decreased to zero value at the end but is spreading more widely from other frequencies. The current distributed same along wave guide for three resonant frequencies but different in extreme current at each frequency.



(a)

(b)



(c)

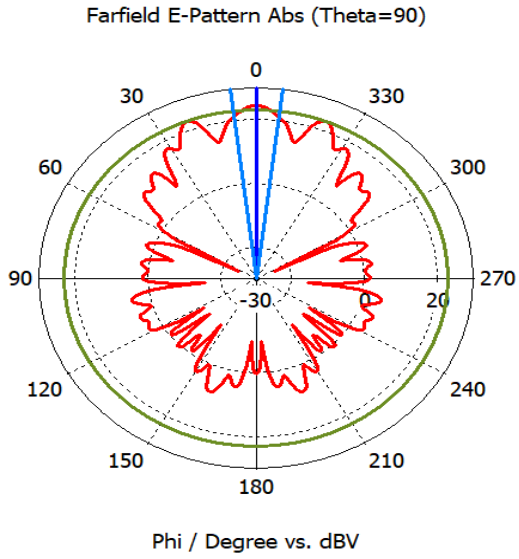
Fig 4.9: The simulated results of current distribution for different resonant frequency of G-SHNA

#### 4.3.4 Radiation pattern

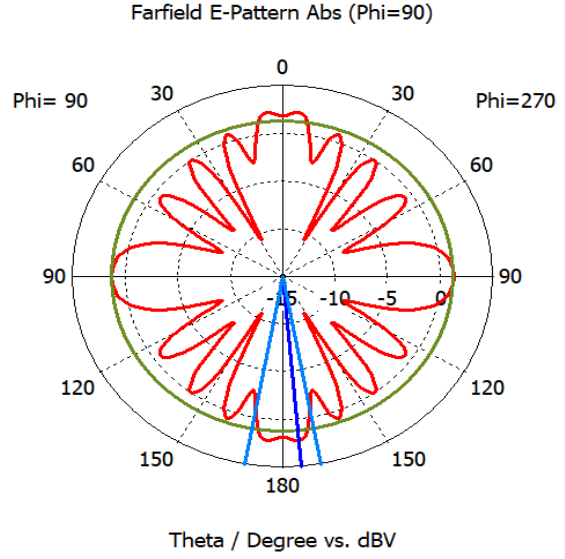
The simulated radiation pattern of the second proposed nanoantenna (G-SHNA) for different resonant frequencies is shown in Fig 4.10. The characteristic far field radiation pattern at 276.49THz, 298.21THz and 320.98THz frequencies is shown in Table 4.3. It is illustrated in x-y plane, x-z plane and y-z plane.

Table4.3: The simulated radiation pattern characteristic for three resonant frequencies of G-SHNA.

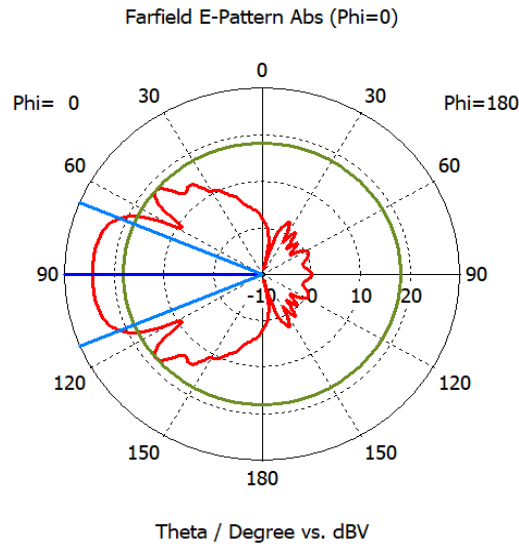
Frequency (THz)	Parameter	x-y plane ( $\theta=90$ )	y-z plane ( $\Phi=90$ )	x-z plane ( $\Phi=0$ )
276.47	Main lobe magnitude(dB)	24.4dB	2.21dB	24.4dB
	Main lobe direction	0°	175°	90°
	Angular width (3dB)	13.7°	21.1°	45°
	Side lobe level (dB)	-1.3dB	-1dB	-6.3dB
298.21	Main lobe magnitude(dB)	24.3dB	1.94dB	24.3dB
	Main lobe direction	0°	0°	90°
	Angular width (3dB)	16.9°	22.9°	42.3°
	Side lobe level (dB)	-2dB	-2.7dB	-7.2dB
320.98	Main lobe magnitude(dB)	24.8dB	3.08dB	24.8dB
	Main lobe direction	0°	0°	90°
	Angular width (3dB)	14.6°	18°	39.3°
	Side lobe level (dB)	-1.7dB	-3.7dB	-9.5dB



X-Y

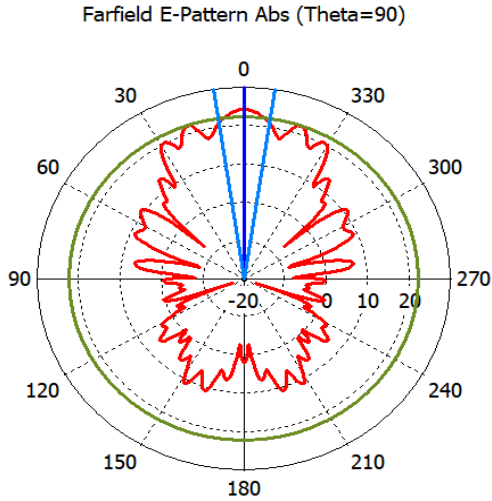


Y-Z



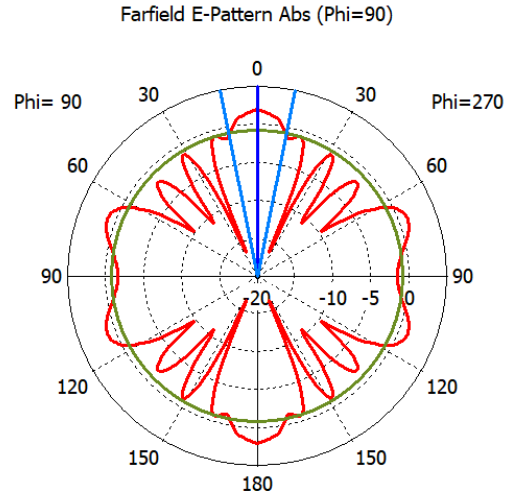
X-Z

(a) at 276.47 THz



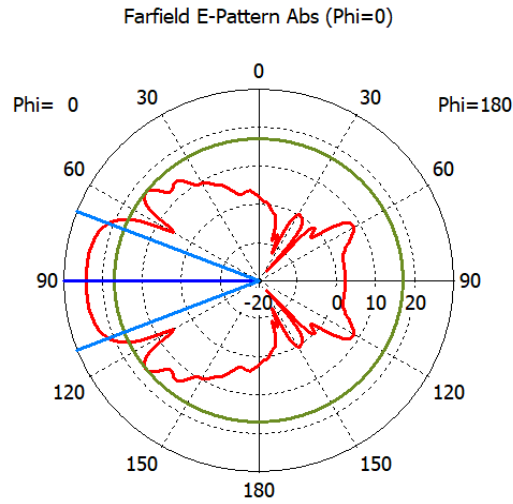
Phi / Degree vs. dBV

X-Y



Theta / Degree vs. dBV

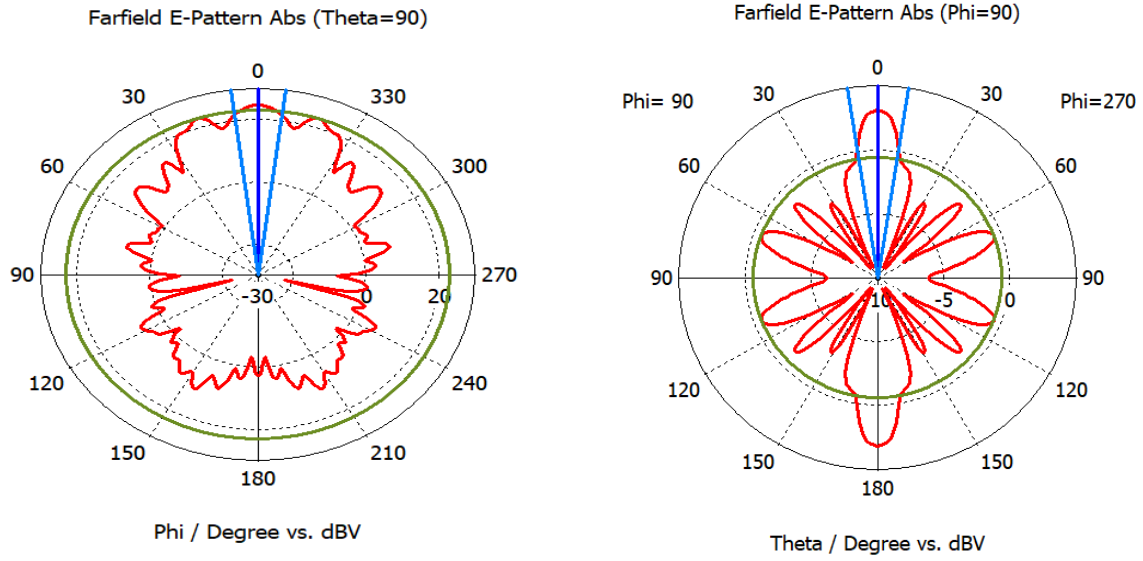
Y-Z



Theta / Degree vs. dBV

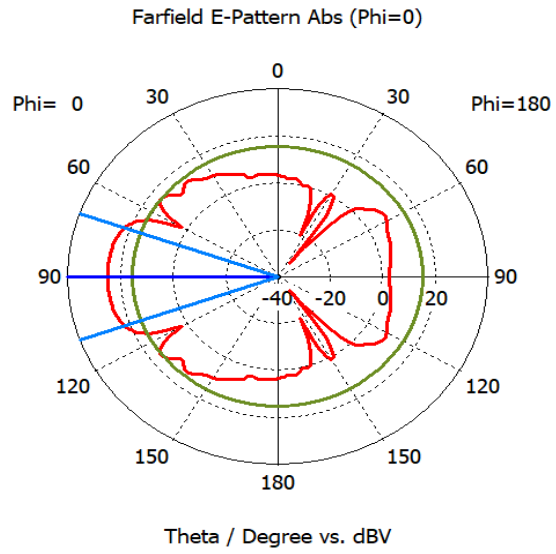
X-Z

(b) at 298.21 THz



X-Y

Y-Z



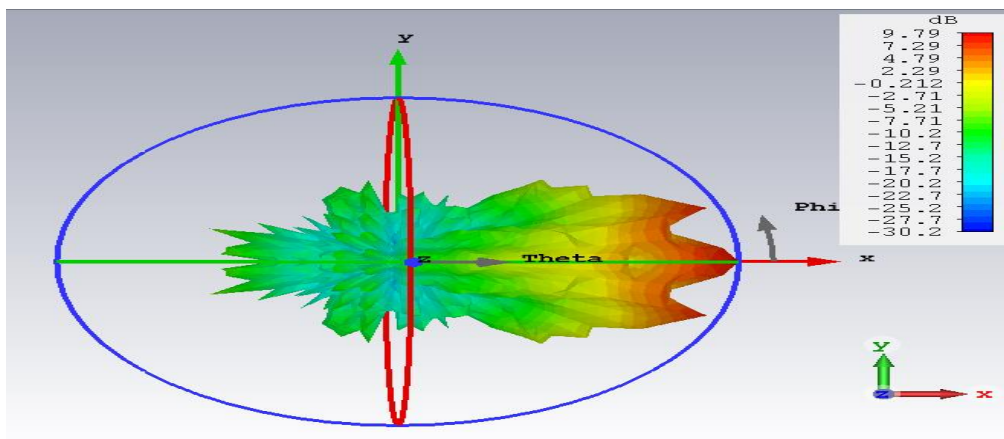
X-Z

(c) at 320.98THz

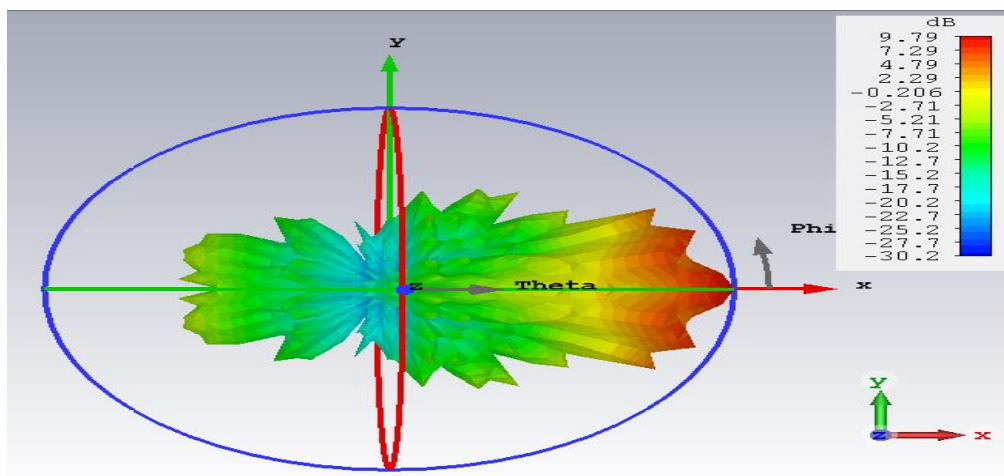
Fig 4.10: The simulated far field radiation pattern of G-SHNA at three resonant frequencies 276.47THz, 298.21THz and 320.98THz.

### 4.3.5 3D Gain

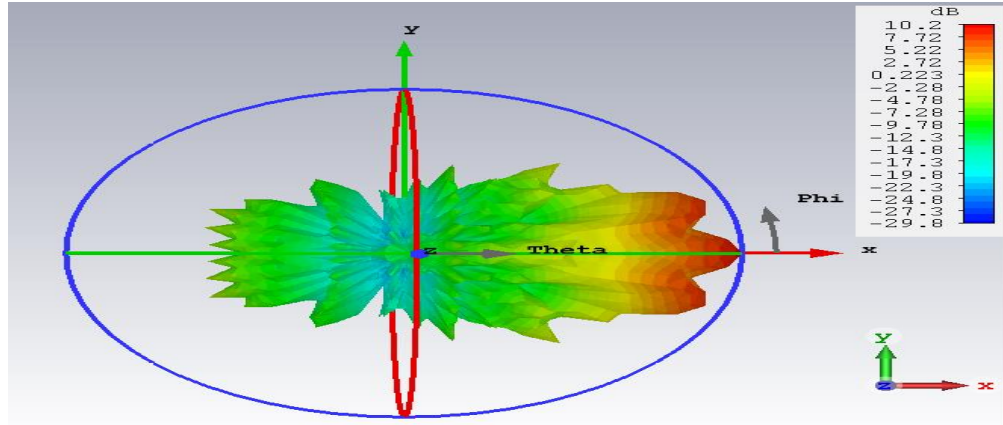
The simulated far field gain pattern is shown in Fig 4.11 for different three resonant frequencies where gain is 9.79dB at 276.47THz, 9.79 dB at 298.21THz and the last value is 10.2dB at 320.98THz. We note that the first and second resonant frequencies of the value of gain is constant but rather increases at last frequency.



(a) Gain at 276.47THz



(b) Gain at 298.21THz

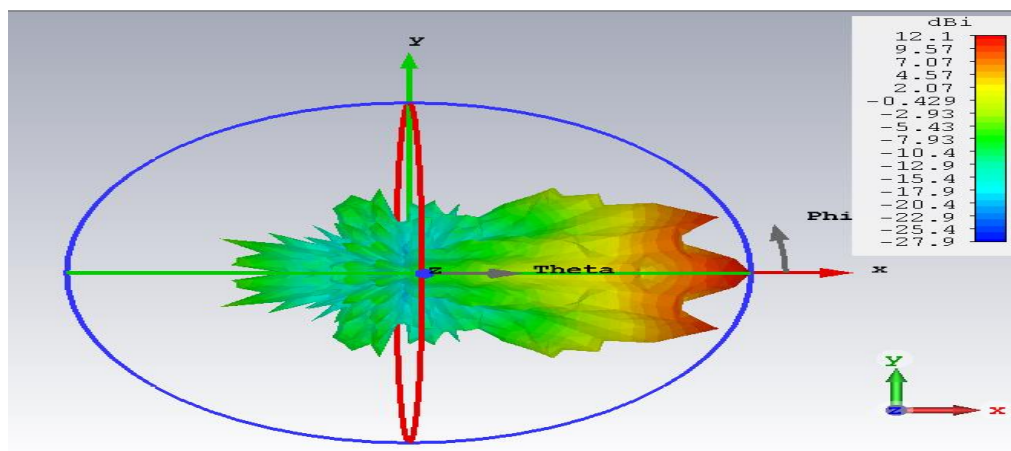


(c) Gain at 320.98THz

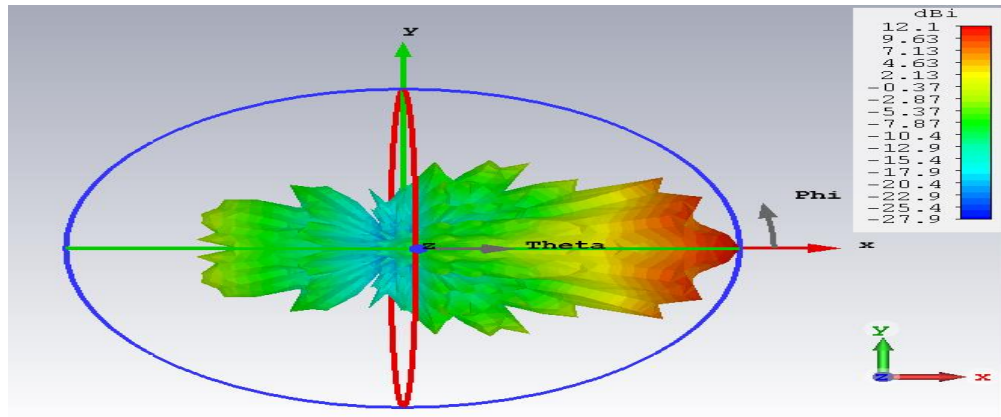
Fig 4.11: The simulated gain for different frequencies

### 4.3.6 3D Directivity

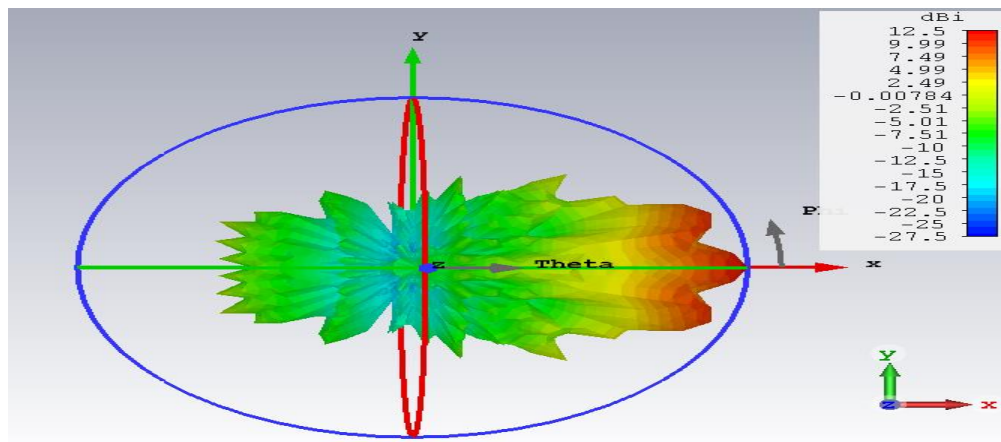
Figure 4.12 shows the simulation of far field directivity pattern at different frequencies of the (G-SHNA). The value of directivity for the first and second resonant frequencies is equal to 12.1dB at 276.47THz and 298.21THz .However, for the last resonant frequency 320.98THz, the directivity value is 12.5dB.



(a) Directivity at 276.47THz



(b) Directivity at 298.21THz



(c) Directivity at 320.98THz

Fig 4.12: The simulated directivity of G-SHNA.

### 4.3.7 Efficiency and bandwidth

Radiation efficiency can be calculated from gain and directivity as illustrated above. Table 4.4 illustrates the efficiency for the second proposed antenna G-SHNA for different frequencies and shows the bandwidth for wide band frequency based on equation (3.18, 3.20)

Table 4.4: The results of efficiency and bandwidth for G-SHNA

Frequency (THz)	276.47	298.21	320.98
Efficiency (%)	81	81	82
Bandwidth (THz)	100		

### 4.3.8 Compression between the first (SHNA) and second (G-SHNA) proposed antenna

The results simulation of two proposed antenna can be compared based on the reflection coefficient  $s_{11}$ , resonant frequencies, gain, directivity, efficiency and bandwidth as shown in Table 4.5.

Table 4.5: The compression between the two proposed antennas

Design	Frequency (THz)	$S_{11}$ (dB)	Gain (dB)	Directivity (dB)	Efficiency (%)	BW (THz)
SHNA	32.49	-22.28	1.02	1.42	72	Multi bands 6.78 7.77 8.38
	53.9	-41.09	5.99	6.46	93	
	71.23	-24.27	9.79	10.3	95	
G-SHNA	276.47	-25.48	9.79	12.1	81	Wide band 100
	298.21	-32.29	9.79	12.1	81	
	320.98	-26.09	10.2	12.5	82	

From the comparison results of the two proposed designs, it is clear that the second proposed antenna is better than the first antenna in terms of gain, directivity and bandwidth because we use vias that reduces the leakage process and locks the signal within the waveguide and high directional signal.

### 4.3.9 The proposed designs validation

Table 4.6: The compression the proposed designs and other references

Design	Frequency (THz)	$S_{11}$ (dB)	Gain (dB)	Directivity y (dB)	Efficiency y (%)	BW (THz)
[32]	185	-18	7.12			85
	200	-34	8.11			
	230	-16	9.31			
[36]	275	-64	-	14.2	66.93	100
SHNA	32.49	-22.28	1.02	1.42	72	Multi bands 6.78 7.77 8.38
	53.9	-41.09	5.99	6.46	93	
	71.23	-24.27	9.79	10.3	95	
G-SHNA	276.47	-25.48	9.79	12.1	81	Wide band 100
	298.21	-32.29	9.79	12.1	81	
	320.98	-26.09	10.2	12.5	82	

## 4.4 Characteristic of Cylindrical-Gold Horn Nanoantenna(C-GHNA)

The simulation results of the third proposed design cylindrical-gold via horn nanoantenna (C-GHNA) are discussed in the following sections:

### 4.4.1 Reflection coefficient $S_{11}$

The simulated results reflection coefficient of C-GHNA are shown in Fig 4.13. It illustrates the resonant frequency at 239.3THz, 263.52THz and 289.32THz with reflection coefficient -23.59dB, -23.89dB and -23.96 dB respectively.

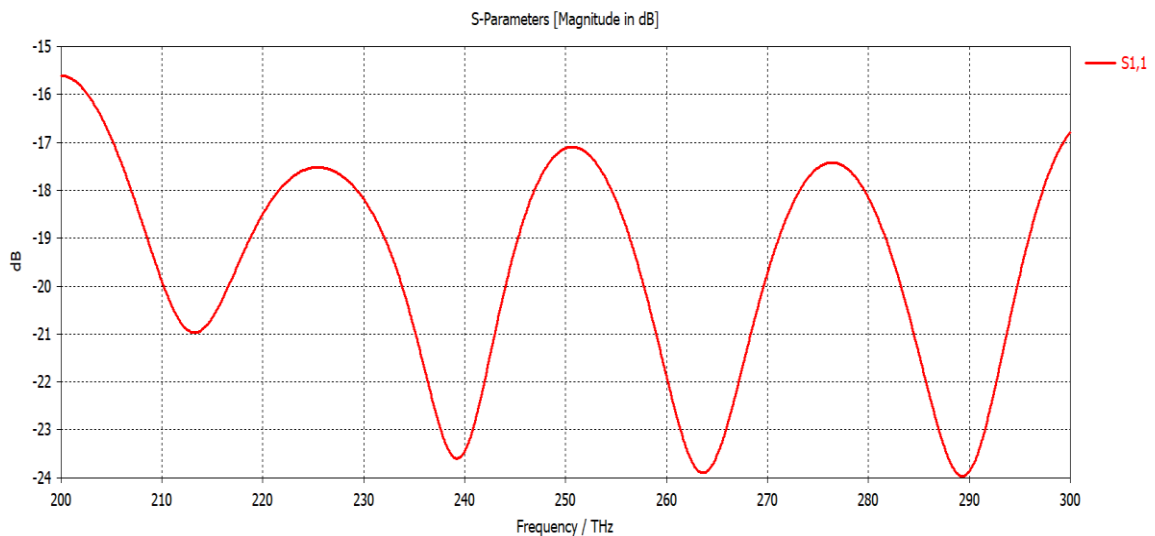


Fig 4.13: The simulation of reflection coefficient of C-GHNA

### 4.4.2 VSWR

The VSWR of the third proposed model C-GHNA is shown in Fig 4.14. It has an appropriate value at three resonant frequencies 239.3 THz, 263.52THz and 289.32 THz located at below 2. Where  $VSWR < 2$  represents the standard value as illustrated in Chapter Three.

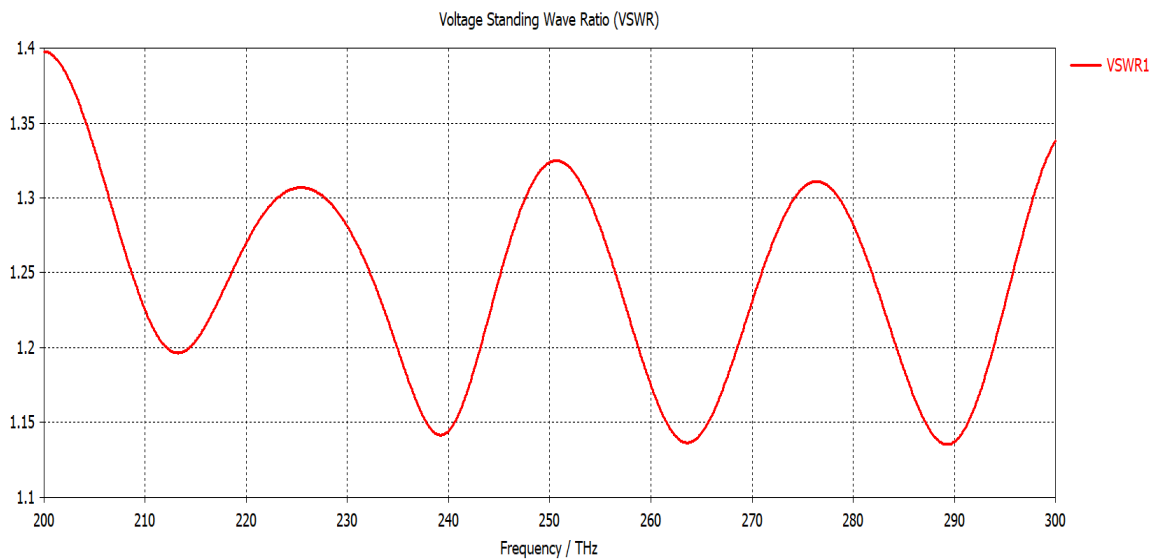
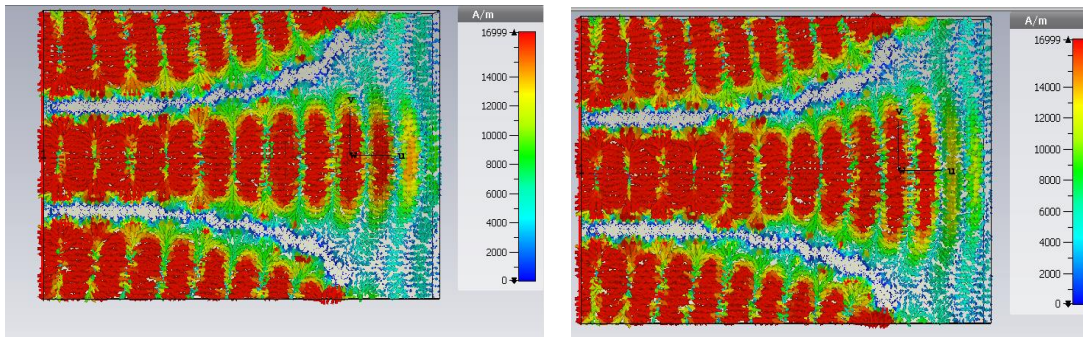


Fig 4.14: VSWR of the proposed model C-GHNA

### 4.4.3 Current distribution

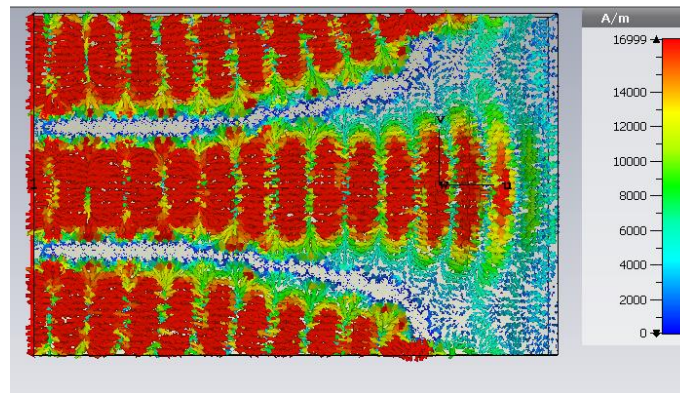
Figure 4.15 shows the simulated results of the current distribution of C-GHNA where Figure (a) shows the current distribution at 239.3THz frequency concentrated inside waveguide and the side of design in narrow shape; Figure (b) at 263.52THz frequency illustrates the current distribution concentrated the starting of waveguide to the

flare end more broadly than other frequencies for the proposed antenna. and Moreover, Figure (c) at 289.32THz shows the current distribution concentrated along the transmission line but less than the second frequency towards the end of the flare.



(a) 239.3THz

(b) 263.52THz



(c) 289.32THz

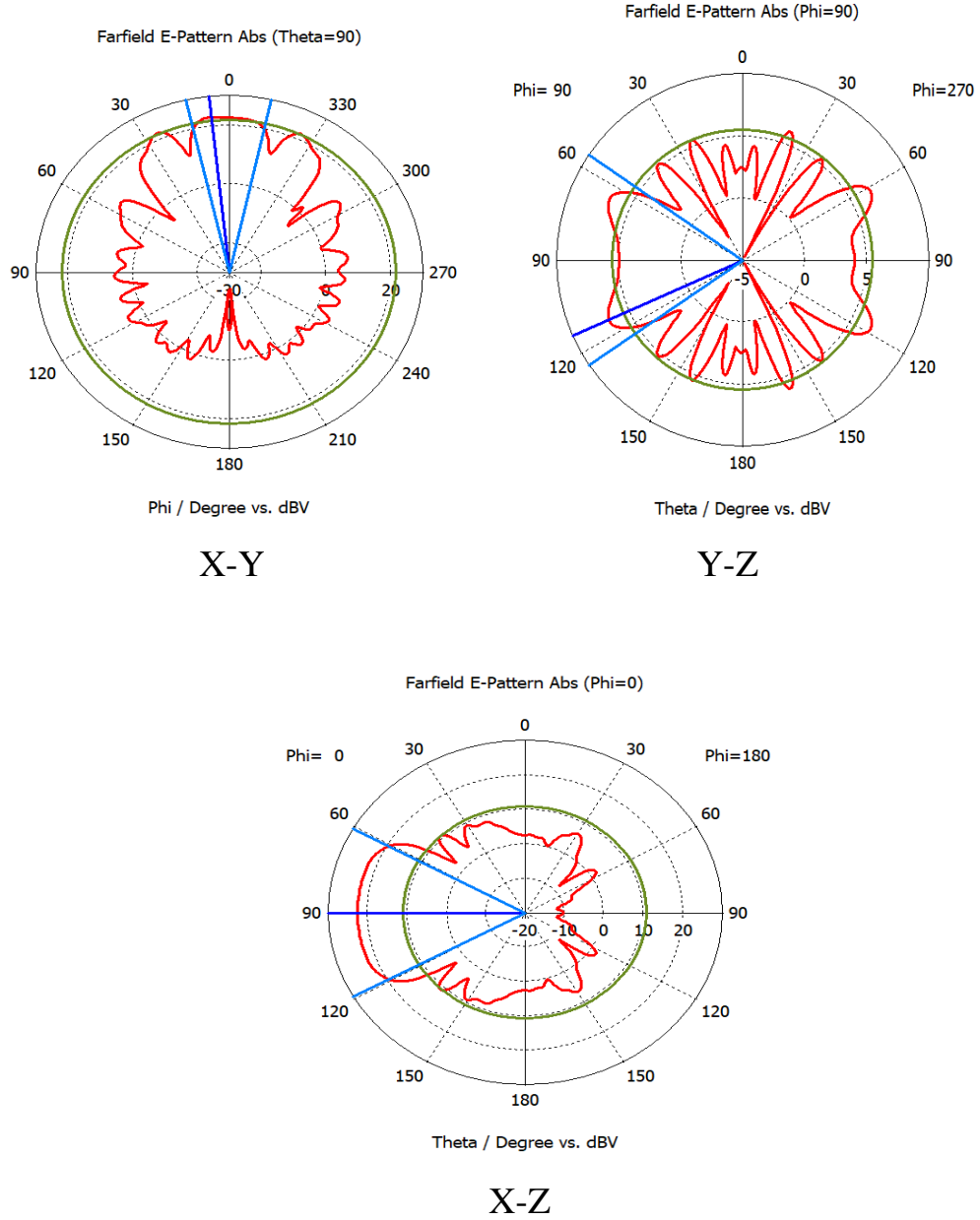
Fig 4.15: The simulated results current distribution for different resonant frequency of C-GHNA

#### 4.4.4 Radiation pattern

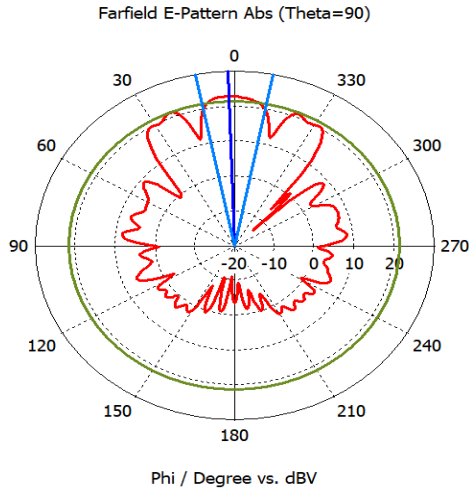
Table 4.7 shows the simulation result of characteristic far field power radiation for different resonant frequencies. Besides Fig 4.16 shows the results of two dimension of radiation pattern for three resonant frequencies 239.3THz, 263.52THz and 289.32THz.

Table 4.7: The characteristic of far field power radiation of C-GHNA

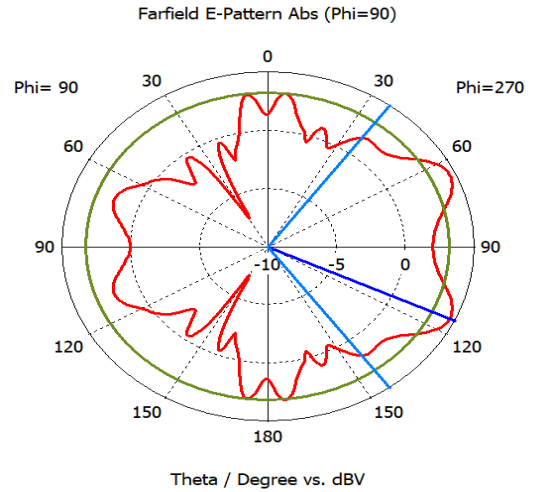
Frequency (THz)	Parameter	x-y plane ( $\theta=90$ )	y- z plane ( $\Phi=90$ )	x-z plane ( $\Phi=0$ )
239.3	Main lobe magnitude(dB)	22.9dB	6.76dB	22.9dB
	Main lobe direction	9°	114°	90°
	Angular width (3dB)	25.4°	68.6°	58.4°
	Side lobe level (dB)	-1.1dB	-1.3dB	-11.5dB
263.52	Main lobe magnitude(dB)	22.8dB	4.56dB	22.9dB
	Main lobe direction	2°	115°	74°
	Angular width (3dB)	22.2°	107.5°	56.7°
	Side lobe level (dB)	-1.4dB	-1.3dB	-11.2dB
289.32	Main lobe magnitude(dB)	23.1dB	5.95dB	23.4dB
	Main lobe direction	2°	110°	74°
	Angular width (3dB)	19.8°	58.7°	52.9°
	Side lobe level (dB)	-1.1dB	-1.5dB	-11.3dB



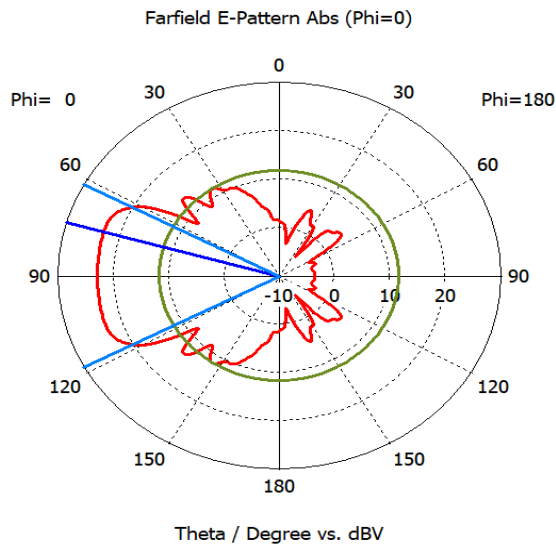
(a) 239.3THz



X-Y

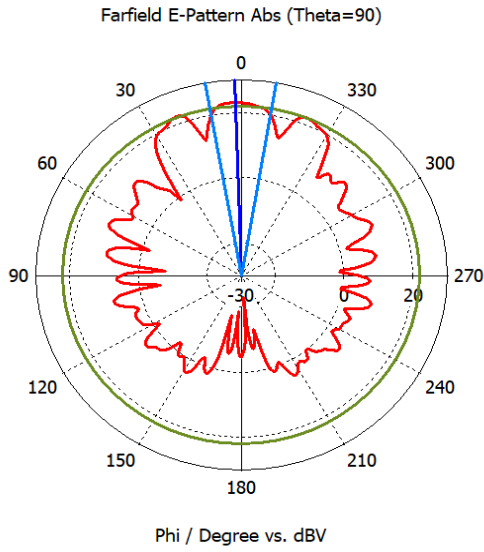


Y-Z

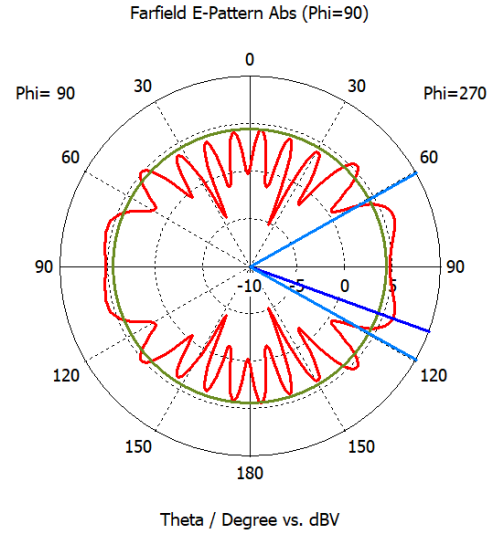


X-Z

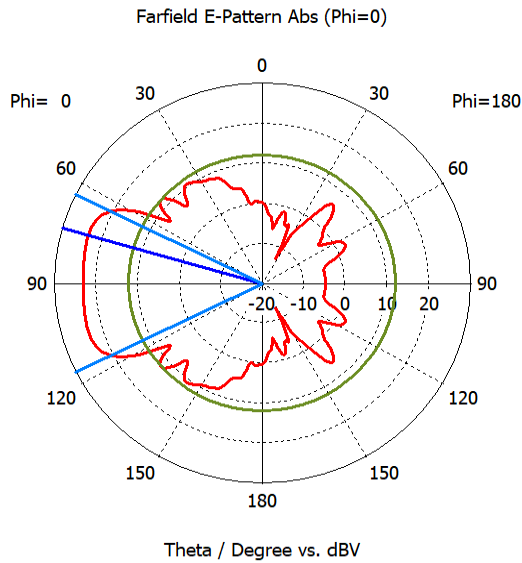
(b) 263.52THz



X-Y



Y-Z



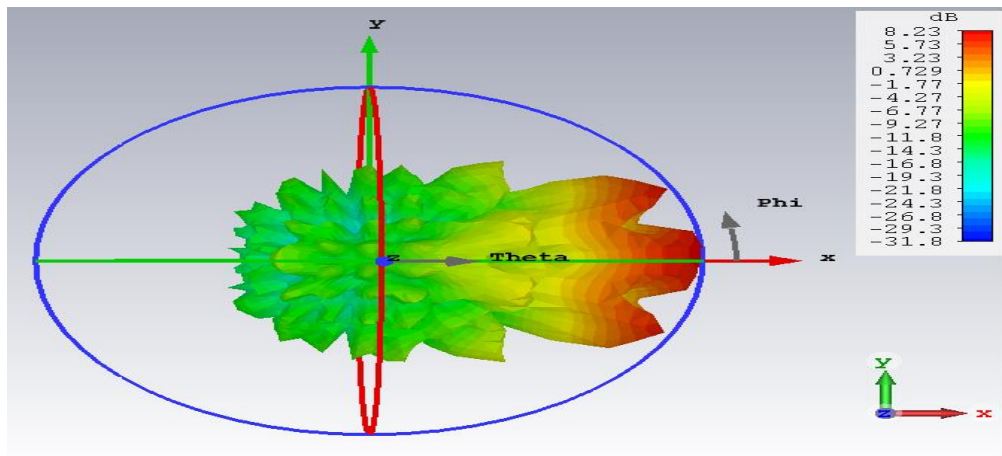
X-Z

(c) 289.32THz

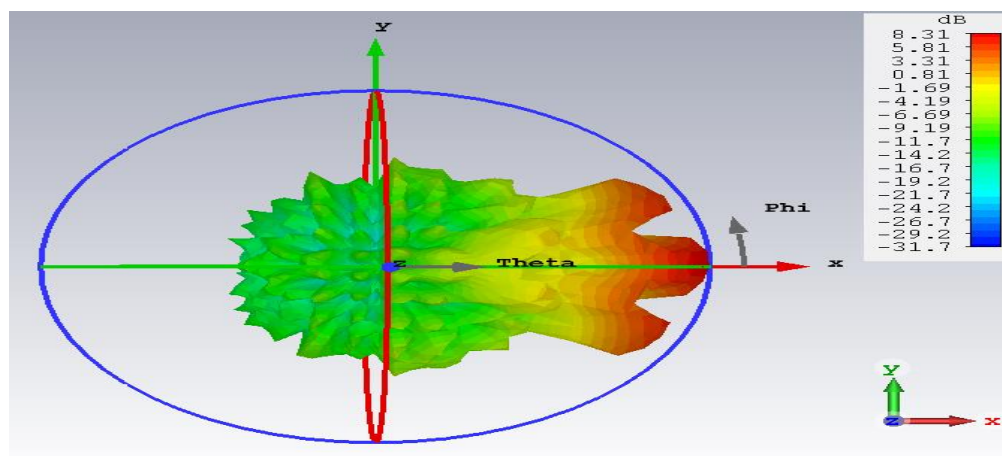
Fig 4.16: The simulated radiation pattern for proposed antenna

### 4.4.5 3D Gain

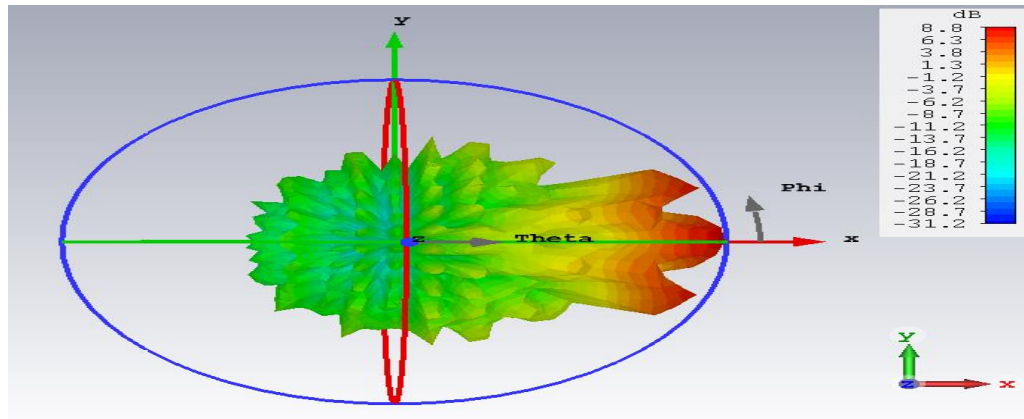
The 3D far field simulated gain is shown in Fig 4.17. The gain value is 8.23 dB at a lower resonant frequency of 239.3THz. The gain is 8.31dB at the second resonant frequency 263.52THz, and 8.8 dB at a higher resonant frequency of 7.9GHz. The value of gain for three resonant frequencies increases with respect of increasing of frequency value.



(a) 239.3THz



(b) 263.52THz

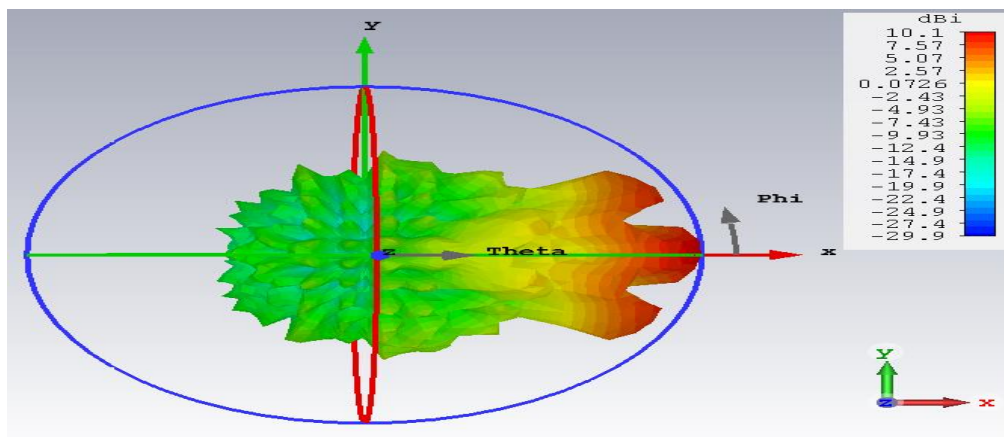


(c) 289.32THz

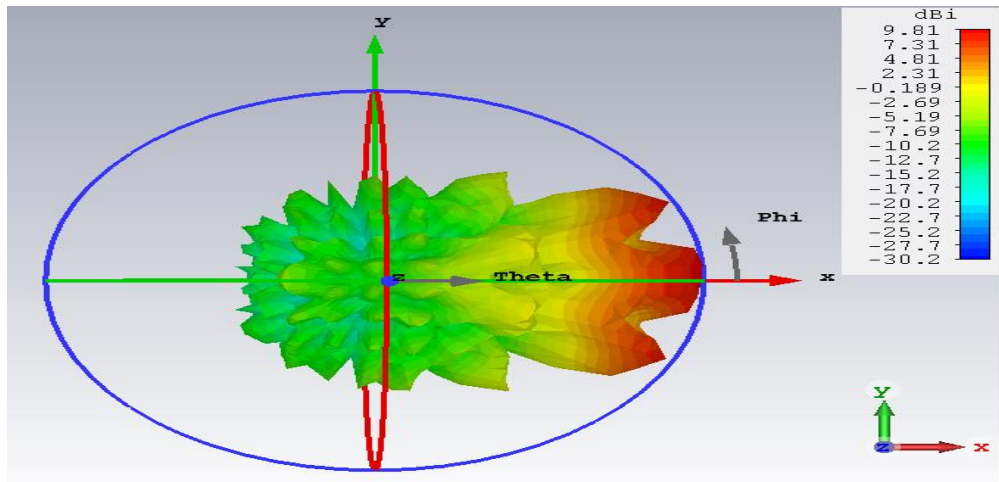
Fig 4.17: 3D far-field gain of different resonant frequencies

#### 4.4.6 3D Directivity

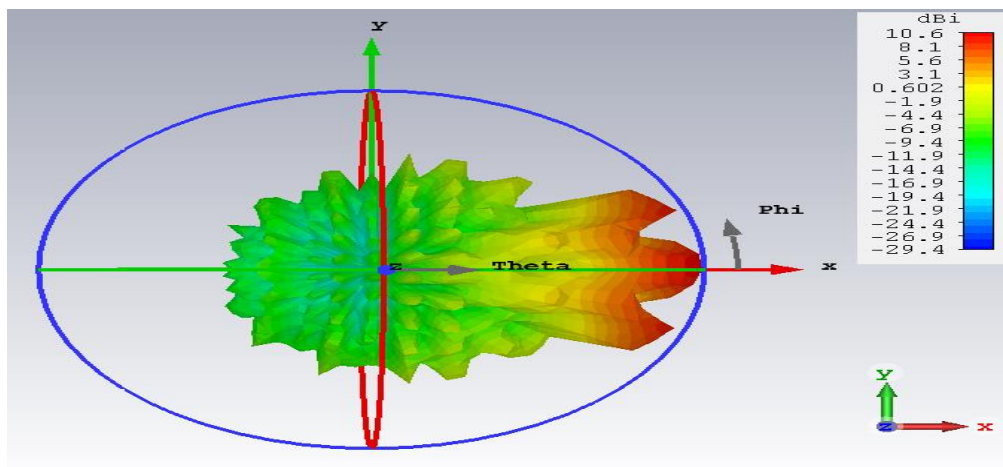
The 3D polar plot the simulated directivity for three resonant frequencies are shown in Fig 4.18. The directivity value is 9.81 dB at a lower resonant frequency of 239.3THz. It increases to 10.1dB at the second resonant frequency 263.52THz, and the higher value of directivity of proposed design is 10.6 dB at the last resonant frequency of 289.32THz.



(a) 239.32THz



(b) 263.52THz



(c) 289.32THz

Fig 4.18: 3D far-field directivity of three resonant frequencies of C-GHNA

#### 4.4.7 Efficiency and bandwidth

Efficiency of the third proposed design can be calculated based on directivity and gain simulated results as shown in Table 4.8. Also, bandwidth can be calculated from high frequency and lower frequency as in equation 3.18 and 3.20.

Table 4.8: Efficiency and bandwidth

Frequency (THz)	239.3	263.52	289.32
Efficiency (%)	84	82	83
Bandwidth (THz)	100		

#### 4.5 Characteristic of Substrate Integrated Waveguide Cylindrical-Gold Horn Nanoantenna (SIW-HNA)

The following sections highlight simulation result of the forth proposed antenna, as we use the substrate roger 5880 between the gold transmission line.

##### 4.5.1 Reflection coefficient $S_{11}$

Figure 4.19 illustrates the reflection coefficient wave of SIW-HNA at different resonant frequencies 203.7THz, 220 THz, 234.75 THz, 264 THz, and 282.79 THz with reflection coefficient -44.58dB,-33 dB,-42.2 dB,-33.3 dB,-27 dB respectively.

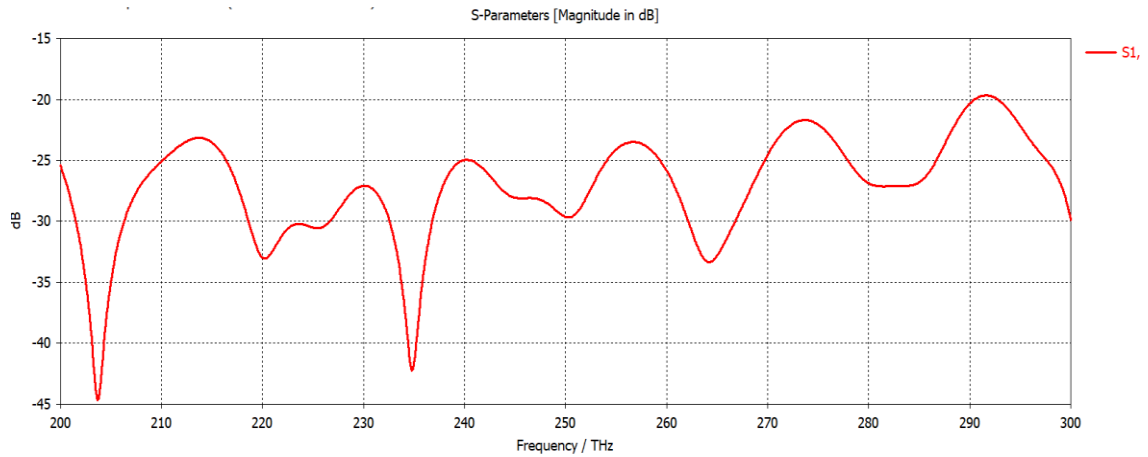


Fig 4.19: The simulated reflection coefficient  $S_{11}$  of SIW-HNA

#### 4.5.2 VSWR

The VSWR of the last proposed model (SIW-HNA) is shown in Fig 4.20. It has an appropriate value at five resonant frequencies (203.7, 220, 234.75, 264, 282.79) THz that should lie below to 2. When VSWR value is higher 2. This means a high mismatch between input impedance of antenna  $Z_{in}$  and the characteristic impedance of transmission line. Therefore, the antenna does not work effectively.

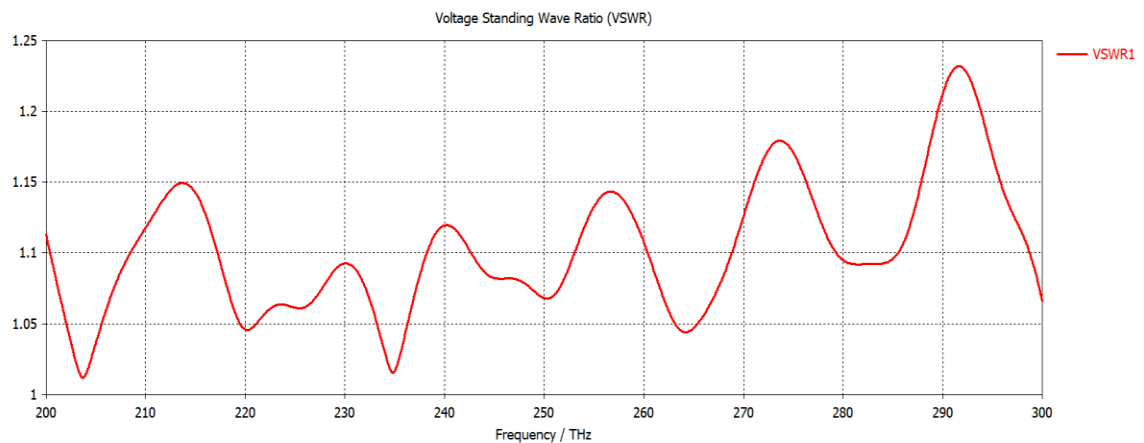
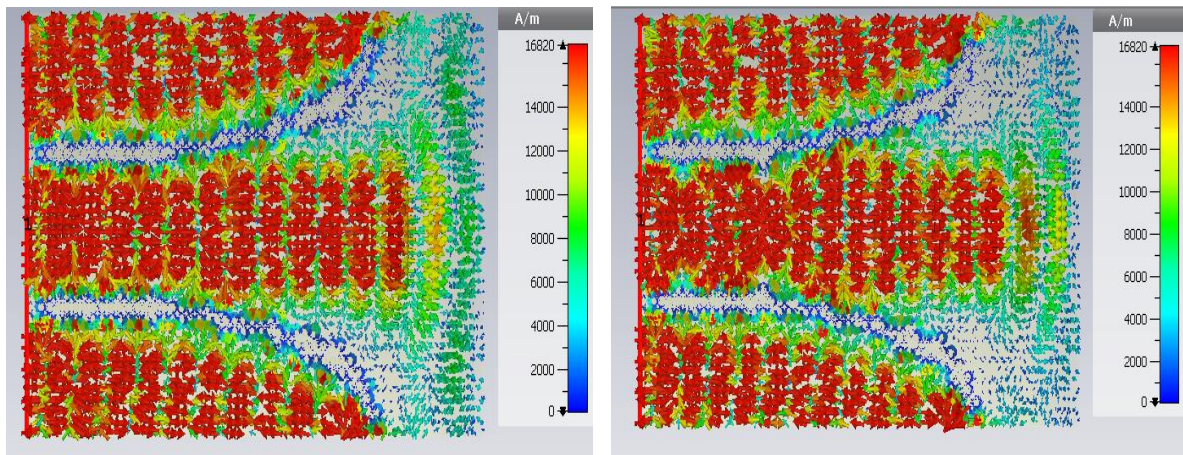


Fig 4.20: Simulated VSWR of the proposed model

### 4.5.3 Current distribution

The simulated current distribution of SIW-HNA at different resonant frequencies is shown in Fig 4.21. The current distribution varies according to different frequencies. The current is distributed at the first frequency (203.7THz) on a regular basis starting from the beginning of the transmission line to the end. The second frequency (220THz) begins with the difference in the center area of the transmission line. The third frequency (234.75THz) is a clearly different distribute at the beginning and then becomes tight in the region and back to be distributed more widely. In addition, the fourth and fifth resonant frequencies (264, 28279) THz the current distribution concentrates the starting of transmission line and then narrows and finally expands to come out of the end of horn antenna.



(a) 203.7THz

(b) 220THz

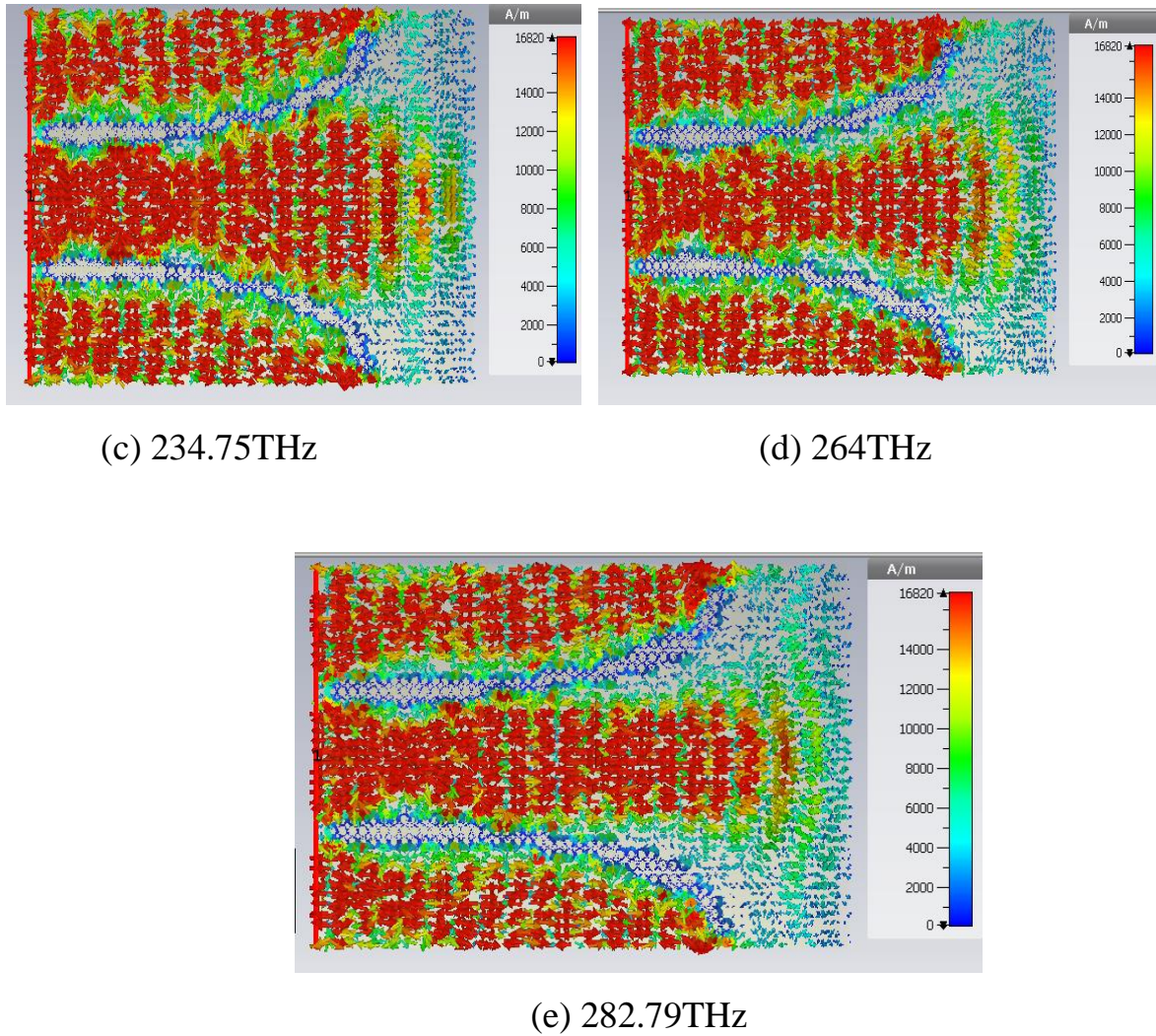


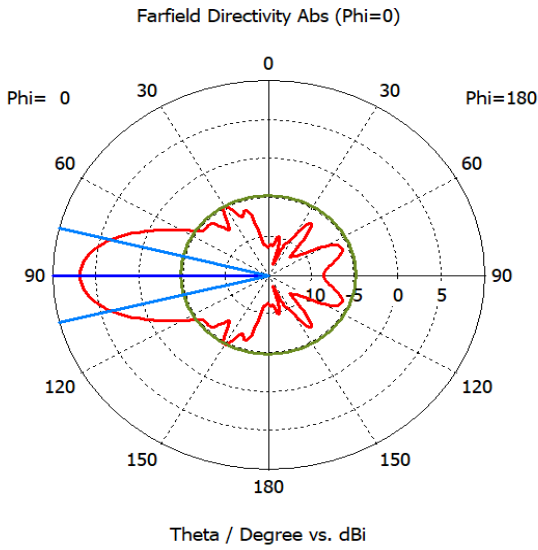
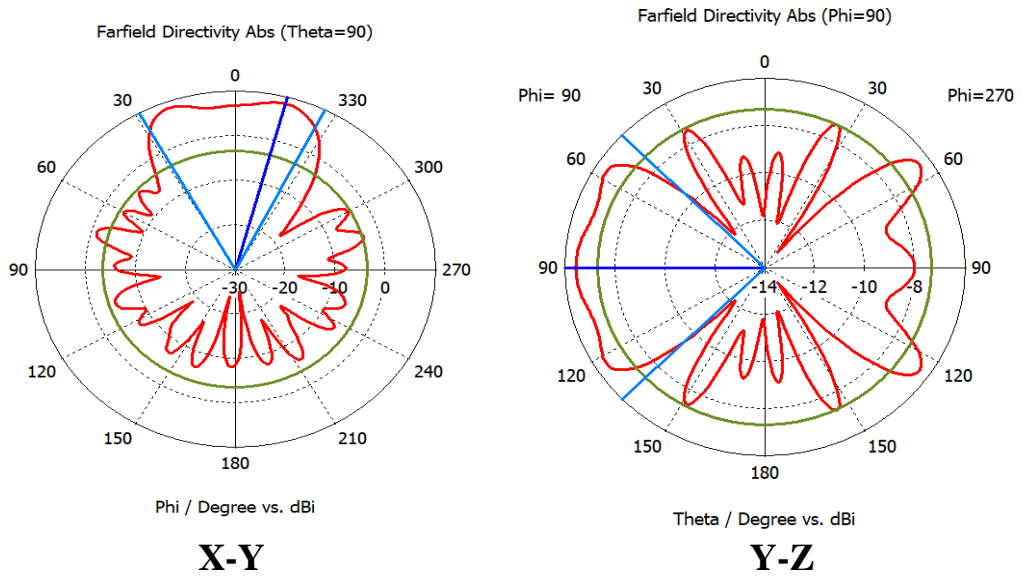
Fig 4.21: Simulated current distribution of the proposed model

#### 4.5.4 Radiation pattern

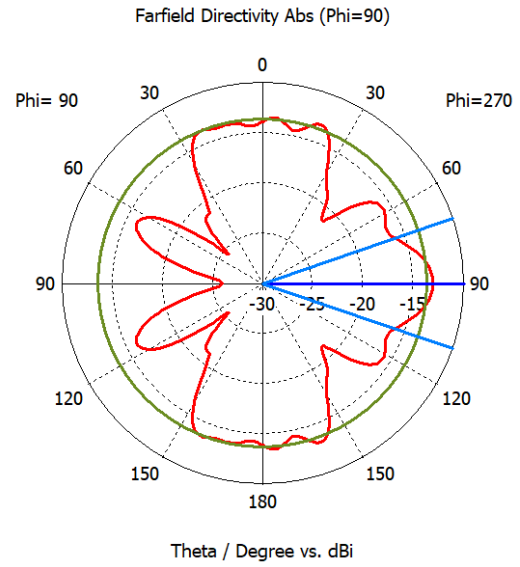
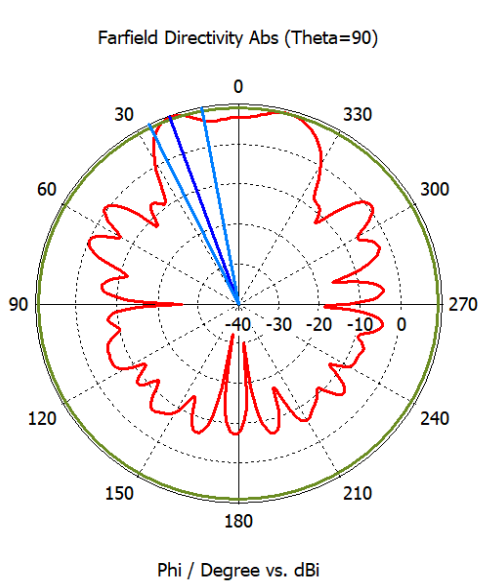
The 2D Radiation pattern of the forth-proposed antenna for five resonant frequencies (203.7, 220, 234.75, 264, and 282.79) THz is shown in Fig 4.22. In addition, we illustrate the characteristic of the power radiation in Table 4.9.

Table 4.9: The characteristic of radiation pattern of SIW-HNA

Frequency (THz)	Parameter	x-y plane ( $\theta=90^\circ$ )	y- z plane ( $\Phi=90^\circ$ )	x-z plane ( $\Phi=0^\circ$ )
203.7	Main lobe magnitude(dB)	21.8dB	6.82dB	20.1dB
	Main lobe direction	345°	90°	90°
	Angular width (3dB)	25.2°	88.6°	28.2°
	Side lobe level (dB)	-11.9dB	-1dB	-11.6dB
220	Main lobe magnitude(dB)	22.7dB	0.04dB	19.8dB
	Main lobe direction	20°	90°	90°
	Angular width (3dB)	15.7°	36.3°	33.6°
	Side lobe level (dB)	-8.8dB	-1dB	-8dB
234.75	Main lobe magnitude(dB)	23.2dB	6.79dB	23.2dB
	Main lobe direction	358°	81°	90°
	Angular width (3dB)	39.3°	52.7°	31.5°
	Side lobe level (dB)	-9.8dB	-4dB	-7.3dB
264	Main lobe magnitude(dB)	23.6dB	7.87dB	20dB
	Main lobe direction	349°	90°	90°
	Angular width (3dB)	21°	47.3°	23.3°
	Side lobe level (dB)	-5.3dB	-2.6dB	-6.6dB
282.79	Main lobe magnitude(dB)	24.9dB	10.7dB	19.7dB
	Main lobe direction	350°	90°	90°
	Angular width (3dB)	12.9°	34.5°	22.2°
	Side lobe level (dB)	-6.1dB	-3.3dB	-2.3dB

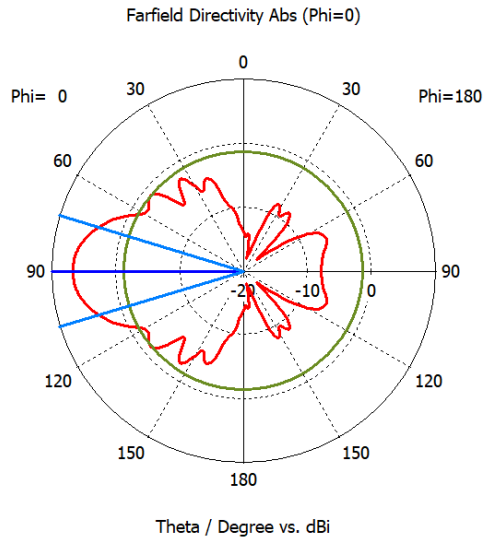


(a) at 203.7 THz



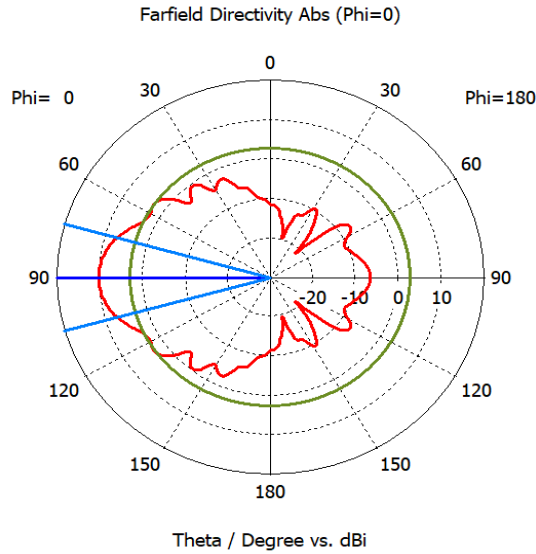
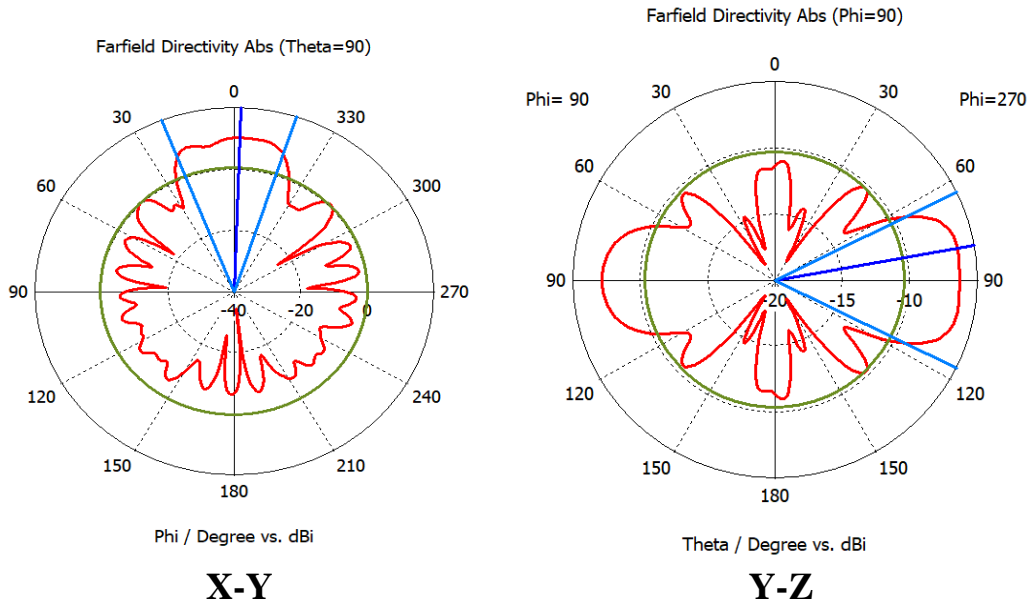
**X-Y**

**Y-Z**

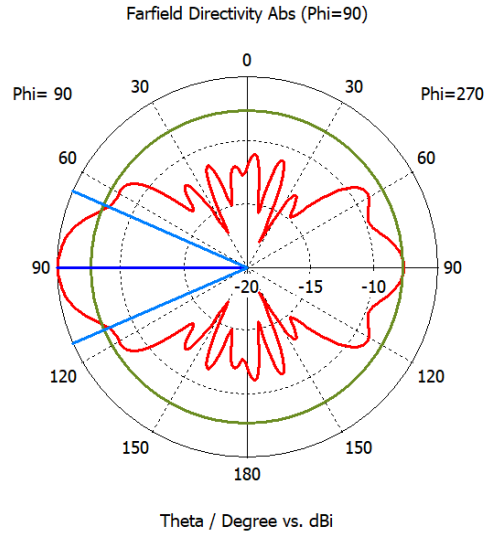
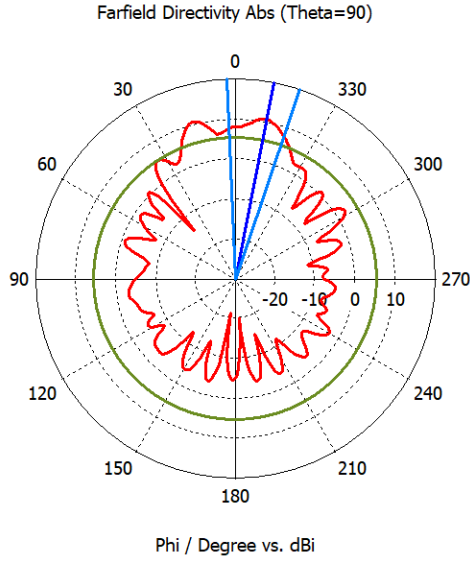


**X-Z**

(b) at 220 THz

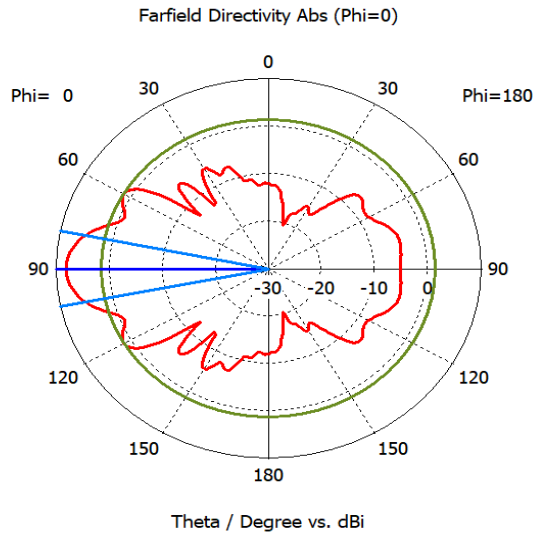


(c) at 234.75 THz



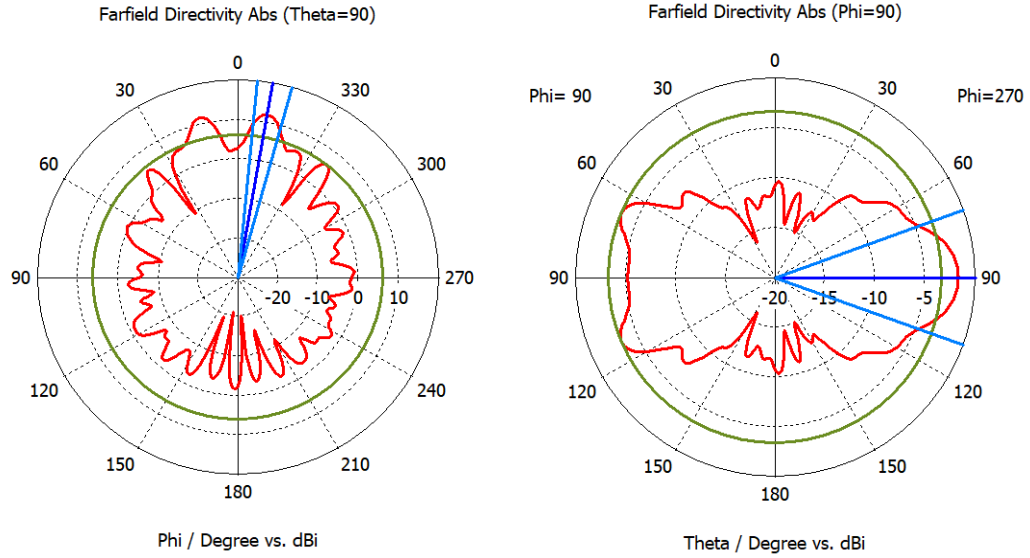
**X-Y**

**Y-Z**



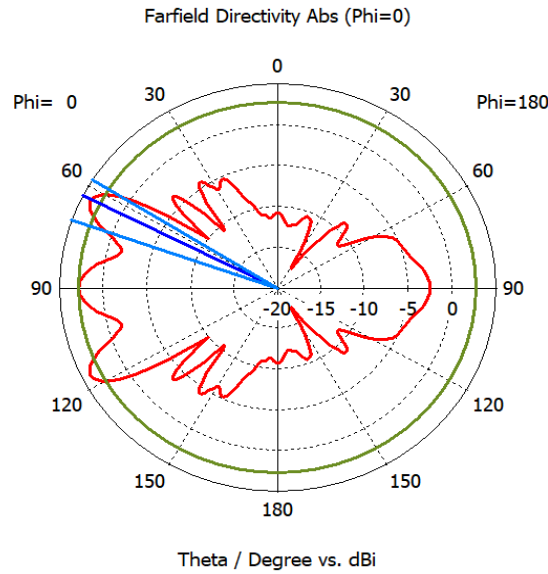
**X-Z**

(d) at 264 THz



**X-Y**

**Y-Z**



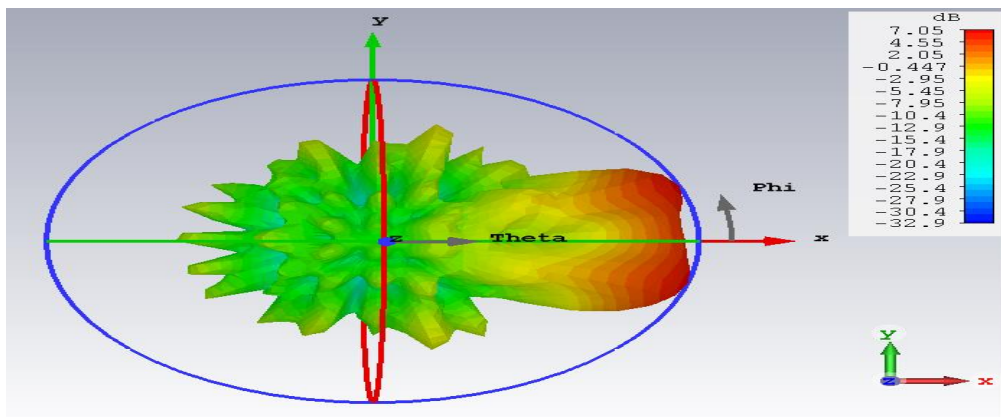
**X-Z**

(e) at 282.79

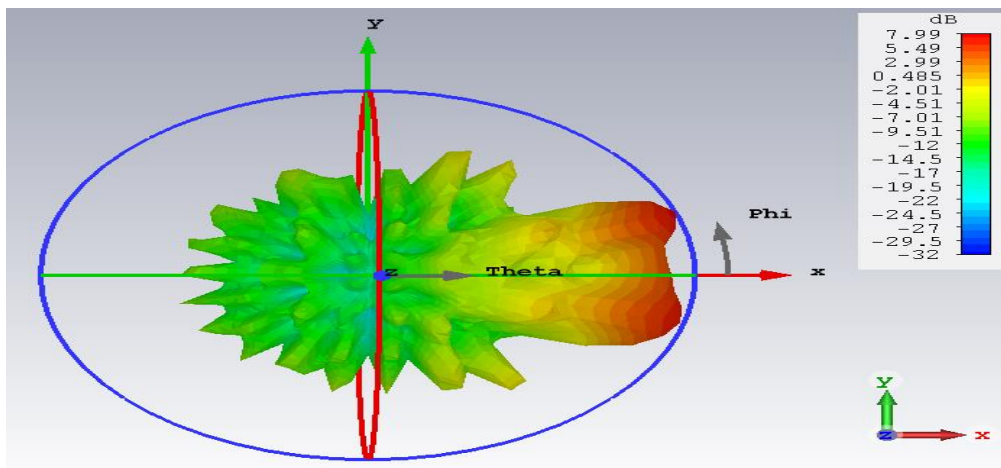
Fig 4.22: The simulated result of 2D radiation pattern

### 4.5.5 3D Gain

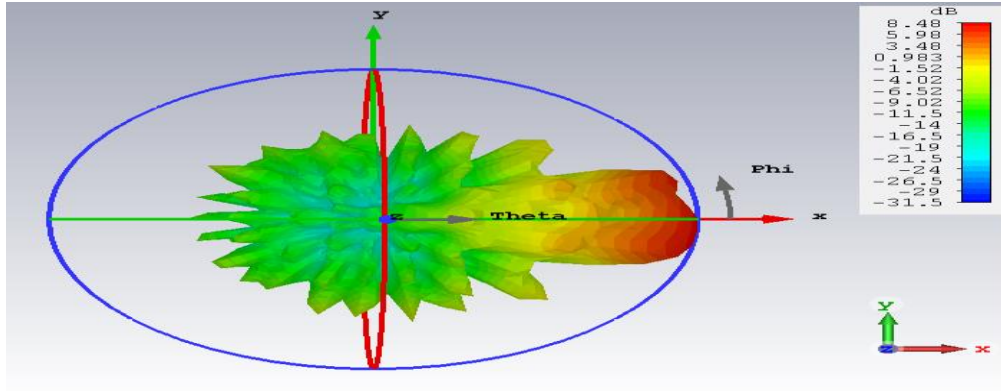
Figure 4.23 illustrates the far field gain simulation. The gain value is 7.05dB at a first resonant frequency 203.7THz, increases to 7.99dB at second resonant 220THz. Also the gain value is 8.48dB at third resonant 234.75THz. At the fourth resonant frequency 264THz the gain increases to 8.89dB and the higher value of gain is 10.2dB at the last resonant frequency 282.79THz.



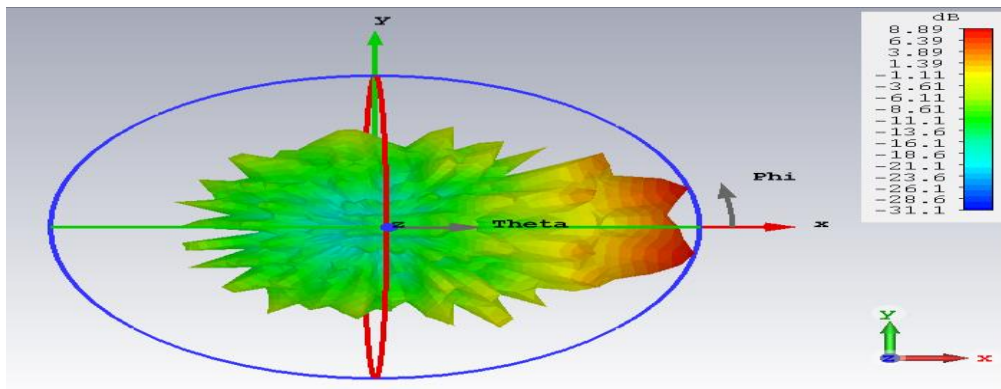
(a) 203.7THz



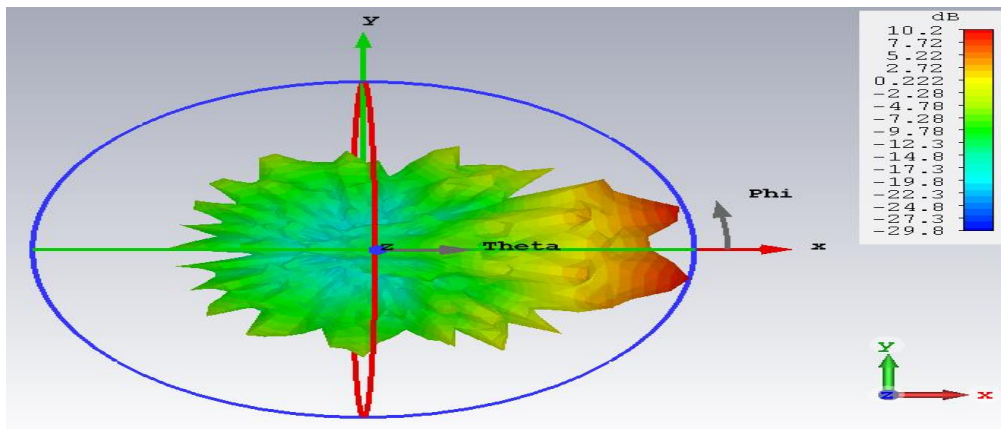
(b) 220THz



(c) 234.75THz



(d) 264THz

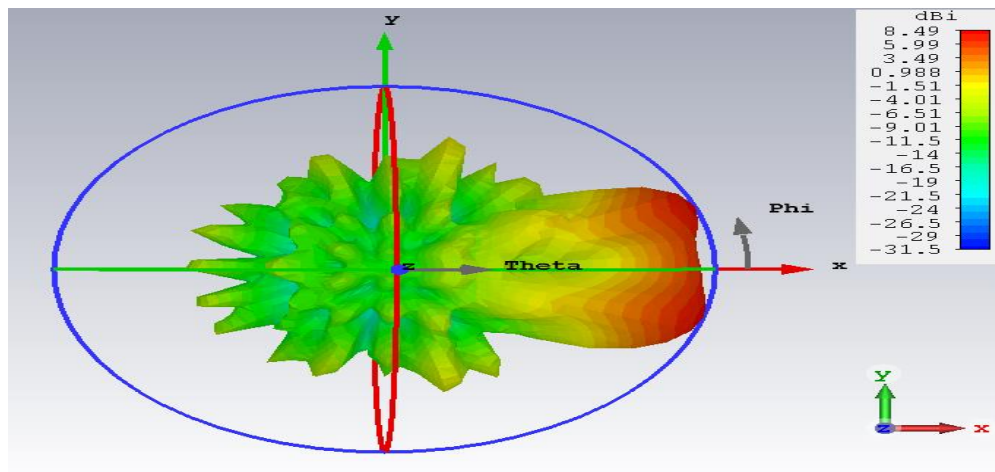


(e) 282.79

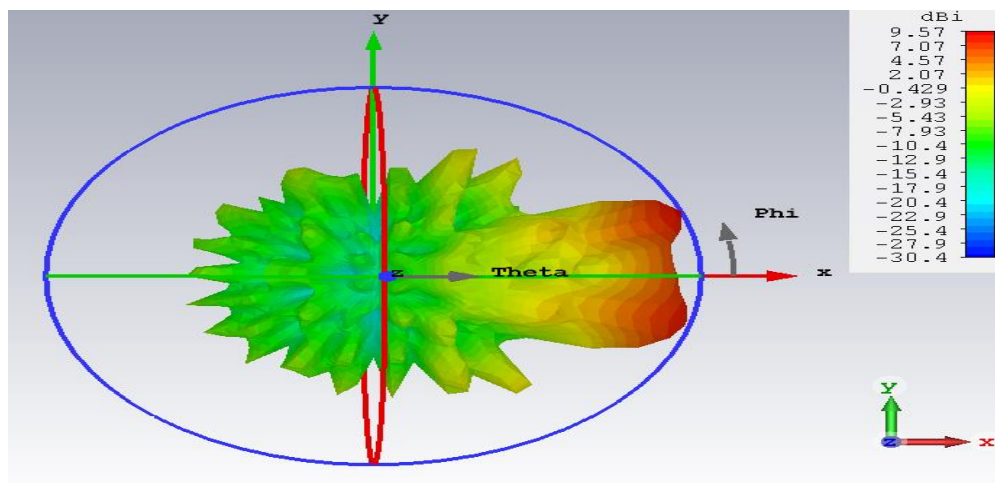
Fig 4.23: Simulation Gain at three various frequencies

### 4.5.6 3D Directivity

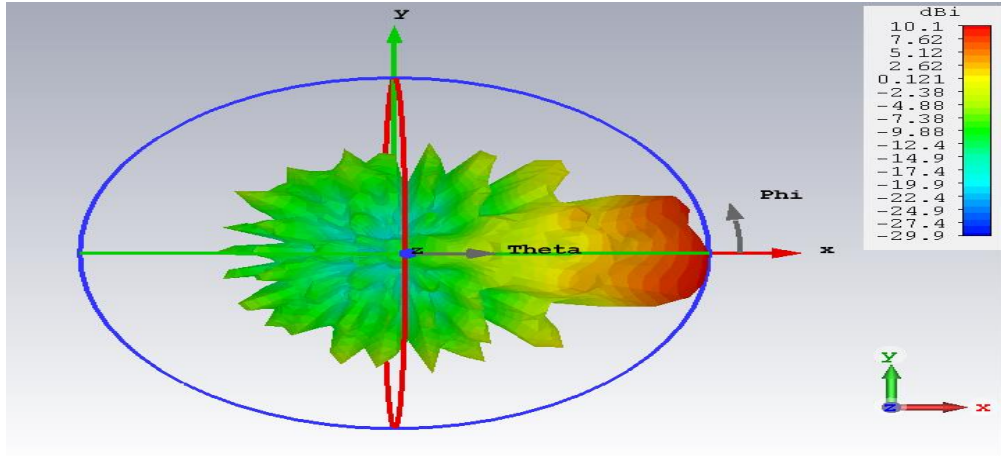
The simulation far field of directivity pattern is shown in Fig 4.24. The directivity value is 8.49dB at a lower resonant frequency 203.7THz. Then directivity is 9.57dB increases at second frequency 220THz. Increased value of directivity is 10.1dB at third frequency 234.75THz and the values of directivity increase to 10.6dB and 12dB at fourth and the last resonant frequencies 264THz and 282.79THz respectively.



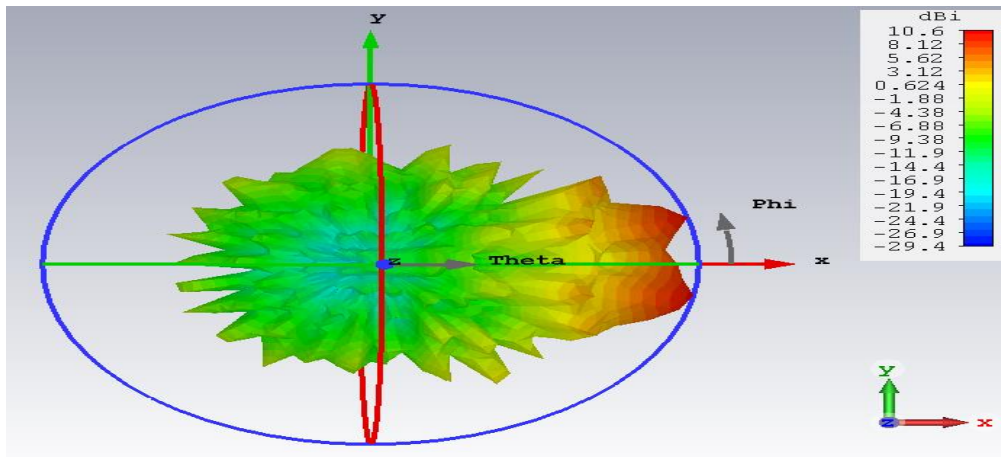
(a) 203.7THz



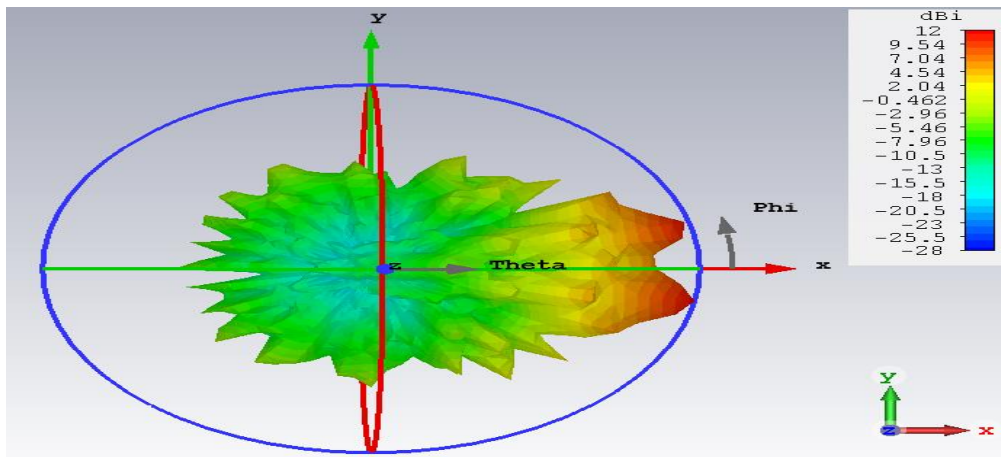
(b) 220THz



(c) 234.75THz



(d) 264THz



(e) 282.79THz

Fig 4.24: The directivity for different frequencies

### 4.5.7 Efficiency and bandwidth

Table 4.10 illustrates the efficiency of the last proposed design. It is calculated on the basis from directivity and gain simulated results. Also, Bandwidth can be calculated for different frequencies (203.7, 220, 234.75, 264, 282.79) THz .it is based on equation 3.18 and 3.20.

Table 4.10: The simulated results of efficiency and bandwidth for various frequencies.

Frequency (THz)	203.7	220	234.75	264	282.79
Efficiency (%)	83	83	84	84	85
Bandwidth (THz)	100				

### 4.5.8 Compression between the third (C-GHNA) and fourth (SIW-HNA) proposed antenna

Based on the simulated results of the last two proposed antennas, we can compared the results with respect to reflection coefficient  $s_{11}$ , resonant frequencies, gain, directivity, efficiency and bandwidth as shown in Table 4.11.

Table 4.11: The comparison between the last two proposed designs

Design	Frequency (THz)	$S_{11}$ (dB)	Gain (dB)	Directivity (dB)	Efficiency (%)	BW (THz)
C-GHNA	239.6	-23.59	8.23	9.81	84	Wide band 100
	263.9	-23.89	8.31	10.1	82	
	289.5	-23.96	8.8	10.6	83	
SIW-HNA	203.7	-44.58	7.05	8.49	83	Wide band 100
	220	-33	7.99	9.57	83	
	234.75	-42.2	8.48	10.1	84	
	264	-33.3	8.89	10.6	84	
	282.79	-27	10.2	12	85	

#### 4.5.9 The validation of the two design with other reference

Table 4.12: Comparison between the last two proposed designs

Design	Frequency (THz)	$S_{11}$ (dB)	Gain (dB)	Directivity (dB)	Efficiency (%)	BW (THz)
[32]	185	-18	7.12			85
	200	-34	8.11			
	230	-16	9.31			
[36]	275	-64	-	14.2	66.93	100
C-GHNA	239.6	-23.59	8.23	9.81	84	Wide band 100
	263.9	-23.89	8.31	10.1	82	
	289.5	-23.96	8.8	10.6	83	
SIW-HNA	203.7	-44.58	7.05	8.49	83	Wide band 100
	220	-33	7.99	9.57	83	
	234.75	-42.2	8.48	10.1	84	
	264	-33.3	8.89	10.6	84	
	282.79	-27	10.2	12	85	

## 4.6 Comparison of the four proposed antennas

A comparison of the four proposed antennas is illustrated in Table 4.13. This comparison is made of different shapes and material that are included in the transmission line (between the two layers of gold) and observation of differences in terms of gain, directivity and other factors.

Table 4.13: The simulation results of the four proposed horn antenna designs

Proposed antenna	S <sub>11</sub> (dB)	Freq. THz	directivity (dB)	Efficiency (%)	Bandwidth (THz)	Side lobe (THz)	Application
SHNA	-22.28, -41.09, -24.27	32.49, 53.9, 71.23	1.42, 6.46, 10.3	72, 93, 95	Multi bands 6.78, 7.77, 8.38	-9,-13.8, -18	Wireless nano link Photo detection Photo emission [45] [35]
G-SHNA	-25.48, -32.29, -26.09	276.47, 298.21, 320.98	12.1, 12.1, 12.5	81, 81, 82	Wide band 100	-1.3,-2,-1.7	Harnessing solar energy [36]
C-GHNA	-23.59, -23.89, -23.96	239.6, 263.9, 289.5	9.81, 10.1, 10.6	84, 82, 83	Wide band 100	-1.1,-1.4,-1.1	Energy harvesting [32]
SIW-HNA	-44.58, -33, -42.2, -33.3, -27	203.7, 220, 234.75, 264, 282.79	8.49, 9.57, 10.1, 10.6, 12	83, 83, 84, 84, 85	Wide band 100	-11.9,-8.8,-9.8,-5.3,-6.1	Smart lighting [31]

# CHAPTER FIVE

## CONCLUSIONS AND SUGGESTIONS

### 5.1 Introduction

In this chapter, we view the work presented in this thesis of proposing four designs of horn nanoantenna to design multiband and broadband for optics wireless communication, smart lighting and energy harvesting applications. We also present conclusion of this work that has been done in previous chapters as well as some recommendations for future work.

### 5.2 Conclusion

In this section, the associated comments about the four designs of Horn Nanoantenna are presented. These four Nanoantennas are proposed with the same general shape but used different sidewall to demonstrate the effect of the geometrical shape of arranged vias inside transmission line on the antenna performance, such as reflection coefficient  $S_{11}$ , gain, directivity and side lobe.

The first design consists of only two gold layer called Simple Horn Nanoantenna (SHNA). This simulation results of proposed design with respect to reflection coefficient multiband with three resonant frequency, which a range of bandwidth (29.3-36) THz, (49.3-57.3) THz and (67.6-75.7) THz, gain are (1.02, 5.99, 9.79) dB, directivity are (1.42, 6.46, 10.3) dB and

efficiency are (72, 93, 95)% for three resonant frequencies (32.49, 53.9, 71.23)THz respectively.

The second design is composed of two gold layers arranged inside between them gold –silicon vias. This design is called Gold-Silicon Horn Nanoantenna (G-SHNA). The range of bandwidth is (230-330) THz, gain (9.79, 9.79, 10.2) dB, directivity (12.1, 12.1, 12.5) dB and efficiency for three resonant frequencies (279.47, 298.21, 320.98) THz are (81, 81, 82) % respectively.

The third design is used cylindrical-gold via as sidewall inside the transmission line, this proposed design called Cylindrical-Gold via Horn Nanoantenna (C-GHNA). The bandwidth is (200-300) frequency range, gain (8.23, 8.31and 8.8) dB, directivity (9.81, 10.1, 10.6) dB, efficiency (84, 82, 83) percentage at three resonant frequencies (239.6, 263.9, 289.5) THz.

The last design composed two gold layers inserted between them dielectric material (Au-Rogers RT5880-Au) used cylindrical via as a sidewall this design called Substrate Integrated Waveguide-Horn Nanoantenna (SIW-HNA). The bandwidth range is (200-300) THz, efficiency for five resonant frequencies (203.7, 220, 234.75, 264,282.79) THz are (83, 83, 84, 84, 85) % respectively, gain are (7.05, 7.99, 8.48, 8.89 and 10.2) dB and directivity are (8.49, 9.57, 10.1, 10.6, 12) dB.

We is concluded from the results of four proposed horn nanoantenna, the second design (G-SHNA) is the best because wideband frequency and high directivity.

### 5.3 Suggestions

The suggestions for future scope can be reviewed as follows:

- 1) Designing a horn nanoantenna with a slotted waveguide such that these slots can be created with different shapes and dimensions.
- 2) Designing a horn nanoantenna with an open end in the form of ladder shape.
- 3) Designing a printed horn nanoantenna based on Substrate Integrated Waveguide (SIW).

## References

- [1] Ramesh G. et al, Microstrip Antenna Design Handbook, london: artechhouse, 2011.
- [2] Constantine A. Balanis, Antenna Theory Analysis and Design, New Jersey: John Wiley & Sons, Fourth Edition 2016.
- [3] Amanti M. et al, "Horn Antennas for Terahertz Quantum CascadeLasers," *ELECTRONICS LETTERS*, vol. 43, no. 10, May 2007.
- [4] Semih C. et al, "Validation of Electromagnetic Field Enhancement in Near-Infrared through Sierpinski Fractal Nanoantennas," *OPTICS EXPRESS*, vol. 22, no. 16, 2014.
- [5] Andrea A. and Nader E., "Wireless at The Nanoscale: Optical Interconnects Using Matched Nanoantennas," *The American Physical Society*, vol. 104, no. 10, May 2010.
- [6] Javier A. et al, "Optical Antennas for Nano-Photonic Applications," *INSTITUTE OF PHYSICS*, vol. 16, no. S230, March 2005.
- [7] Mu"hlischlegel P. et al, "Resonant Optical Antennas," *SCIENCE*, vol. 308, no. 10, June 2005.
- [8] Pai-Yen C. and Andrea A., "Optical Nanoantenna Arrays Loaded with Nonlinear Materials," *The American Physical Society*, vol. B82, December 2010.
- [9] Allan W. Love, Electromagnetic Horn Antennas, New York : IEEE, Press, 1976.
- [10] Constiane A. Balanis, Advanced Engeineering Electromagnetics, New York: John Wily& Sons, 1989.
- [11] Shubhendu S., "Design and Analysis of Pyramidal Horn Antenna at 8

- GHz Frequency," *International Journal of Advanced Research in Electronics and Communication Engineering*, vol. 3, no. 2, February 2014.
- [12] Krasnok A. et al, "Optical Nanoantennas," *Physics - Uspekhi*, vol. 56, no. 6, November 2012.
- [13] Tadao N. et al, "Advances in Terahertz Communications Accelerated by Photonics," *NATURE PHOTONICS*, vol. 10, June 2016.
- [14] Kumud R. Jha and Singh G. , "Terahertz Planar Antennas for Future Wireless Communication: A technical review," *Elsevier*, 2013.
- [15] Garcia-Parajo M., "Optical Antennas Focus in on Biology," *Nat. Photon.* 2, 2008.
- [16] Andrea A. and Nader E., "Theory, Modeling and Features of Optical Nanoantennas," *IEEE*, 2013.
- [17] Ivan S. Maksymov et al, "Optical Yagi-Uda nanoantennas," *Walter de Gruyter*, 2012.
- [18] Steven D. Novack and Dale K. Kotter, "Theory and Manufacturing Processes of Solar Nanoantenna Electromagnetic Collectors," *Journal of Solar Energy Engineering*, vol. 132, 2010.
- [19] Babu L. Shahu et al, "A Compact Super Wideband Monopole Antenna Design using Fractal Geometries," *Microwave Review*, 2014.
- [20] Dipika S. Sagne et al, "Design of Modified Geometry Sierpinski Carpet Fractal Antenna Array for Wireless Communication," *IEEE* , 2012.
- [21] Lukas N. and Niek v. Hulst, "Antennas for Light," *nature photonics*, vol. 5, 2011.
- [22] Dheif I. Abood, Wideband Nano Fractal Antenna Design, University of Technology: master Thesis, 2015.

- [23] Andrea A. and Nader E., "Optical Nanotransmission Lines: Synthesis of Planar Left-Handed Metamaterials in The Infrared and Visible Regimes," *OPTICS LETTERS*, vol. 23, no. 3, 2006.
- [24] Majid A. Azimi et al, "Design of Broadband Constant-Beamwidth Conical Corrugated-Horn Antennas," *IEEE Antennas and Propagation Magazine*, vol. 51, no. 5, 2009.
- [25] Hao W. et al, "Dielectric Loaded Substrate Integrated Waveguide (SIW) H-Plane Horn Antennas," *IEEE TRANSACTIONS ON ANTENNAS AND PROPAGATION*, vol. 58, no. 3, 2010.
- [26] Mahdi O. and Mohammad S. Abrishamian, "Corrugated SIW K Band Horn Antenna," *International Journal of Electronics and Communications*, 2014.
- [27] Adam J. and Romier M. , "Design Approach for Multiband Horn Antennas Mixing Multimode and Hybrid Mode Operation," *IEEE*, 2016.
- [28] Bing Z. et al, "Metallic 3-D Printed Antennas for Millimeter- and Submillimeter Wave Applications," *IEEE TRANSACTIONS ON TERAHERTZ SCIENCE AND TECHNOLOGY*, 2016.
- [29] Muhannad A. Al-Tarifi<sup>1</sup> and Dejan S. Filipovic, "On The Design and Fabrication of W-band Stabilised-Pattern dual-Polarised Horn Antennas with DMLS and CNC," *IET Microwaves, Antennas & Propagation*, vol. 11, no. 14, 2017.
- [30] Ariffuddin Joret et al , "Design and Simulation of Horn Antenna Using CST Software for GPR System," *IOP Publishing*, 2017.
- [31] Ramaccia D. et al, "Efficient and Wideband Horn Nanoantenna," *OPTICS LETTERS*, vol. 36, no. 10, 2011.
- [32] Ramaccia D. et al, "Electrical and Radiation Properties of a Horn Nano-

- Antenna at Near Infrared Frequencies," *IEEE*, 2010.
- [33] Ramaccia D. et al, "Boosting PV Cell Performances by using Horn Nano-Concentrators," *IEEE*, 2012.
- [34] Bondarenko T. et al, "THz Band Horn Antenna Design," *PAC*, 2013.
- [35] Yuanqing Y. et al, "Plasmonic Sectoral Horn Nanoantennas," *OPTICS LETTERS*, vol. 39, no. 11, 2014.
- [36] Sumukha P. et al, "Design and Analysis of a Nano Horn Antenna for Harnessing Solar Energy," *International Journal of Current Engineering and Technology*, vol. 4, no. 2, 2014.
- [37] Zhongyu L. et al, "A Design of On-chip Terahertz Horn Antenna With Microstrip Feed," *IEEE International Conference on Integrated Circuits and Microsystems*, 2016.
- [38] Adell L. A. and Sukure E. Kocabas, "Beam Steering and Impedance Matching of Plasmonic Horn Nanoantennas," *OPTICS EXPRESS*, 2016.
- [39] Sundaramurthy A. et al, "Toward Nanometer-Scale Optical Photolithography: Utilizing the Near-Field of Bowtie Optical Nanoantennas," *Nano Lett.*, vol. 6, p. 1, 2006.
- [40] Chen p., and Alu A. , "Optical Nanoantenna Arrays Loaded with Nonlinear Materials," *Phys. Rev. B*, vol. 82, 2010.
- [41] Taminiau T., Stefani F., and van N. Hulst, "Enhanced Directional Excitation and Emission of Single Emitters by a Nano-Optical Yagi-Uda Antenna," *OPTICS EXPRESS*, vol. 16, 2008.
- [42] Alu A., and Engheta N., "Input Impedance, Nanocircuit Loading, and Radiation Tuning of Optical Nanoantennas," *Phys.Rev.Lett*, vol. 101, 2008.
- [43] Zhao Y., Engheta N., and Alu A., "Effects of Shape and Loading of Optical Nanoantennas on their Sensitivity and Radiation Properties,"

*OPTICS*, vol. 28, 2011.

- [44] Mohammad H. et al, "Design and Analysis of Disordered Optical Nano-antenna Structures," *IEEE. Journal of Lightwave Technology*, pp. 1-5, 2016.
- [45] Adeel A., Design and Analysis of Plasmonic Nanoantennas with Ground Plane and Impedance Matching, MSC thesis, Koc University, 2016.
- [46] Saif N., Design and Analysis of Slotted Patch Antenna for Wideband Applications, MSC thesis, Al-Mustansiriyah University, 2016.
- [47] Otasowie P. and Ogujor E., "Voltage Standing Wave Ratio Measurement and Prediction," *International Journal of Physical Sciences*, vol. 4, no. 11, 2009.
- [48] Pavel M. et al, "Antenna Radiation Efficiency Measurement in an Ultrawide Frequency Range," *IEEE Antennas and Wireless Propagation Letters*, vol. 8, 2009.
- [49] Sikiru O. Zakariyya, Modeling of Miniaturized, Multiband and Ultra-Wideband Fractal Antenna, Gazimağusa, North Cyprus: MSC thesis, Eastern Mediterranean University, 2015.
- [50] Giampiero L. et al, "Fundamental Properties and Optimization of Broadside Radiation From Uniform Leaky-Wave Antennas," *IEEE TRANSACTIONS ON ANTENNAS AND PROPAGATION*, vol. 54, no. 5, 2006.
- [51] Giuseppe V. et al, "Review of Substrate Integrated Waveguide Circuits for Beam-Forming Networks Working in X-Band," *SCINCE*, 2019.
- [52] Dominic D. and Yves C., "The Substrate Integrated Circuits - A New Concept for High-Frequency Electronics and Optoelectronics," *IEEE*, 2003.

- [53] Tarek D. and Ali D., Substrate Integrated Waveguide Antennas, Springer Science, Handbook of Antenna Technologies, 2015.
- [54] Cassivi Y. et al, "Dispersion Characteristics of Substrate Integrated Rectangular Waveguide," *IEEE MICROWAVE AND WIRELESS COMPONENTS LETTERS*, vol. 12, no. 9, 2002.
- [55] Bozzi M. et al, "Review of Substrate-Integrated Waveguide Circuits and Antennas," *IET Microwaves, Antennas & Propagation*, vol. 5, no. 8, 2011.
- [56] Feng X. and Ke W., "Guided-Wave and Leakage Characteristics of Substrate Integrated Waveguide," *IEEE TRANSACTIONS ON MICROWAVE THEORY AND TECHNIQUES*, vol. 53, no. 1, 2005.



جمهورية العراق  
وزارة التعليم العالي والبحث العلمي  
جامعة الفرات الاوسط التقنية  
الكلية التقنية الهندسية-نجف



# تصميم وتقييم الاداء لهوائيات نانويه من النوع البوقي للتطبيقات الحديثة

رسالة مقدمة الى  
قسم هندسة تقنيات الاتصالات  
كجزء من متطلبات نيل درجة ماجستير تقني في هندسة تقنيات الاتصالات

تقدم بها

دعاء مريم عباس محمد  
بكالوريوس في هندسة تقنيات الاتصالات

إشراف

الاستاذ المساعد الدكتور فارس محمد علي الجعفري

المدرس الدكتور سالم محسن وادي

تشرين الاول / 2019

## الخلاصة

الهدف الرئيسي من هذه الرسالة هو تصميم ومحاكاة هوائي البوق النانوي الجديد الذي يعمل في مدى التيرا هيرتز. والذي يدخل في العديد من تطبيقات الميكروويف والبصريات والاتصالات اللاسلكية مثل الإضاءة الذكية، الاستشعار، التصوير، وحصاد الطاقة وغيرها من التطبيقات المطلوبة ذات النطاق العريض.

يستخدم هوائي البوق في الهندسة بسبب الخصائص الجذابة، مثل الاتجاهية والربح والنطاق العريض. درس العديد من الباحثين هذا النوع من الهوائيات، بما في ذلك المخروطية والهرمية. التصميمات المقترحة لها نفس التصميم العام ولكنها مختلفة في الجزء الجانبي ودراسة تأثير الشكل على خصائص الهوائي. استخدمنا في هذه الرسالة اعمدة أسطوانية ومربعة الشكل بالإضافة الى اختلاف المواد المستخدمة

في هذه الرسالة ، قمنا بتصميم ومحاكاة أربعة تصميمات من طراز البوقي النانوي ، حيث تعمل التصميمات المقترحة في تيرا هيرتز ولديها ترددات متعددة النطاق أو عريضة النطاق. جميع التصميمات المقترحة للهوائي بأربعة قرون تتكون من طبقتين من الذهب المعدني لأن الذهب يمثل موصلًا كهربائيًا مثاليًا ، والذي لا تتغير خصائصه في القياسات النانوية بسمك 50 نانومتر. يستخدم نوع التغذية للإثارة خط النقل ل Horn Nanoantennas الدليل الموجي عند 50 اوم. جميع أبعاد طبقتين مستخدمة في تصميمات الهوائي الأربعة المقترحة في نفس النطاق، يبلغ طول الدليل الموجي  $\ell_{wg} = 4000\text{nm}$  ، ويبلغ طول القرن  $\ell_{horn} = 2000\text{nm}$  وعرض دليل الموجة  $w_{wg} = 2500\text{nm}$  بسمك 50 نانومتر. من أجل

تنفيذ أداء كل من التصاميم المقترحة، يتم استخدام محاكي برمجيات متاح تجارياً يسمى STUDIO CST  
STUDIO SUITE 2018 للحصول على الهدف المرغوب به.

يتكون التصميم هوائي القرن النانوي الأول من طبقتين فقط من خط النقل يطلق عليه الهوائي القرن  
النانوي البسيط (SHNA). يعطي هذا الهوائي نطاقاً متعدد النطاقات بثلاثة ترددات رنانة، حيث يبلغ عرض  
نطاق الأول (29.3-36) تيرا هيرتز، الثاني (49.3-57.3) تيرا هيرتز والنطاق الأخير (67.6-75.7)  
تيرا هيرتز.

يتكون التصميم الثاني أيضاً من طبقتين من الذهب، لكنهما يضيفان الأسطوانات المربعة من  
الذهب والسيلكون بالتعاقب داخل خط النقل يعرف هذا التصميم ذهب-سيلكون هوائي القرن النانوي  
(G-SHNA). هذا التصميم يعطي نطاق عريض. مجموعة عرض النطاق الترددي من (200 - 300)  
تيرا هيرتز.

يتألف تصميمات الهوائي القرن النانوي الثالث والرابع من طبقتين من الذهب بإضافة اعمدة  
الاسطوانية داخل خط النقل ولكن التصميم الأخير مختلف حيث تستخدم المادة عازلة بين طبقتين الذهب  
نعمل ثقوب او حفر داخل المادة العازلة وبعد ذلك نملئ هذه الحفر بمادة موصلة يفضل من نوع مادة  
الطبقتين للحصول على أفضل موائمة. لذلك، يطلق عليه اسطوانية-ذهب الهاوي القرن النانوي (C-GHNA)  
والركيزة دمج الدليل الموجي الهوائي القرن النانوي (SIW-HNA)، هذين النوعين تعطي نفس مجموعة  
النطاق الترددي من (200-300) تيرا هيرتز.